THESIS FOR THE DEGREE OF LICENTIATE OF ENGINEERING

Frequency Response by Wind Farms in Islanded Power Systems with High Wind Power Penetration

MATTIAS PERSSON

Department of Energy and Environment
CHALMERS UNIVERSITY OF TECHNOLOGY
Gothenburg, Sweden, 2015

Frequency Response by Wind Farms in Islanded Power Systems with High Wind Power Penetration
MATTIAS PERSSON

Division of Electric Power Engineering
Department of Energy and Environment
Chalmers University of Technology
SE–412 96 Gothenburg
Sweden
Telephone +46 (0)31–772 1000

Printed by Chalmers Reproservice
Gothenburg, Sweden, 2015

Dedicated to my family.

Frequency Response by Wind Farms in Islanded Power Systems with High Wind Power Penetration

MATTIAS PERSSON
Department of Energy and Environment
Chalmers University of Technology

Abstract

The integration of variable speed wind turbines (VSWT) in power systems keep increasing in order to reduce the emission of green house gases. This increase of power electronic converter interfaced generation causes a decrease of power system inertia and issues previously existing in power systems tend to become more complicated and new solutions should be evaluated.
This thesis investigates the impacts on frequency stability that can be caused by a decreased inertia in weak power systems. This by firstly investigating the frequency behavior and the roots and causes of the decreasing frequency quality in the Nordic power system (NPS). This by means of phasor measurement units (PMU) from different locations in the NPS. In particular the focus has been on large power imbalances, the rate of change of frequency (ROCOF) and the impact of location of disconnected generation, frequency quality and the evaluation of a new automatic frequency restoration reserve (FRR-A) service that was introduced in the NPS in 2013.
Furthermore, the concept of inertia emulation to handle large power imbalances is developed further with the adaptation to handle variable wind. Two strategies of utilize the rotating mass of the VSWT in order to balance 20 and 50 % VSWT instantaneous wind penetration ratios (WPR) in a islanded power system based on a hydro unit. The temporary frequency drop for a wind penetration of 50 % was improved from 47.33 Hz, for the uncontrolled case, to 49.10 Hz utilizing the suggested adaption of inertia support responindg to a disturbance of 0.1 pu.
Lastly, the capability of a VSWT to provide temporary primary frequency support in islanded power systems with 50 % through an alternating generation mix based on hydro, reheat or thermal units in charge of automatic generation control (AGC) considering delays, dead band settings and a combined pitch and droop controlled control strategy. The combined strategy showed clear improvements to the span of 49.9 Hz $\leq f <$ 50.1 Hz of 28 percentage points for a hydro based power system, this while only reducing the energy produced by 6 %.

Index Terms: Synthetic inertia, inertia emulation, frequency control, variable speed wind turbine, rate of change of frequency, frequency stability, transient stability, low inertia power systems, AGC.

Acknowledgments

My sincere gratitude goes to my supervisor Assoc. Prof. Peiyuan Chen for his guidance, never ending professionalism and support. Thank you for the motivation during frustrating times, your friendship and your continuously open mind. I also would like to thank my supervisor and examiner Prof. Ola Carlson for his inputs throughout the thesis and nice discussions. This project was a part of Chalmers Energy Initiative and the support is greatly acknowledged.
I would like to thank Prof. Torbjörn Thiringer for his willingness to share, listen and help with anything at any time.
Thanks to Dr. Morten Hemmingson at Gothia Power for the providing PMU data is greatly appreciated.
A big thanks also to Lars Olsson, for his knowledge on practical applications and his contribution on the industry view on the research conducted within the reference group.
Furthermore, I would like to thank Christer Bäck at Svenska Kraftnät for his supporting discussions on frequency behavior in the Nordic system and for sharing information.
A special thank goes to my roommates Amin Bahmani and Mebtu Beza, their attention to detail, willingness to perform in any task is truly inspiring. I would also like to thank my dear colleagues at the division of Electric Power Engineering and my students for creating such a nice working place.
I would like to thank my family and friends for their support and belief in me all these years, but also their patience in me when I disappear into work or drift of during conversations into research.
Last but certainly not least I would like to thank my girlfriend, Elin for her love, support during the sometimes endless nights of work. Without her I would truly be lost.

Mattias Persson
Gothenburg, Sweden
Feb, 2015

List of Acronyms

AGC	Automatic Generation Control
APM	Active Power Management
ASP	Ansluta Större Produktionsanläggning
CE	Continental Europe
DFIG	Doubly-Fed Induction Generator
DG	Distributed Generation
DK1	Danish Western Operating System
DK2	Danish Eastern Operating System
ENTSO-E	European Network of Transmission System Operators for Electricity
EWEA	European Wind Energy Association
FCPA	Frequency Controlled Pitch Actuator
FCR	Frequency Containment Reserve
FCR-D	Frequency Containment Reserve for Disturbances
FCR-N	Frequency Containment Reserve for Normal Operation
FI	Finish operating system
FDR	Frequency Controlled Disturbance Reserve
FNR	Frequency Controlled Normal Operation Reserve
FPC-WT	Full-power Converter Wind Turbine
FRR	Frequency Restoration Reserve
FRR-A	Automatic Frequency Restoration Reserve
FRR-M	Manual Frequency Restoration Reserve
GB	Great Britain
IM	Induction Machine
IRE	Ireland
LFC	Load Frequency Control
MFS	Minimum Functional Specification
MPP	Maximum Power Point
MPPT	Maximum Power Point Tracking
NERC	North American Electric Reliability Corporation
NO	Norwegian Operating System
NPS	Nordic Power System
PMU	Phasor Measurement Unit
PMSG	Permanent-Magnet Synchronous Generator
ROCOF	Rate of Change of Frequency
RR	Replacement Reserve

REV	Relative Energy Value
SE	Swedish Operating System
SONI	System Operator of Northern Ireland
SVK	Svenska Kraftnät
TMF	Temporary Minimum Frequency
TSO	Transmission System Operator
VSWT	Variable Speed Wind Turbine
WPR	Wind Power Penetration Ratio
WT	Wind Turbine

Contents

Chapter 1

Introduction

1.1 Background and motivation

In order to reduce CO_2 emission there is a growing demand for renewable power generation. One of the main renewable energy sources is wind. Turbines are installed to replace existing generation or increase the overall generation capacities. Even though they are becoming larger an average European offshore wind turbine installed in 2014 had a rating of 3.7 MW [1]. The central scenario for the European Wind Energy Association (EWEA) for 2020 predicts an installed capacity increase of 64 % compared to that of 2013, reaching 192.5 GW installed wind power capacity. This would reflect a 14.9 % share of wind energy in the European demand [2].

Due to wind variability and low predictability the occurrence of power imbalance in the system might increase due to increased wind power penetration[3]. These power imbalances could increase the variations of frequency, due to constrained or slow reserves, further worsening the frequency quality in a future power system. Furthermore, with a growing wind power penetration in the grid there is an increasing need for regulation from variable speed wind turbines (VSWTs), also known as doubly-fed induction generator (DFIG) or full power converter (FPC)-WT, to provide support in the form of spinning reserve and for reducing frequency instabilities in the grid. This need originates from the lack of inertia response provided by VSWT in their basic configuration [4]. An increase in wind power penetration ratio (WPR) may cause a decrease in total power system inertia. These factors could result in an worsened frequency stability during large power imbalances (trip of large generator units or n-1 contingencies).

1.2 Literature review

As existing problems related to frequency stability and quality might worsen due to a increased WPR of VSWT research has focused on the ability to control turbines in order to solve existing problems. The main findings of a literature study is presented below.

A study on angular stability can be seen in [5]. This paper presents the improvement on rotor angle stability utilizing the wind farms for reactive power support during disturbances, thus

decreasing the angular deviation during disturbances. Angular stability during large wind integration is also studied in [6] where synchrophasor measurements are utilized in order to estimate impact of wind power on angle stability and estimation of power system inertia.

[7] presents a centralized frequency control strategy and discusses the impact of spatial smoothing and how it reduces power fluctuations. It indicates a larger amount of kinetic energy is able to extract from VSWT compared to conventional fossil powered plants. Future research on timings between wind turbines (WTs) and conventional plants is proposed.

Frequency support strategies mainly for primary frequency control and through the use of the rotational energy and de-loading of the turbine is presented in the following papers: [8] considers the frequency support from VSWT when replacing current electric generation up to a WPR up to 51.9 %. Five different strategies for control is presented and evaluated, the most beneficial being the ”Static and dynamic frequency dependent voltage control”. The frequency control is initiated after a loss of 2.5 % of the total generation. Voltage and frequency dependent loads are considered in the modeling. Conclusions made from the paper are that an increasing WPR causes an increased initial frequency drop after a disturbance prior to activation of VSWT-support. [9] presents a deloaded optimum power extraction curve in order to boost the power output during frequency changes due to a load step of 0.15 pu subjected to a grid with a WPR of 25 % backed up with a thermal unit. Frequency nadir occurs at 49.2 Hz without support and at 49.4 Hz with the suggested support strategy. A similar study with an other concept of when to move to derated operation can be seen in [10] whom uses a high WPR of 65 % and backup generation beeing a thermal unit. The paper provides alot of insight to the operation of each component in the studied power system. Inertia emulation has been evaluated in [11] and has been proved to give a larger contribution from a VSWT than to a similarly sized directly coupled WTs. Interesting investing studies on a deeper level especially regarding synthetic inertia, weak power systems with good analytical contributions can be found in [12],[13].

Frequency data from the Nordic power system (NPS) have previously been studied in [14] and [15] utilizing phasor measurement units (PMU) measurements. The effect of sampling rate of the data was however not considered. An overall deterioration of the frequency quality was observed.

In order to increase the capability to handle large power imbalances VSWT are also retrofitted with supporting storage. [16] studies the control of a 2 MW permanent-magnet synchronous generator (PMSG)-based VSWT and its transient response. The DC-link is modeled with good accuracy and provides parameters. Other papers present support functions (through larger capacitors) to be put into the DC-link in order to boost the power imbalances [17] and [18].

Overview papers within the area are listed below and their main take aways according to the author of this thesis. [19] describes the inertia emulation and droop control but also the interaction between generation units’ automatic generation control (AGC) and the local support provided by VSWT. [20] describes future trends such as local voltage control, inertia emulation and power oscillation damping (mainly 0.15 - 2 Hz). [21] considers the different types of topologies for VSWT but also concludes that grid frequency support as inertia emulation and droop control are emerging issues.

Lacking in research is however a connection to the power system frequency behavior in normal

operation and the apparent problems of frequency stability and quality and how they might increase or decrease in regards to a change in power system inertia or but not only the introduction of frequency controlled VSWT.

Sampling frequencies are of importance when considering rate of change of frequency (ROCOF) studies, and need to be investigated. The ability to provide inertia emulation during various wind operations should be addressed after a careful modeling of the aerodynamic performance as suggested in [13].

The transmission system operator (TSO), Svenska Kraftnät (SVK), in Sweden is evaluating the possibility of running the major cities in island operation during sever disturbances [22]. The WPR can vary greatly during a future islanded operation of a grid with VSWTs. Therefore different support strategies for power imbalance needs to be evaluated, issues and benefits of the increased WPR should be evaluated towards a variety of backup generation.

In low inertia power systems the impact of frequency dependent loads should be of importance considering their interaction during large power imbalances, this since larger variations of frequency is expected in the low inertia grid.

Thorough frequency quality studies is still needed to further evaluate the risks of a reduced power system inertia due to integration of VSWT. Local frequency measurements should also be evaluated in order to realize if local control algorithms is sufficient for frequency support or if a centralized frequency signal should be provided through supervisory control.

1.3 Purpose of the thesis and main contributions

The main purpose of this thesis is to present the implications on power system frequency during reduced inertia in the power system and the effect of increasing WPR.

To re-evaluate the frequency quality in recent years in the NPS, evaluate the roots and causes the frequency quality, when the deviations occur and to link these findings towards a frequency control application in a VSWT.

To study the implications of inertia support from VSWT and their ability to handle variable wind during the activation period of the support strategy.

To Evaluate the possible primary frequency support that can be provided by VSWT in islanded power systems with varying backup generation and during high WPR. The control strategy needs to be based on temporary support prior to the AGC of the backup generators catch up.

The main contributions of this thesis are according to the knowledge of the author:

1. Frequency evaluation of NPS considering the ways to evaluate and behaviors that might increase during a possible decrease of power system inertia.
2. Inertia control with added control for handling real wind variations.
3. Continuous primary frequency support of VSWT through adapted droop implementation and frequency controlled pitch actuator. Improved frequency behavior independently of type of

backup generator, low amount of spilled wind and reduced wear and tear of backup generation.

1.4 Structure of the thesis

The thesis is structured in the following way:

Chapter 2 describes the most relevant theories on frequency control and various support strategies. It also gives a short description of how a frequency deviation occurs after the disconnection of a generator in a power system. It is finalized with a short review of grid codes put on generators in the countries with the highest wind power penetration (by installed capacity).

Chapter 3 contains an initial literature review of the impacts that poor frequency quality could lead to and is followed by an evaluation of the frequency quality of the NPS based on PMU data from 2006, 2012 and 2013. The chapter gives recommendations on the applied sampling frequency in the measurements for frequency duration studies as well as for the rate of change of frequency (ROCOF) studies. The chapter ends with a discussion and evaluation regarding the new frequency support strategy introduced in the NPS in January of 2013.

Chapter 4 contains the basic power system generation units and their models that are used in both Chapter 5 and 6. Chapter 5 considers the support strategies from variable speed wind turbines (VSWT) during large disturbances (loss of 0.1 pu generation). Reflections on frequency responding loads and their contribution to the overall frequency nadir are also considered. An adaption to a previous model to handle variable wind data is presented and evaluated. A short description of interconnected wind-hydro systems is also considered briefly.

Chapter 6 reflects on the frequency deviations caused in a power system with large amount of wind power to maintain its frequency when altering the different types of generation supporting the automatic generation control. Different wind speeds from real data are evaluated through their effect on power system frequency. Two frequency control strategies for VSWT are combined and evaluated. This by comparing the loss of produced power due to spillage of energy when trying to control the frequency using the VSWT on the deviations caused by the wind power fluctuations.

Finally, Chapter 7 presents the main conclusions and future work.

1.5 List of publications

I. M. Persson, P. Chen, O. Carlsson, ”Frequency Support by Wind Farms in Islanded Power Systems with High Wind Power Penetration,” in *PowerTech (POWERTECH), 2013 IEEE Grenoble*, pp. 1-6, June 16, 2013.

II. B. Motamed, P. Chen, M. Persson, ”Comparison of Primary Frequency Support Methods for Wind Turbines,” in *PowerTech (POWERTECH), 2013 IEEE Grenoble*, pp. 1-5, June 16 2013.

The author has also contributed to the following publications not included in the thesis.

1. M. Persson, ”Flicker evaluation of 45 kW WindEN turbine,” at *Chalmers University of Technology*, Göteborg,2013.
2. M. Persson, T. Thiringer ,W. Baig, ”Measurements and Modeling of three and five-limbed Transformer Behavior During Large Voltage and Frequency Disturbances”, submitted to *IET Generation, Distribution and transmission*, jan, 2015.

Chapter 2

Frequency and wind power

2.1 Introduction

The Nordic power system bases its power production on several renewable generation sources mainly hydro. Base power demand in Sweden and Finland is to great extent covered by nuclear while Norway main source is hydro production. Denmark's base power comes from thermal units, distributed or centralized. Denmark is however split in two areas electrically, DK2 connected to NPS while DK1 is connected to Continental Europe (CE). Several HVDC interconnections connect NPS to CE but also interconnect Sweden to Finland to increase the transfer capacities between the countries.

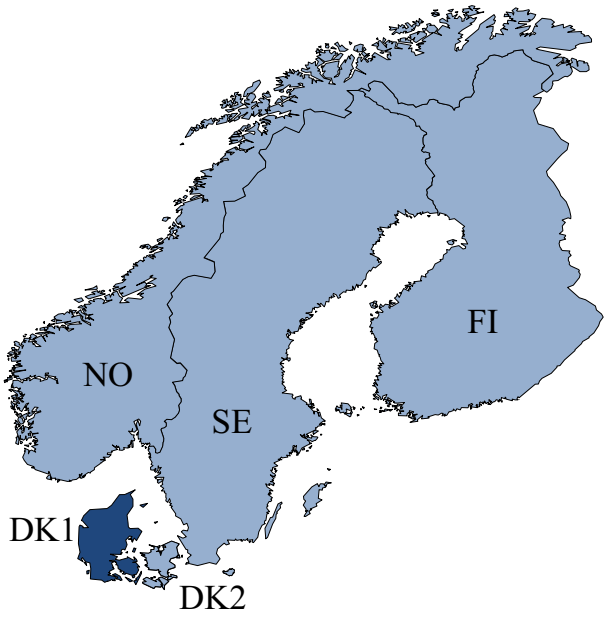

Figure 2.1: A sketch representing the Nordic synchronous area as well as DK1.

Considering the installed capacity of the countries in the NPS the different sources of electricity

can be shown in Table 2.1. It should be noted that this contains reserve generators and that the wind does not produce at rated capacity all the time. However, as a goal of the European region to increase their renewable several countries will introduce more wind power in the future thus reducing operational capacities in mainly thermal units.

TABLE 2.1: Generation mix capacity in the Nordic power system by the end of 2012 in accordance with [23],[24], [25]

Type of generation	DK2 [MW]	FI [MW]	NO [MW]	SE [MW]	Total [MW]	Total [%]
Nuclear power	0	2732	0	9363	12095	13
Thermal power	3361	11051	1108	8018	23538	26
Hydro power	0	3164	30700	16203	50067	55
Wind power	957	286	704	3745	5692	6
Solar power	0	0	0	24	24	0
Total [MW]	4318	17233	32512	37353	91416	100

These generation units are scheduled in the market in accordance with the Nord Pool Spot and it hourly clearing of energy from each unit. There is also a reserve market in order to handle system imbalances that might occur during the different operational hours of the NPS. The services and their response time and terminology are further discussed in section 2.2.

2.2 Frequency regulation

Considering Table 2.1 the main contribution of the frequency control in the NPS has been provided by the hydro governors and non-nuclear thermal units. The behavior of these sources though stable is relatively slow when compared to the control of VSWT. To consider a future scenario with high penetration of wind turbines it is important to consider the work already performed in countries with high levels of these intermittent sources. Different countries legislation on frequency control when dealing with large amounts of intermittent power production is of interest to detect control settings, restriction in connection and demanded performance put on generators.

2.2.1 Terminology

Grid codes on frequency reserves has been evaluated continuously as the system integrates more countries, new services and products and thoughts of joint markets even between synchronous areas. In order to clarify and reduce the risk of misapprehension of results the terminology used by the North American Electric Reliability Corporation (NERC), the ENTSO-E and the previous and current Nordic TSO's are presented in Figure 2.2.

NERC	ENTSO-E	Previous Nordic Terminology	New Nordic Terminology
Primary Reserve	Frequency Containment Reserve (FCR)	Frequency Controlled Normal Operation Reserve (FNR)	Frequency Containment Reserve for Normal Operation (FCR-N)
		Frequency Controlled Disturbance Reserve (FDR)	Frequency Containment Reserve for Disturbances (FCR-D)
Secondary Reserve/AGC control	Frequency Restoration Reserve (FRR)	Manual reserve	Automatic Frequency Restoration Reserve (FRR-A), Manual Frequency Restoration Reserve (FRR-M)
Tertiary Reserve	Replacement Reserve (RR)		

Figure 2.2: The terminology used in power systems related to frequency controlling reserves [26], [27], [28], [29].

The time for and speed of the different frequency regulation services are presented in Figure 2.3 for a generation trip in a fictitious power system with the Nordic reserve terminology.

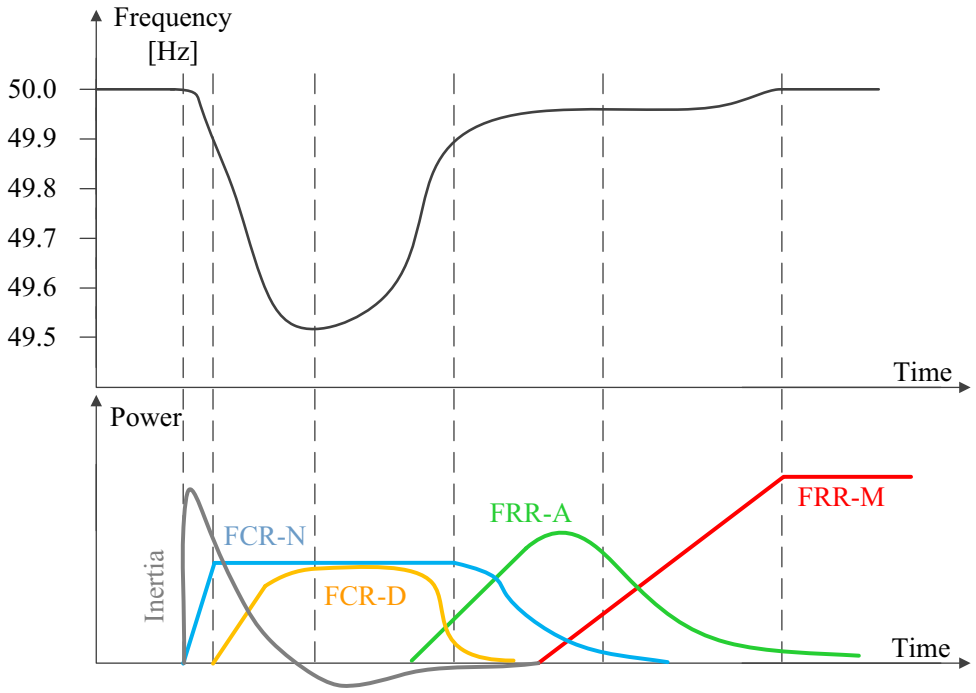

Figure 2.3: A sketch representing frequency regulation support strategies during a fictive frequency dip in the Nordic power system.

In Figure 2.3 the different activation of frequency regulation services are presented. Firstly the inertia response covers the loss of generation. Secondly the FCR is activated to balance the disturbance and once the frequency passes 49.9 Hz the FDR is also activated. The inertia being an inherent behavior of directly coupled generators while FCR-N and FCR-D are automatic reserves provided by assigned generators. These are then balanced by the FRR whose responsibility is to manually or automatically balance out the reserve used so that the power system can be ready for a new disturbance within 15 minutes.

2.2.2 Inertia

The inertia is provided only by directly coupled generators and is an inherent kinetic energy released immediately after a load imbalance. The initial reaction of inertia initially solely depends on the distance to the disturbance while after a while the individual inertia constant of the generators is the deciding factor of the speed decrease (see section 2.3).

TABLE 2.2: Typical inertia constants of generation units [30], [31].

Type of generation	H
Nuclear power unit	5-8 s
Other Thermal unit	2-7 s
Hydro unit	2-4 s
Wind turbine	2.4-6 s

Even though FPC-WT and DFIG units do not provide inertia they can provide, through control, a similar product called. Synthetic inertia, virtual inertia, inertia emulation. All in various ways trying to utilize the rotating mass in order to provide short support fast from VSWT with an added control loop. For more information see Chapter 6.

2.2.3 Frequency containment reserves (FCR)

The bids for these services are continuously updated or specified throughout the year and updated for every hour at Elbas.

TABLE 2.3: Various FCR properties in the different synchronous areas [28].

Property	CE	GB	IRE	NPS
Accuracy of measurement	>10 mHz	>10 mHz	>10 mHz	>10 mHz
FCR Activation delay (incl. dead band)	10 mHz	15 mHz	15 mHz	10 mHz
FCR Activation time to full	30 s	10 s	15 s	30 s [1]
FCR Full activation deviation	± 200 mHz	± 500 mHz	± 500 mHz [2], ±1000 mHz [3]	± 500 mHz

[1] If f_{sys} is outside standard frequency range of ±100 mHz.
[2] Valid for dynamic FCR, from HVDC inter connectors [32].
[3] Valid for static FCR.

However in the Nordic region the reserves have long time been divided into a specific type for the continuous operation and a specific one designed to handle bigger disturbances.

The Frequency Containment Reserve - Normal Operation (FCR-N)

The Frequency Containment Reserve - Normal Operation (FCR-N), is the power available to control the frequency in the Nordic system within its standard frequency range ($\pm$100 mHz) [27], [28] and is automatically activated by deviations in the power system frequency. If a step wise change of the frequency occur from 50 - 49.9 Hz it must be activated to 63 % within 60 seconds and to 100 % within 3 minutes [26]. 600 MW should be available at 50 Hz.

The Frequency Containment Reserve - Disturbed Operation (FCR-D)

The Frequency Containment Reserve - Disturbed Operation (FCR-D), is the power available for frequency regulation within the area of 49.9 - 49.5 Hz. It also is automatically activated by deviations in the power system frequency. If a step wise change of the frequency occur from 49.9 - 49.5 Hz it must be activated to 50 % within 5 seconds and to 100 % within 30 seconds [26].

2.2.4 Frequency restoration reserves (FRR)

Automatic and manual reserve that has the objective to regulate the balance in the Nordic power system. It is hence also used in order to reset the FCR [26].

The Frequency Restoration Reserves - Automatic (FRR-A)

The Frequency Restoration Reserves - Automatic (FRR-A) started as a solution to the increasing frequency deviations in the NPS in the beginning of 2013 with a capacity of 100 MW. It is an automatic reserve with the objective of restoring the system frequency to 50 Hz. The FRR-A scheduled from hydro in the NPS has to act within 30 seconds and produce full output power after 120 seconds. The support should be provided stepwise in steps of 5 MW. For the thermal units active in the FRR-A they should act according to the transfer function (2.1) below;

$$P_{th} = \frac{1}{(1 + sT_{th})^4} \tag{2.1}$$

where T_{th} is the time constant/activation time of the unit set to maximum 35 s and P_{th} is the power output after a set point shift. The set points are set by the TSO after monitoring the frequency and converting it to the required power in MW needed. The signals are then spread out to the providers of the FRR-A services who then distribute the set points to their own units. The update setting needs to be less than 10 seconds in order to act as reserve providers in all stages of the communication [26], [28],[33].

The Frequency Restoration Reserves - Manual (FRR-M)

Used in order to replace the FCR and the FRR-A and to bring the frequency back to 50 Hz. Manually regulated by the TSOs. The reserve can also be used in order to de-load transmission lines close to their thermal overloading limits or to increase head room in the power system [26]. The minimum bid size is 10 MW and should be activated fully within 15 minutes [26],[27].

2.3 Frequency stability in power systems

Definition:

Power system stability is the ability of an electric power system, for a given initial operating condition, to regain a state of operating equilibrium after being subjected to a physical disturbance, with most system variables bounded so that practically the entire system remains intact [34].

For the sake of wind power integration it is considered less of a necessity to consider the small-signal stability of the system for even islanded systems as shown in [35], [36].

In order to understand what happens during a disturbance causing a power imbalance, a simplified system is considered. Two identical generation units connected at the same busbar transfer power to an infinite bus via a transmission line, as can be seen in Figure 2.4. The disturbance is considered when one of the generators is disconnected. The descriptions and figures are based on [37] mainly p. 351-363.

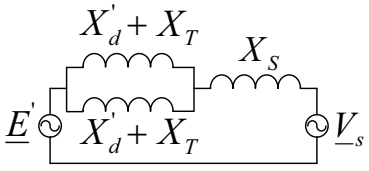

Figure 2.4: Equivalent circuit of two parallel generators connected to an infinite busbar through a transmission line.

Where $\underline{E'}$ is the transient back-emf of the generator and $\underline{V_s}$ is the voltage at the infinite bus. X'_d is the generator transient reactance, X_T, the transformer reactance and X_s is the system reactance.

1. Rotor swings in the generators (first few seconds)

   Disconnection of one of the two generators cause two effects. Firstly, the equivalent reactance increases thus lowering the power-angle characteristics from the generators to the infinite bus in accordance with 2.2.

$$P_-(\delta'_0) = \frac{E'V_s}{\frac{X'_d+X_T}{2} + X_s} sin(\delta'_0) \quad , \quad P_+(\delta'_0) = \frac{E'V_s}{X'_d + X_T + X_s} sin(\delta'_0) \tag{2.2}$$

Where $P_{-}(\delta'_0)$ and $P_{+}(\delta'_0)$ is the power-angular characteristic of the system prior and after the disconnection of the generator respectively.

Secondly, the mechanical power delivered to the system is reduced by half. This due to the loss of the other generator unit, assuming equal size, thus $P_{m+} = 0.5P_{m-}$. Figure 2.5 shows the implication of equal-area-criterion on this power imbalance. Where ΔP_0 is the power lost due to the generator disconnection and ΔP_{r1} is the initial power burst of kinetic energy provided by the closest still connected generator, ΔP_{s1} is the kinetic energy from other generators in the system behind the infinite bus.

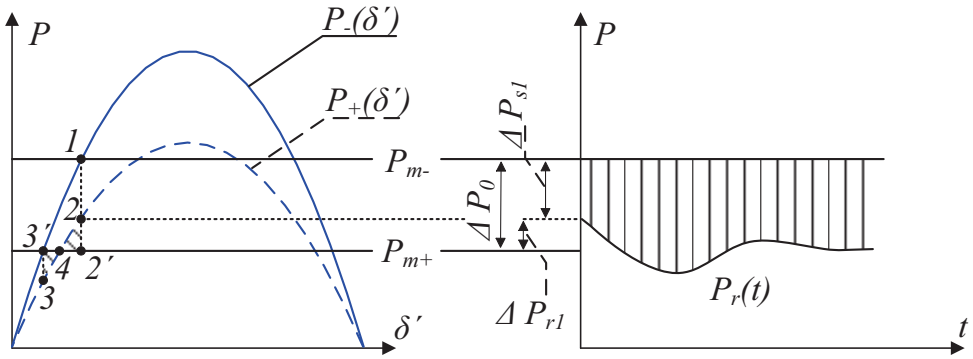

Figure 2.5: Rotor swing during first stage of dynamics in accordance with equal area criterion. Power on y-axis indicating the transfer from $\underline{E'}$ to $\underline{V_s}$ [37].

The rotor angle of the remaining generator cannot change instantaneously, thus the abundance of electrical power (compared to mechanical power delivered by the prime mover). This occurs at location 2, thus causing the de-acceleration of the rotor corresponding to the area $2 - 2' - 4$. The momentum causes the rotation to pass location 4 and stops at location 3 when the de-acceleration area is equal to that of the acceleration area (of $4 - 3 - 3'$). The damping torque[1]then cause the oscillations to decrease to location 4. The amplitude of ΔP_{r1} depends on the amount of lost generation that it covers immediately after the disconnection of the nearby generator. This amount of power depends on the system equivalent reactance in accordance with 2.3.

$$\frac{\Delta P_{r1}}{\Delta P_{s1}} = \frac{X_s}{X'_d + X_T} \tag{2.3}$$

Even though (2.3) here is considered for parallel generating units a similar expression can be obtained for the multi-machine case. The conclusion of (2.3) being that the share of any generator in meeting a power imbalance depends on its electrical distance, X_s representing the distance to other generation and X'_d + X_T is the distance to the unit remaining in operation at the same bus, as the one of the two parallel generators discussed here.

[1]For more information regarding damping torque see p. 202-206 in [37].

However, assuming that the contribution from the contributing generators to the inertia response are equal to:

$$P_{inertia-r} = 2H_r f_r \frac{df_r}{dt} \tag{2.4}$$

and

$$P_{inertia-s} = 2H_s f_s \frac{df_s}{dt} \tag{2.5}$$

Where H_s and H_r are the inertia constants of the two generators and S_s and S_r are the rating of them . Combining these two with 2.3 the following expression can be derived assuming the initial frequency (f_{s0} = f_{r0} = f_0) is the same in steady state at the both locations.

$$\frac{\frac{df_1}{dt}}{\frac{df_2}{dt}} = \frac{X_s}{X'_d + X_T} \frac{H_s S_s}{H_r S_r} \tag{2.6}$$

Equation 2.6 is only valid at the instant of where the frequency starts to fall representing the local phenomena close to the generator being disconnected to have a steeper derivative than that further away. For more information and results from real measurements see Section 3.4.1.

2. Frequency drop (a few seconds to several seconds). The share of any generator in meeting the power imbalance depends solely on its inertia, and not on its electrical distance. After a few rotor swings, all generators will slow down at the same rate assuming they remain in synchronism. Here the share of the generators interaction towards the system imbalance is solely based on the inertia of each generator. This may be written as:

$$\frac{d\Delta\omega_1}{dt} \approx \frac{d\Delta\omega_2}{dt} \approx ... \approx \frac{d\Delta\omega_N}{dt} = a \tag{2.7}$$

where $\Delta\omega_i$ is the speed deviation of the i^{th} generator, N is the number of generators and a is the average acceleration.

Considering the famous swing equation:

$$2H\frac{d^2\delta}{dt^2} = P_m - P_e - P_D = P_{acc} \tag{2.8}$$

In accordance with [37], assuming a non frequency dependent load, the equations can be rewritten and combined to:

$$\Delta P_i = 2Ha = \frac{H_i}{\sum_{k=1}^{N} H_k} \Delta P_0 \tag{2.9}$$

Where it can be observed that the i:th generator contribution P_i to the disturbance ΔP_0 is a main function of the ratio of inertia of itself and surrounding generators.

3. Primary control by the turbine governor system (several seconds)

   During this stage the frequency variations mainly depend on the settings and loadings of the turbine and its governors but also the frequency dependence of the load, assuming that the voltage is constant. Assuming a linear approximation of the loads frequency dependence the operating frequency can be determined by the intersection of the following equations:

$$P_T = P_{T0} + \Delta P_T = P_{T0} - K_T \Delta f \frac{P_{T0}}{f_n} \tag{2.10}$$

$$P_L = P_{L0} + \Delta P_L = P_{L0} - K_L \Delta f \frac{P_{L0}}{f_n} \tag{2.11}$$

where, P_T is the generation characteristics , P_{T0} is the pre-disturbance power output, K_T is the reciprocal of droop for the total system generation characteristic. P_L is the load characteristics,P_{L0} is the pre-disturbance power demand ,K_L is the frequency sensitivity characteristics of the load (active power). These typical load and generation patterns are presented in Figure 2.6. Here P_{T-} and P_{T+} are the pre-disturbance and post-disturbance static characteristics of the turbine system.

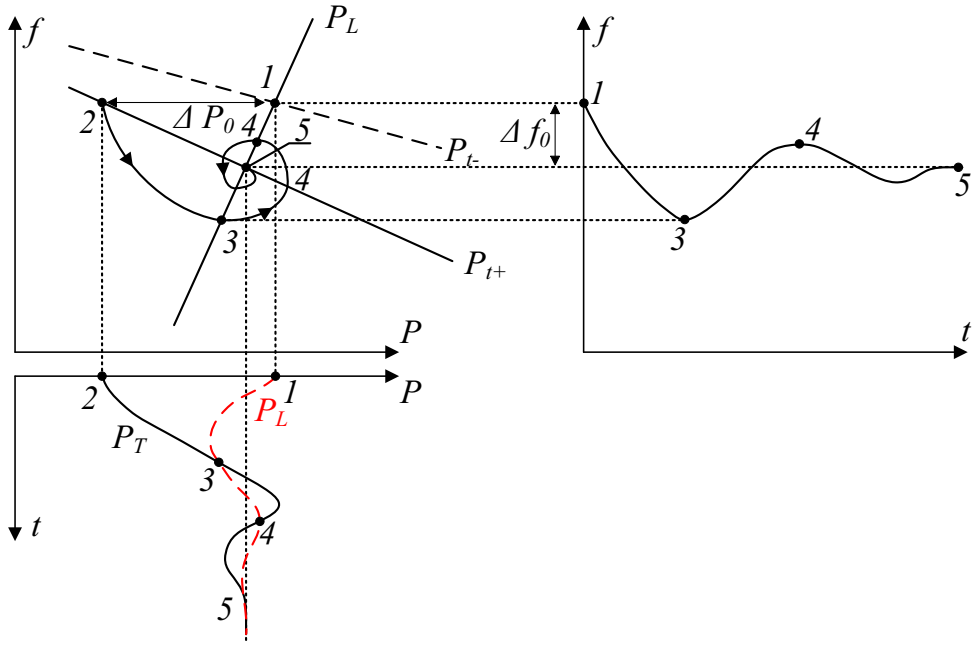

Figure 2.6: Primary control after initial stages of frequency variations [37].

In Figure 2.6 the generation is disconnected at location 1, changing the generation operating point (while rotor swings) to location 2. The generator then tends to move towards

location 5 the intersection between the load and new generation characteristics. However, due to time delays in the governors leaving location 2 the trajectory is below that of P_{T+}. At location 3 however load and generation match but due to the inertia and time delays the power keeps increasing further increasing the frequency. This continues until location 4 where a new equilibrium can be found causing a new local maximum in the frequency. These oscillations are eventually removed and the steady state deviation occurs at location 5. The value of the final frequency can be determined by:

$$\frac{\Delta f_5}{f_n} = \frac{-1}{K_T + K_L} \frac{\Delta P_0}{P_L} \tag{2.12}$$

4. Secondary control by central regulators After the stages of initial stages of the frequency deviation it is time for the TSO to cover the imbalance in frequency still available or/and to replace the reserves currently active in the system. This is commonly done by either AGC or Load-frequency control (LFC) or a manual reserve or replacement reserve (as specified in Section 2.2.1). This in order to balance out the system to be ready for the next disturbance.

   The power system support functions try to maintain the system frequency stability. The frequency deviations might however occur, especially with reduced system inertia. Generators are enforced through legislation (grid codes) to handle these variations and still stay connected in order not to worsen a already dire situation by tripping. These laws of the power system will be studied further in 2.4 for the countries able to reach the highest levels of instantaneous penetration of wind.

2.4 Grid code evaluation

The various synchronous areas each have their grid codes on generators enforcing their connection to the grid during power imbalances. Individual countries can still enforce stricter regulation if deemed necessary. Spain and Portugal seem to rely mainly on the ENTSO-E grid code for their grid code content.

TABLE 2.4: Wind power penetration in Europe, 2012 [38].

Country	Wind power penetration [%]
Denmark	27
Portugal	17
Spain	16
Ireland	13
Germany	11

The grid codes of these countries are then of interest in order to evaluate the need or regulation put on a future frequency responding VSWT. The grid codes also present minimum values of frequency in order to not loose generation units.

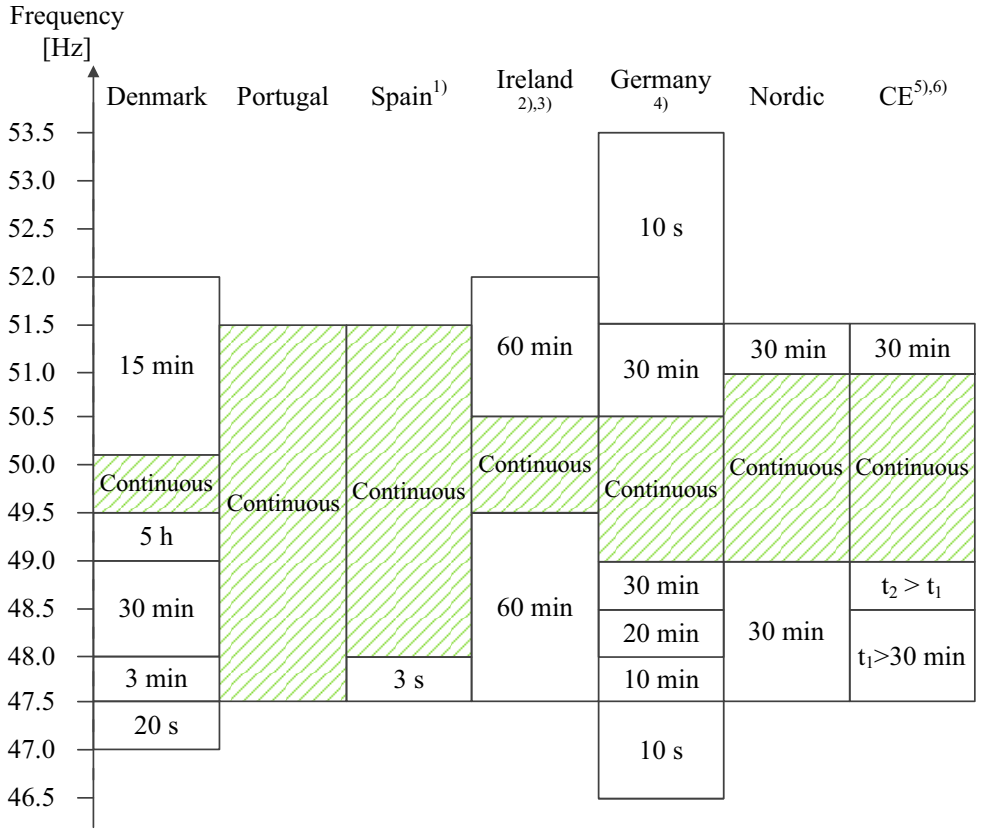

Figure 2.7: Grid code related to frequency deviations of countries with high WPR in Europe in accordance with: [39],[40],[41],[42],[43],[44],[27],[45].

It is interesting to note that Denmark having large levels of WPR have a very detailed grid code, but demand a shorter duration of over frequency connection from wind generators. Probably due to the ease of shutting down wind turbines but also as a direct result of distributed thermal units that are less stable during over frequency events. In addition the E.ON Netz grid code provides a more detailed grid code than for example the current Nordic grid code. Most probably due to the lack of wind power in the NPS. The Irish grid code forces its generators to be connected for a long time but is also a continuously updated grid code also containing demands on handling steep ROCOFs during disturbances, mainly due to their instantaneous wind penetration ratio that lowers the inertia in the system further increasing the steepness of the frequency derivative.

[1]Spanish grid code enforces generators to be able to handle instantaneous frequencies below 47.5 Hz.

[2]Irish grid code also states that no new wind generation is allowed to start if f >50.2 Hz.

[3]Irish grid code enforces generators to be able to handle ROCOF levels of 0.5 Hz/s.

[4]The added constraints of E.ON Netz offshore grid code for wind farms, covers $51.5 < f < 53.5$ Hz and $46.5 < f < 47.5$ Hz.

[5]Continental Europe allows the TSO to decide the time of duration (t_1) between $47.5 < f < 49.0$ Hz as long as it is at least 30 min.

[6]Continental Europe allows the TSO to decide the time of duration (t_2) between $49.0 < f < 49.9$ Hz as long as it is longer than t_1.

Chapter 3

Frequency characteristics of Nordic power system

The Nordic power system (NPS)(NO, DK2, SE and FI) dominated by hydro and nuclear units (the latter not providing frequency regulating services), is still looking to increase its share of wind production units. This is done in order to cover the production deficit from decommissioned old reactors and to reduce the impact on global warming. The increase of this converter interfaced generation sources will put additional strains on the frequency regulation by the TSOs of the NPS. A regulation that is already strained according to [33]. It can also be seen that the lack of power system inertia due to higher penetrations of converter interfaced generation can cause dangerous levels of rate of change of frequency (ROCOF) during big disturbances [46]. To combat the increasing frequency deviations and to improve the frequency quality the TSO's in the NPS implemented an automatic frequency responding reserve (FRR-A) of initially 100 MW in 2013 and later increased to 300 MW by the autumn of 2013 since the initial capacity was deemed too small. Frequency data have previously been studied in [14] [15] for the power system in the Nordic region. [15] uses a down sampled 50 Hz data (to 10 Hz), but no context has been described to the need of the quality of the measurements with respect to its sampling frequency nor any consideration to the ROCOF. Still a lot of data has been presented showing deterioration from 2005-2009. [46] uses a measuring window of 500 ms in order to evaluate the systems dynamics but still remove short term transients.

This section is aimed at providing knowledge to the use of PMU measurements for frequency quality evaluation through the examination of frequency data from 2006, 2012 and 2013 in the NPS. Furthermore the impact of the FRR-A and its various capacities will be investigated as well as an overview of current issues and reasons for the poor frequency quality in the NPS. Finally the effect of increasing the wind penetration ratio in a future NPS and its impact on the frequency quality will be addressed.

3.1 Implications of poor frequency quality

This section is meant to describe different consequences caused by poor frequency quality in a power system that can be found in existing literature. The focus is on frequency quality since a poor such parameter indicate long occasions outside of operation rage for a power system.

Steam turbines

Used in various types of converting steam to electric power generation is a man contributor to power generation in for example the USA [47]. The blades of a steam turbine has several natural frequencies associated with higher mechanical stresses, deviation in frequency thus forces the turbine of its rated speed and closer to these hazardous regions of operation. The damage to the system is not instant but rather cumulative in its nature. Turbine manufacturers try to avoid placing their resonance frequencies close to rated operation, it is typically not a concern unless the frequency deviates more than 5 %. Under frequency events are however more stressful since a unit at the rated output can not increase its production in order to help with the frequency deviation. [48],[49]

Flux density

Some of the main components of a power system such as the generators and transformers are based on magnetic material, which are sensitive to the flux density passing through them. V/f is directly proportional to flux density; thus under frequency might cause saturation of magnetic material causing heating in generators and transformers, perhaps even tripping due to overheating. In components with magnetic cores the flux density corresponding to V/f is a sever factor proportional to heat losses and cause of saturation of the magnetic core. In an already constrained power system it is likely that transformers are pushed towards its limits, this in combination with a under frequency event could cause the transformer to saturate. This in turn forcing more magnetizing current to be drawn which might trip over current protection or breakers further worsening the situation [48],[50]. Certain over-excitation relays are common to try to act to not just frequency but the perhaps devastating combination of low frequency and high voltage.

Auxiliary systems

In most plants the auxiliary systems providing essential cooling, feeding of boilers and fans for combustion air etc. are commonly coupled with induction machines (IM). These IM would during an under frequency event reduce their performance when the frequency drops. This can cause low flow of coolant relays to trip in for example nuclear power plants, especially in combination with slightly saturated transformers further up in the system. Over heating could also cause tripping of other generators/appliances in the grid [51].

Governor stress

During frequency variation above and below the dead bands for governors, the prime movers of assigned generation units are controlled with frequency regulation. These actions cause wear and tear on the units, especially if they occur often and rapidly [52].

Industrial load impacts

Most industrial processes that are sensitive to frequency variations usually have variable frequency drives as a separation stage in between the grid and a sensitive appliance, these drives are usually insensitive to frequency disturbances. Many electronic loads convert their AC source to DC and are therefore unaffected to $\pm$ 5 % frequency change [48].

Load shedding

The Nordic Grid Code, specifies the different stages of automatic frequency controlled load shedding that will occur if the reserves are depleted and the frequency keeps falling below 49.0 Hz [27].

TABLE 3.1: Load shedding in the Nordic power system [27].

Country	Action at frequency level
DK2	10 % of consump. if f <48.5 Hz momentary or f <48.7 Hz for 20 s.
	10 % of consump. if f <48.3 Hz momentary or f <48.5 Hz for 20 s.
	10 % of consump. if f <48.1 Hz momentary or f <48.3 Hz for 20 s.
	10 % of consump. if f <47.9 Hz momentary or f <48.1 Hz for 20 s.
	10 % of consump. if f <47.7 Hz momentary or f <47.9 Hz for 20 s.
NO	7000 MW (during peak load) in stages from 49.0 to 47.0 Hz
SE [1]	Electrical boilers and heat pumps
	P = 35 MW. if f <49.4 for 0.15 s
	35 >P >25 MW if f <49.3 Hz for 0.15 s
	25 >P >15 MW if f <49.2 Hz for 0.15 s
	15 >P >5 MW if f <49.1 Hz for 0.15 s
	30 % of consumption in 5 stages
	Stage 1: f <48.8 Hz for 0.15 s
	Stage 2: f <48.6 Hz for 0.15 s
	Stage 3: f <48.4 Hz for 0.15 s
	Stage 4: f <48.2 Hz for 0.15 s OR f <48.6 Hz for 15 s
	Stage 5: f <48.0 Hz for 0.15 s OR f <48.4 Hz for 20 s
FI	10 % of consump. if f <48.5 Hz 0.15 s. f <48.7 Hz 20 s
	10 % of consump. if f <48.3 Hz 0.15 s. f <48.5 Hz 20 s

In 3.1 one can observe that the NPS considers both long term deviations (20 s for DK2) and shorter for temporary frequency durations (stage 4-5 for the SE region).

[1] South of cross section 2, location between Gävle and Hudiksvall, see page 32 of [27].

For the Central European synchronous system a more general load shedding scheme is recommended.

TABLE 3.2: Load shedding recommendation by ENTSO-E for the Central European synchronous system [30].

Frequency	Amount of load [%]
49.0	10-20
48.7	10-15
48.5	10-15

Generator protection

In order to keep distributed generation (DG) from running in island operation after system separation, generators are equipped with anti-islanding protection. This disconnects the DG usually based on either phase-shift or ROCOF-relays. The ROCOF relays have been shown to perform better during loss of mains, especially when subjected to network disturbances [53],[54]. High levels of ROCOF in combinations with improper or outdated settings can thus cause disconnection of generation during an under frequency event further worsening the situation.

3.1.1 Grid codes on ROCOF

In the Swedish grid code considering the connection of larger production units ”Anslutning av Större Produktions anläggning” (ASP) of sizes above 25 MW the ROCOF limit is set to 0.1 Hz/s. This has however been seen as a too tight setting since the rate of change in the Nordel system has been exceeding this value at least 4 times during 2004-09-30 - 2005-11-04 when disconnection of production sources occurred for different reasons. The frequency data of these measurements are from a PMU unit with a time window of 150 ms. During blackout scenarios the ROCOF has reached several Hz/s such as during the Swedish blackout of 1983 [55], [56], [57].

System operator of Northern Ireland (SONI) expect conventional generators to be capable of handling ROCOF events greater than 1 Hz/s. SONI expects according to their Minimum Functional Specification (MFS) to connected generators to apply to a ROCOF value of 1.5 Hz/s. However the current grid code states a ROCOF limit to 0.5 Hz/s to which generators need to stay synchronized. The text does however reflect on the possibilities to handle ROCOF levels up to 4 Hz/s [58]. The article also argues for the unification of agreement of ROCOF Measurements and definition. It concludes that the TSO’s consider 500 ms as an appropriate time frame to calculate ROCOF. A measurement window of 1 ms would result in a far steeper ROCOF even though it is unclear how that high sampling rate can be obtained.

3.2 Sampling frequency implications

3.2.1 On frequency duration evaluations

PMU measurements are usually sampled at 50 Hz sampling rate. This in turn results in large quantities of data that have to be processed in order to evaluate the frequency quality of a power system. This subsection aims to evaluate the impact that the sampling frequency has on the results of frequency quality.

The 50 Hz data are down scaled using a moving average window of sizes in accordance with Table 3.3.

TABLE 3.3: Implicit sampling frequency of PMU-data.

Case	Sampling Time	Implicative Sampling Frequency f_{is}	Averaged number of samples
1	20 ms	50 Hz	1
2	100 ms	10 Hz	5
3	200 ms	5 Hz	10
4	500 ms	2 Hz	25
5	1 s	1 Hz	50
6	2 s	0.5 Hz	100
7	5 s	0.2 Hz	250

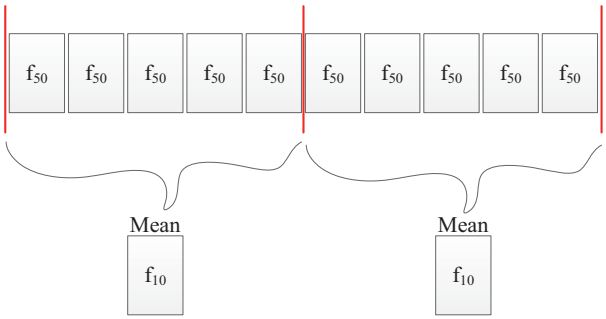

Figure 3.1: Moving average window used in order to re-sample the 50 Hz PMU-data to a new implicit sampling frequency, f_{is}.

The data set of 2013 was subjected to the moving average algorithm in Figure 3.1 and the duration for the frequency to deviate under 49.9 Hz was then computed and evaluated for the different f_{is} of Table 3.3. The result is presented in Figure 3.2 and Figure 3.3 below. The error due to the implicit sampling frequency is calculated as per 3.1.

$$Error_{f<49.9Hz}[\%] = 100\frac{Duration_{f<49.9Hz@50Hz} - Duration_{f<49.9Hz@f_{is}Hz}}{Duration_{f<49.9Hz@50Hz}} \tag{3.1}$$

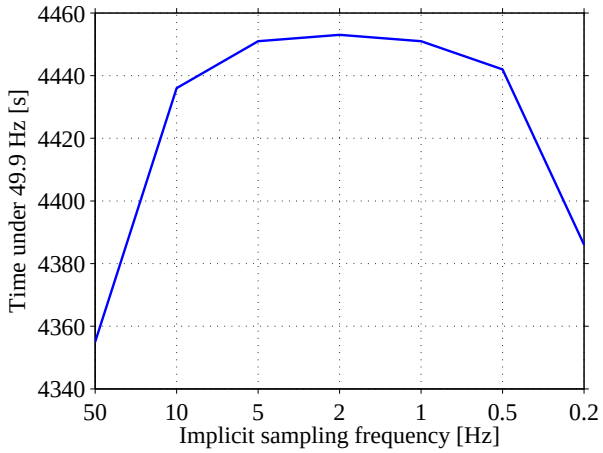

Figure 3.2: Result from alternating the implicative sampling frequency f_{is} for frequency data of 2013 based on 50 Hz data.

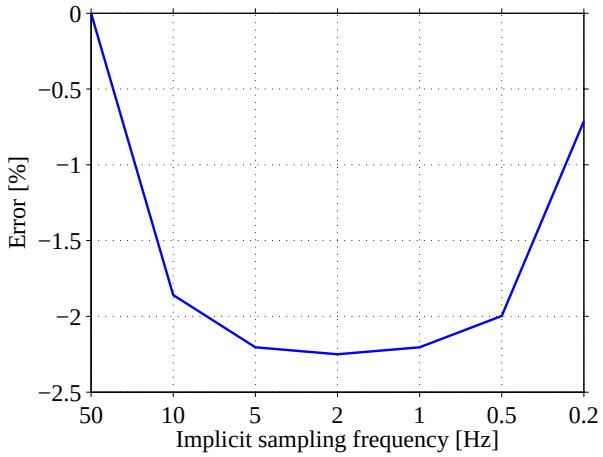

Figure 3.3: The error resulting from alternating the implicative sampling frequency f_{is} for frequency data of 2013 based on 50 Hz data.

It can be seen that the averaging of the data causes some variations, these depend on the occurrences where the frequency have some samples below 49.9 Hz in the average window but most above or vice versa. This would cause an over or under estimation on the evaluation of that specific average window. The largest error for the evaluation of various implicit sampling frequencies is about 2 %, thus for the sake of duration evaluation one can utilize any of the f_{is} without compromising the quality of the evaluation. It is possible that for shorter durations the implications of altering the implicit sampling frequency is not applicable. In [15] a sampling frequency of 50 Hz is used for the raw data, then data are sampled out of that each 100 ms (10 Hz). This seems like a reasonable choice especially if one compares large data sets. How this process of handling data impacts the result has not been investigated. The impact of transients on specific samples might cause deviations in duration evaluations over and under specific limits. Thus by chance giving more or less weight to these occurrences. By using an

implicit sampling frequency one would filter these out, neglecting them in the overall dataset.

3.2.2 On frequency nadir evaluations

In order to ensure that the temporary minimum frequency (TMF) is logged in an appropriate way to evaluate if the implicit sampling frequency has any effect on the its value, or if it causes an error to choose a rather slow sampling frequency. A random fault from January 2013 (see Figure 3.4) was chosen in order to evaluate the effect of sampling frequency on the TMF.

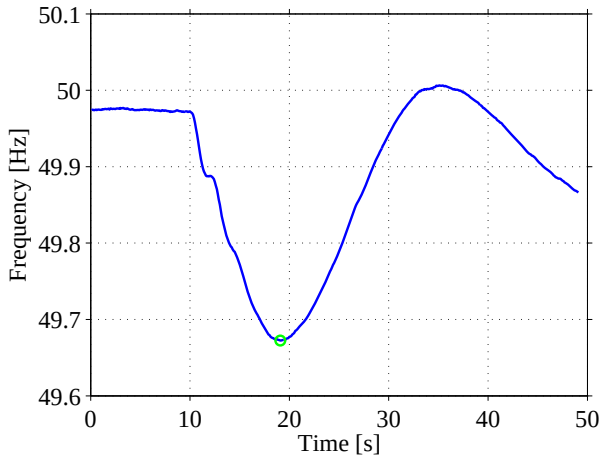

Figure 3.4: A random fault chosen for frequency nadir evaluation from January 2013, f_{is} = 10 Hz.

TABLE 3.4: Effect on frequency nadir, considering various implicit sampling frequencies.

f_{is}	50 Hz	10 Hz	5 Hz	2 Hz	1 Hz	0.5 Hz	0.2 Hz
TMF [Hz]	49.6700	49.6724	49.6727	49.6729	49.6733	49.6755	49.7098

The effect of sampling frequency is as expected not that sever as long as the data are sampled more than once every second. Beyond this point it is more random where the averaged points occur and what interval of data is covered and transformed into each new implicit sample point. However if data were picked out of raw data instead (as in [15]) this would cause a greater mismatch between the different datasets. However, for the sake of storing less data and still obtaining a good accuracy of frequency behavior even 1 Hz seems to be reasonable.

3.2.3 On ROCOF evaluations

During evaluations of the ROCOF, a single event of the data was first evaluated with respect to various implicative sampling frequencies. However it was rapidly seen that the case with f_{is} = 50 Hz had too many small random noises recorded this causes the largest ROCOF to be outside

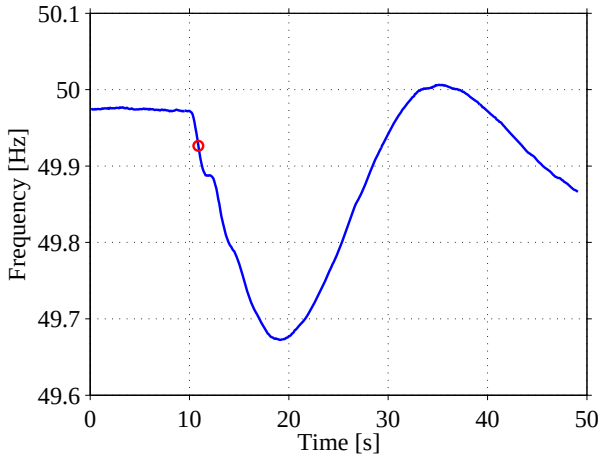

Figure 3.5: A random fault chosen for ROCOF evaluation from January 2013

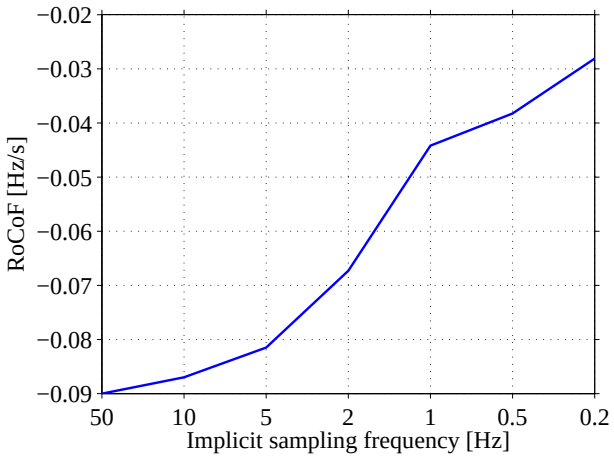

Figure 3.6: The variation in ROCOF resulting from alternating the implicative sampling frequency f_{is} for the event of January 2013 from 50 Hz - 0.2 Hz.

of the initial dip frequency deviation. Thus the value was obtained with f_{is} = 10 Hz and then analyzed at the same time stamp, but for the higher sampling frequency of 50 Hz.

From Figure 3.6 we can see the decrease of ROCOF as a function of sampling frequency. The maximum ROCOF has almost decreased 50 % when moving from a sampling frequency of 10 Hz to 1 Hz. Even though the 50 Hz and 10 Hz ROCOF are close in comparison the 10 Hz is to be considered a more suitable alternative as high frequency noises are filtered out. It is important that when considering ROCOF studies to always evaluate the time series of the event to make sure no transients or loss of data has occurred. It sould be clean as per the one in Figure 3.5 and the time stamps of the PMU-unit should also be evaluated so that no glitches are occurring in the evaluated window.

3.3 Frequency duration evaluations

In order to get an insight into how big the problem of frequency deviations are the statistics of the deviations of 2006, 2012 and 2013 has been evaluated. It is important to note the poor coverage of data from 2006, however trends can still be seen in the different data sets.

TABLE 3.5: Frequency evaluation of 2006 frequency data.

Frequency data of 2006, coverage of data = 76.0 %						
Frequency (Hz)	<49.95	<49.90	<49.85	<49.80	<49.75	<49.70
Total duration	2306944 s (640 h)	100899 s (28 h)	2674 s (45 min)	175 s	68 s	31 s
Frequency (Hz)	>50.05	>50.10	>50.15	>50.20	>50.25	>50.30
Total duration	3411051 s (948 h)	347695 s (97 h)	20084 s (335 min)	527 s	28 s	3.6 s

TABLE 3.6: Frequency evaluation of 2012 frequency data.

Frequency data of 2012, coverage of data = 93.2 %						
Frequency (Hz)	<49.95	<49.90	<49.85	<49.80	<49.75	<49.70
Total duration	3543673 s (984 h)	270727 s (75 h)	8509 s (142 min)	282 s	89 s	44 s
Frequency (Hz)	>50.05	>50.10	>50.15	>50.20	>50.25	>50.30
Total duration	3607552 s (1002 h)	374473 s (104 h)	23115 s (385 min)	1240 s	26 s	2.7 s

TABLE 3.7: Frequency evaluation of 2013 frequency data.

Frequency data of 2013, coverage of data = 91.3 %						
Frequency (Hz)	<49.95	<49.90	<49.85	<49.80	<49.75	<49.70
Total duration	3281631 s (912 h)	273127 s (76 h)	11824 s (197 min)	1030 s	235 s	119 s
Frequency (Hz)	>50.05	>50.10	>50.15	>50.20	>50.25	>50.30
Total duration	3411051 s (948 h)	347695 s (97 h)	20084 s (335 min)	527 s	28 s	3.6 s

From the data presented in Table 3.5, Table 3.6 and Table 3.7 one can see the worsening of the frequency situation from 2006 to 2012 and 2013. The worsening seems to have decreased between 2012 and 2013 considering the deviation from the frequency band of 49.9 - 50.1 Hz. This is mainly due to the introduction of a FRR-A and its response to the frequency in 2013. More about this in Section 3.3.4. There are more over frequency than under frequency occurrences throughout the evaluated periods. Seen to the extreme events such as $f > 50.30$ Hz and $f < 49.70$ Hz, the under frequency events corresponding to generator tripping are more common than the load rejections. It seems that even though frequency quality has increased from 2012

to 2013 the duration of time under 49.7 Hz has increased a lot even though FRR-A has been active through large parts of the year. Compared to previous publication [14] investigates the under frequency events and its results are evaluated for a time period of one year (April 2005 to April 2006) states a total duration of f <49.90 Hz to be 27 h (or 98709 s). [15] considers both over and under frequency studies of January 2009 to October 2009 founds that f <49.90 Hz has a total duration of 52 h while f >50.10 Hz has a total duration of 62 h. For more information see the individual publications.

3.3.1 Frequency deviations during varying load

This section intends to show when the frequency variations occur and during what loading level of the Nordic power system. Nord Pool Spot load data is used in order to evaluate the dependence of frequency variations on system load levels. Variations are then within a certain load level and hour throughout the year of 2013. The evaluation was performed with 50 Hz sampled data, deviations with durations of less than 30 s has been discarded from the plots. These smaller deviation still occurred in a similar pattern, as to those of longer duration, i.e. in the high load cases. The deviations are separated into over (>50.1 Hz) and under-frequency events (<49.9 Hz) and added together for a specific loading hour.

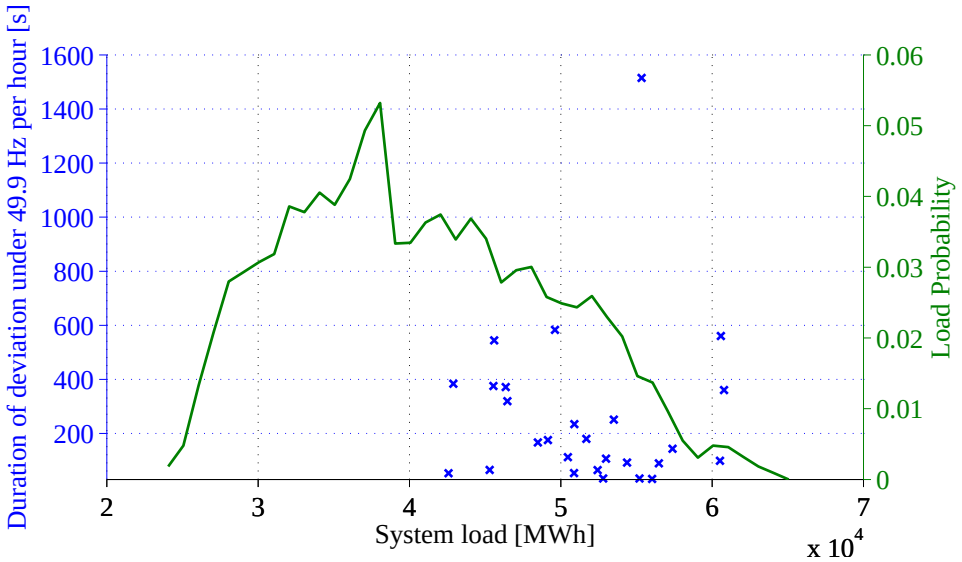

Figure 3.7: Duration of under frequency events and load probability curve of 2013.

It can be observed that at least the number of long over frequency events, in Figure 3.8, are more than the long under frequency events, in Figure 3.7. The hourly average system load is 41153 MWh. Most of the long duration events occur during high system load. The overall cumulative duration of the under frequency events are more spread out but probably concerning the tripping of large production units. It has been observed during the evaluation of the frequency data of 2013 that it on some occasions takes a long time for the steady state frequency to reach above 49.9 Hz. The load is alternating severely, seen in the spread of the empirical load

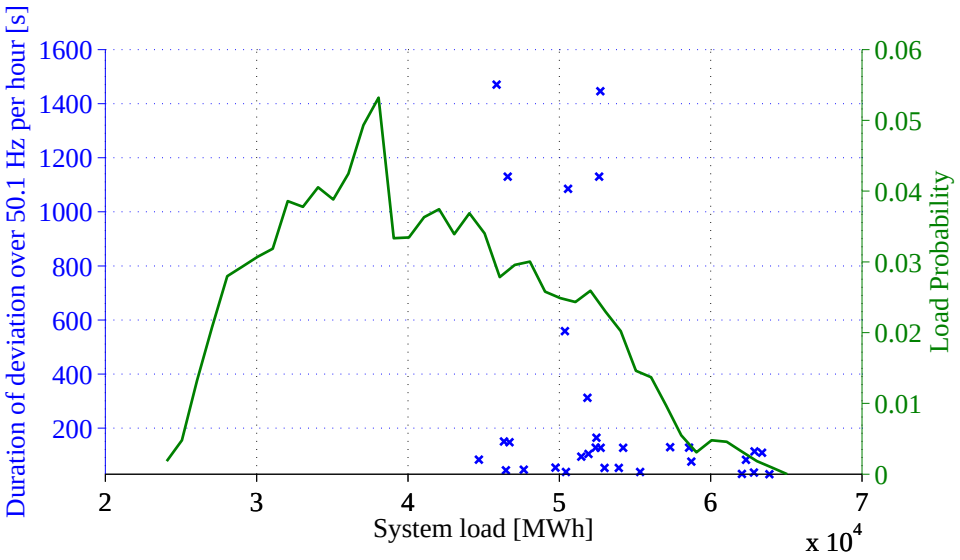

Figure 3.8: Duration of over frequency events and load probability curve of 2013.

distribution. Several interactions of high load and large frequency deviations (both over and under frequency events). No large disturbances occur during low loading conditions, at least not exceeding 30 s in duration. This might imply that loading level is not a big cause of frequency deviation, thus we turn to the load variance.

3.3.2 Hourly load variation in the Nordic power system

Since frequency is related to the balance of the load and generation it is of interest to observe the change in the load and when this occurs. This could give indications on when it is important to provide certain ancillary services or increase the bids on the frequency regulation market. Hourly data from 2013 is considered, steep derivatives imply a large need during those hours for frequency regulation.

TABLE 3.8: Hourly load data of 2013 for the Nordic power system, source: Nord Pool spot

Maximum derivative of load	5092 MWh/h
Minimum derivative of load	-3144 MWh/h
Maximum load	65248 MWh
Minimum load	24062 MWh
Average load	41153 MWh

Cumuatitive Commutativ As can be seen from Figure 3.9 the load deviations during high positive load derivatives (during morning hours) are larger than the negative derivatives (in the evening hours) seen in Figure 3.10. Maximum derivatives of 5092 MWh/h and minimum derivatives of -3144 MWh/h can been observed in Figure 3.9. The high values of positive derivatives could imply a greater need for up-regulating in the morning hours and down-regulating in the

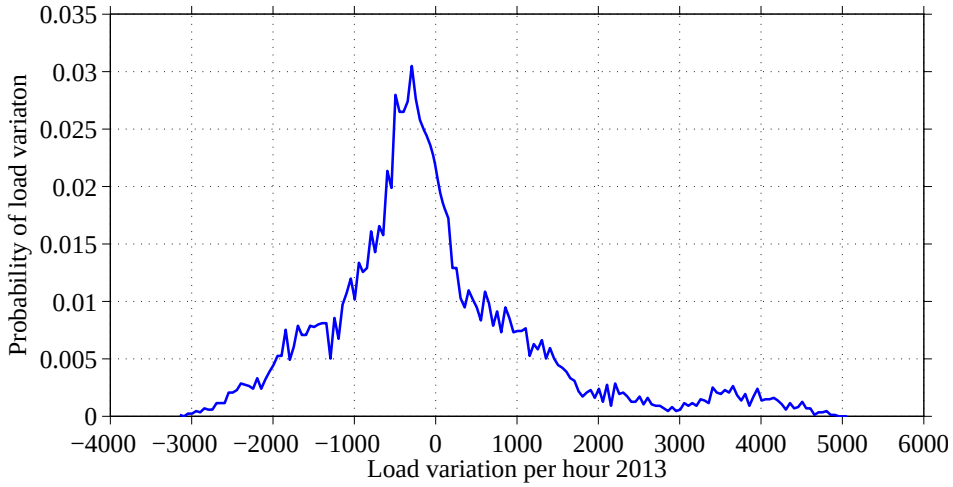

Figure 3.9: The probability of the deviation of the load in 2013.

evening. This is not necessary the case since the hourly demand does not reflect the actual one during the hour. This would imply a larger need for down-regulating in the first time of the hour and a need for up-regulation in the later part of the hour to counteract the actual load increase.

It is important to note that the need for this regulation, if needed, is not required all the year around since the load profiles vary a lot throughout the year as seen in Figure 3.10.

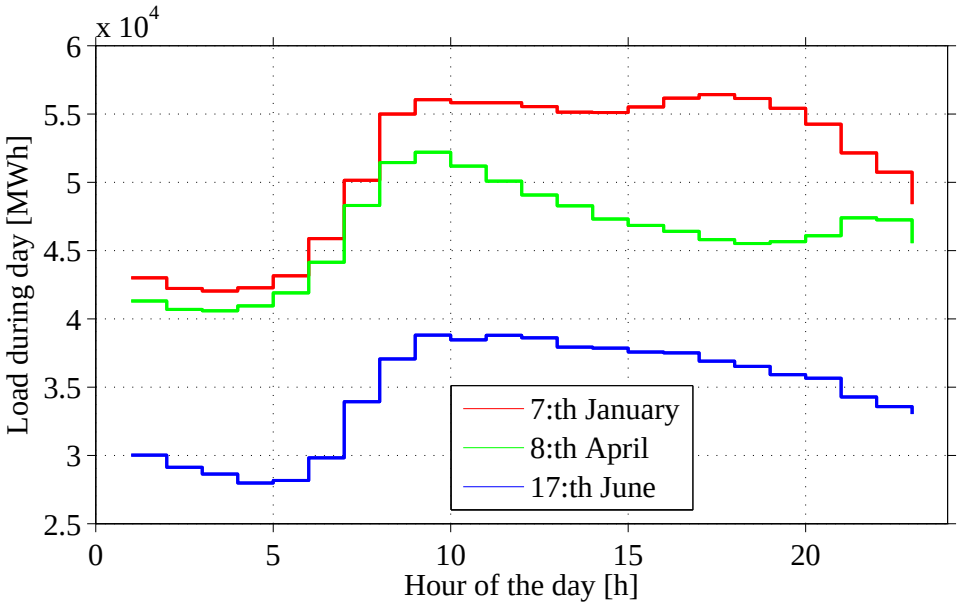

Figure 3.10: Typical load curves of the specified days of 2013, all representing Mondays.

3.3.3 Hourly frequency variations

In order to investigate when during the day the variations occur a high (January, see Figure 3.11), medium (April, see Figure 3.12) and low (June, see Figure 3.13) loading month was considered and the 50 Hz frequency data was separated into minute intervals over one day and then aggregated for the entire month. The data was then separated for over and under frequency by the limits of 50.1 Hz $>$ f and f $<$ 49.9 Hz respectively. The y-axis representing the total duration that the frequency is under (represented by negative time) or over the frequency band for that specific minute of the day for one month. In addition, the common vacation month of July was considered, and can be seen in Figure 3.14.

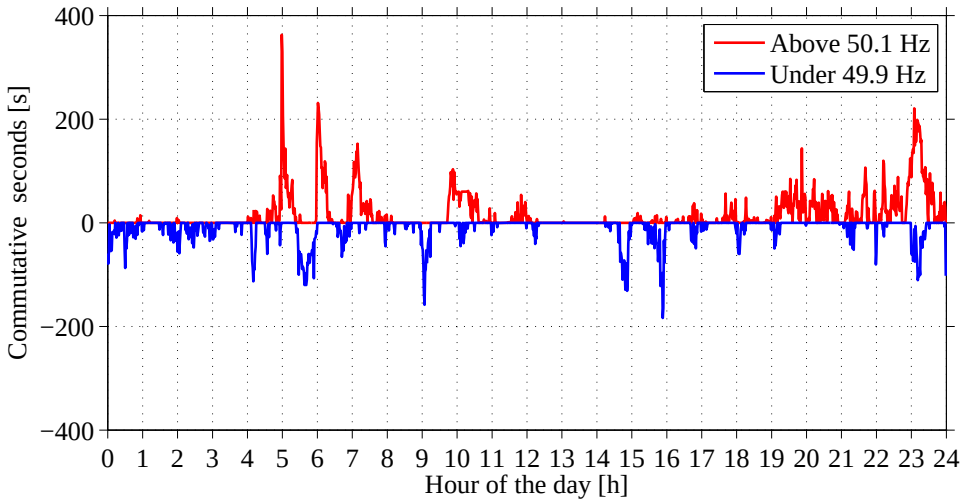

Figure 3.11: The minute-by-minute allocation of under and over frequency of January 2013 over the 24 hours of an aggregated day.

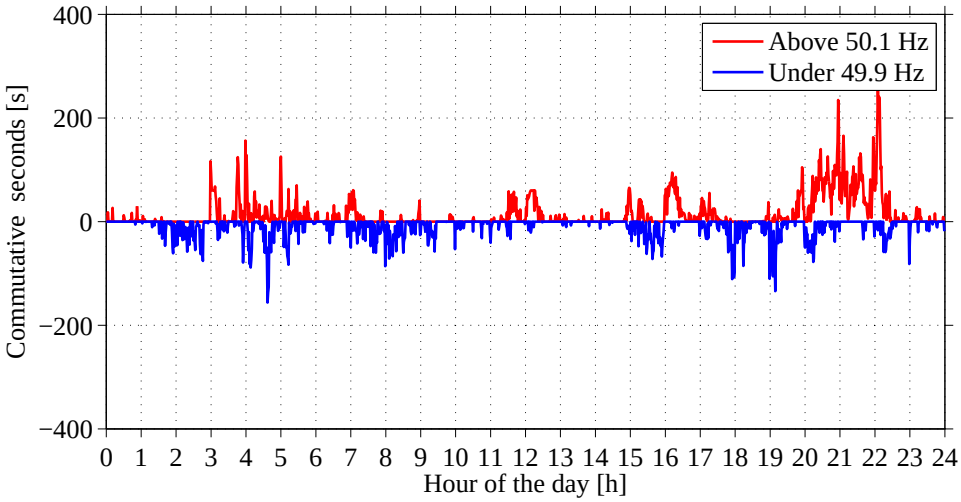

Figure 3.12: The minute-by-minute allocation of under and over frequency of April 2013 over the 24 hours of an aggregated day.

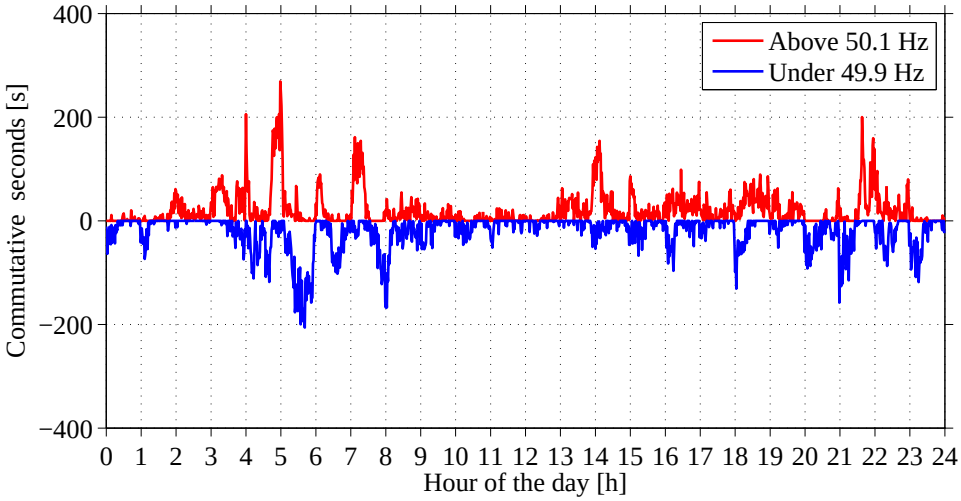

Figure 3.13: The minute-by-minute allocation of under and over frequency of June 2013 over the 24 hours of an aggregated day.

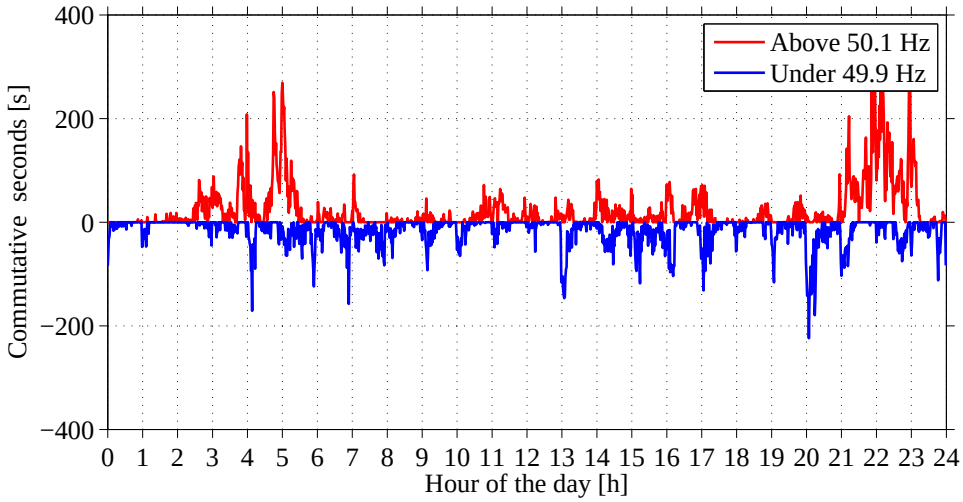

Figure 3.14: The minute-by-minute allocation of under and over frequency of July 2013 over the 24 hours of an aggregated day.

The results clearly show a relation to both the diurnal load variation in Figure 3.10 that the deviations occur for a longer duration during the high load occasions in January. It coincides with the anticipations of Figure 3.9. This implies that the actual load variation as expected is not similar to the anticipated load curve. This and the stepwise clearance of Nord Pool Spot market results in big hourly deviations. An enhanced view of Figure 3.11 is presented in Figure 3.15. One of the reasons behind this behavior is seen Figure 3.16 where assuming a step-wise generation increase one should be able to observe over frequency events more commonly in the first minutes after the hour clearing than during the last minutes of the same hour. The opposite behavior should be observed in the afternoon hours when the load is decreasing, still due to the lack of derivative this might not be noticeable.

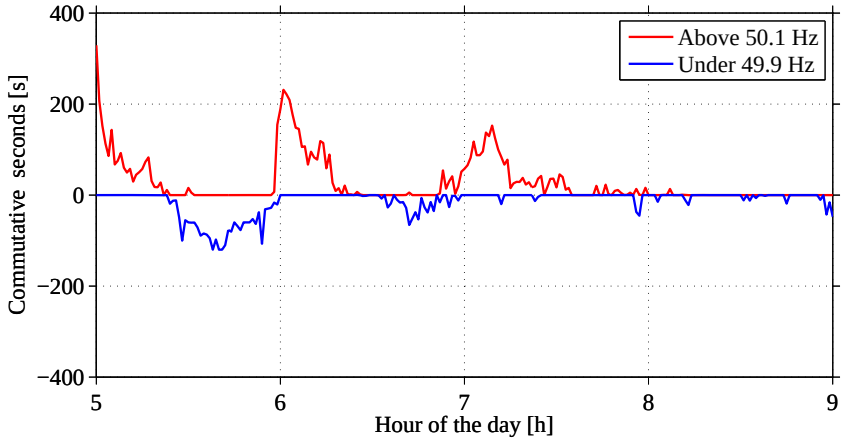

Figure 3.15: An extracted first 5-9 h of the minute by minute allocation of under and over frequency of January 2013 over the 24 hours of an aggregated day in Figure 3.11.

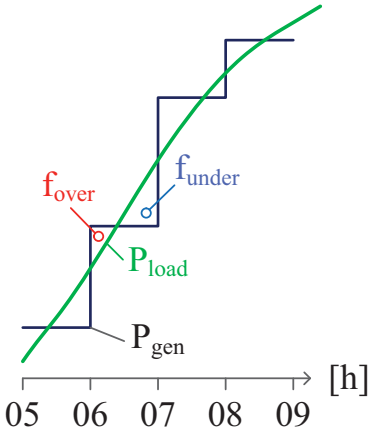

Figure 3.16: A schematic diagram over the proposed reason behind the hourly frequency variations.

In order to understand in more detail how the market clearing cause the frequency quality at the hour shift, the following four statistics for each hour are presented. This even though the argument for morning hours only is valid for 2 and 3 in the following list, the other are in order

to compare and evaluate the evening hours where the argument is valid for 1 and 4, assuming a steep load derivative.

1. % of under-frequency duration occurs in the FIRST 15 min of an hour (as compared to the whole hour)
2. % of under-frequency duration occurs in the LAST 15 min of an hour (as compared to the whole hour)
3. % of over-frequency duration occurs in the FIRST 15 min of an hour (as compared to the whole hour)
4. % of over-frequency duration occurs in the LAST 15 min of an hour (as compared to the whole hour)

The behavior of Figure 3.16 is seen in Figure 3.17.

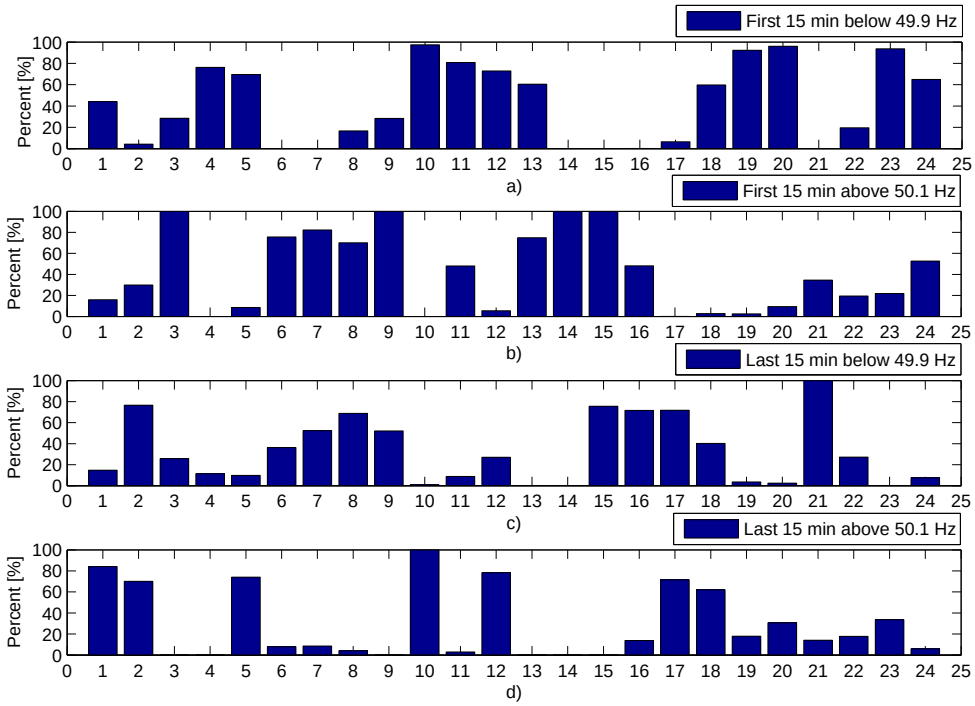

Figure 3.17: Percentage of the first/last 15 minutes of an hour that over/under frequency occurs for January 2013.

In Figure 3.17 the different percentages of the overall deviation for that specific hour that occurs in the first 15 minutes or the last 15 minutes of that hour. One can note that since Figure 3.17 is total percentage out of the total deviation the argument of Figure 3.16 should only be applied to the time spans containing large frequency deviations.

There is a risk that small disturbances during a time span of low disturbances are over interpreted as can be seen in Figure 3.12 for hours 14-15. The deviations occur, but more of a random

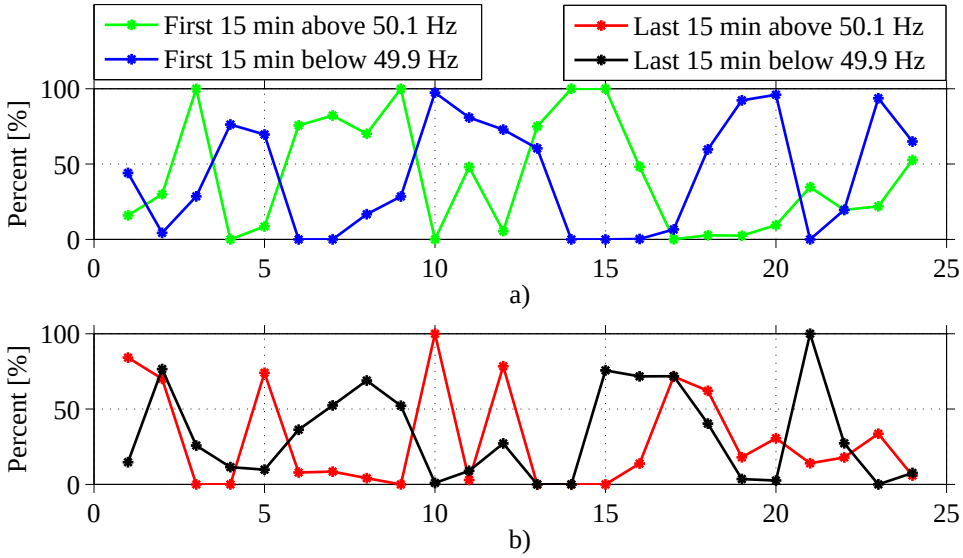

Figure 3.18: Other visualization of Figure 3.17 Percentage of the first/last 15 minutes of an hour that over/under frequency occurs for January 2013.

character could then give such an over interpreted bar in Figure 3.17. The small amount of disturbances above 50.1 Hz is within the first 15 minutes of hour 14, thus it would then coincide with a 100 % bar in Figure 3.17.

In correlation with Figure 3.16 a clear observation in the figure b) can be seen in hour 6-9. A significant part of the frequency variations in the first 15 minutes are above 50.1 Hz. This can be validated by observing figure a) displaying the same 15 minutes but below 49.9 Hz, here few deviations occur out of the total occurring under frequency deviations for that hour. The first part has been investigated, the focus is now shifted towards the last 15 minutes and in accordance with Figure 3.16 one can observe in the c) plot that more than 40 % of the under frequency deviations for those hours (6-9) occur in the last 15 minutes. The analysis is strengthened by observing the over frequency events for the last 15 minutes of the specified hours. It is important to note that since the load derivative is steeper in the 6-9 hours of the day this phenomena is mostly occurring at this time.

Another interesting area i Figure 3.11 is the load decrease region (see Figure 3.10) in the evening between 21-23. If we consider the opposite behavior and

3.3.4 Introduction of FRR-A and its impact of frequency quality

Monday the 7/1:e 2013 at 10 o-clock FRR-A was introduced in the Nordic system that activates within 150 s including a filter time of 30 s, each individual bid of the volume of a minimum step of 5 MW. Initially the capacity was 100 MW, distributed depending on the load of the various countries the previous year, Sweden for example had 39 MW in 2013 based on 2012 annual load [33]. The 4/3 2013 the volume was increased to 200 MW and tested for one week. On the 18/3 the volume was increased for one week to 350 MW and after that the volume varied between 100-350 MW until the test period was planned to end after the summer of 2013 [59]. In May the Nordic TSO's realized that there was a lack of FRR-A capacity due to seasonal "spring flood" conditions, this limited capacity would then only have a small effect on the frequency quality. Spring flood causes productions during spring and autumn to be fairly high leaving less head room for reserve in the hydro units. It was thus decided that the capacity from 20 May to 16 September of the FRR-A should be 0 MW [60]. The FRR-A was then set to 100 MW the 16 September and additional tests to evaluate it was performed from 7 of October 2013 [61]. With the knowledge of both price and the timings of the biggest frequency deviations it seems that the TSO's started a new strategy to only acquire FRR-A during hours with many frequency deviations [REF to frequency variation at hour shifts]. In week 49 of 2013 300 MW of FRR-A was procured between 05:00 and 08:00 CET. No other FRR-A was available this week [62]. In 2014 the testing continued and strives towards improving the behavior at various time intervals. In Week 3 - 5, 300 MW was contracted between 00:00-01:00 CET, 05:00-08:00 CET, and 22:00-24:00 CET on week days (Monday to Friday) only. In week 6-9, 16:00-19:00 was added to the previous intervals for all days of the week, the other timings were still only during week days [63]. Further tests emerged and Week 19-26 The time intervals were 05:00-08:00 and 22:00-24:00 CET on week days only, still with a capacity of 300 MW [64]. No evaluation of these different timings yet exists in the research community.

Frequency deviations during various FRR-A capacities

An overview of the frequency deviations during the specific periods of various FRR-A capacities are presented in respect with the corresponding time the previous year. It is important to note that the price and load levels are not identical between the years of 2012 and 2013, trends might be viable but too sharp conclusions should not made unless knowing the system state during the various years.

TABLE 3.9: Different sizes and durations of various volumes of FRR-A in 2013 and their corresponding date interval in 2012.

Week	Date	FRR-A Capacity	Time over 50.1 Hz [s]	Time under 49.9 Hz [s]	Data Coverage	Date Session
w 2	08-Jan-2013 10:20:00[2] - 11-Jan-2013 23:59:59	100 MW	4611	2052	100.00 %	S1
w 2	10-Jan-2012 10:20:00 - 13-Jan-2012 23:59:59	-	3792	1431	97.75 %	S1
w 10	04-Mar-2013 00:00:00 - 08-Mar-2013 23:59:59	200 MW	3982	3535	100.00 %	S2
w 10	05-Mar-2012 00:00:00 - 09-Mar-2012 23:59:59	-	7951	4679	100.00 %	S2
w 12	18-Mar-2013 00:00:00 - 22-Mar-2013 23:59:59	350 MW	3270	2261	99.72 %	S3
w 12	19-Mar-2012 00:00:00 - 23-Mar-2012 23:59:59	-	3563	4567	100.00 %	S3

Table 3.9 shows the different date sessions for comparisons with Figures 3.19(a), 3.19(b) and 3.19(a). At the date sessions of the various years the price and load data was also compared with their 1 hour data from the Nord Pool data base. These did not seem to coincide at any of the short sessions of various capacities. This was thought to give some insight to the state of the power system at the different times if they in fact were similar. No such conclusion could be drawn from the load and price data. However, it is clear that the 350 MW FRR-A improved the systems frequency quality seen to the compared date sessions.

[2]Due to lack of data for the initial days of week 2 in 2013 a smaller date span was used for the comparison in date session 1.

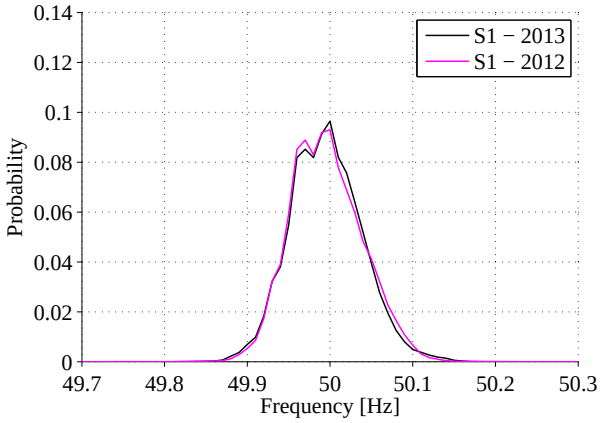

(a) S1

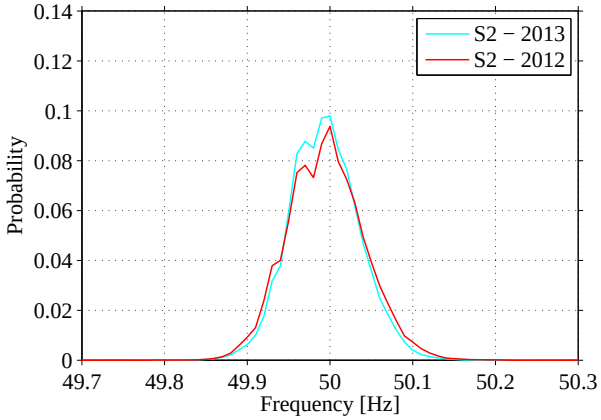

(b) S2

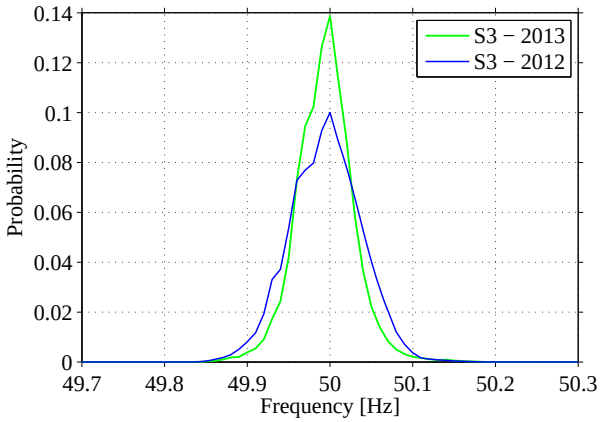

(c) S3

Figure 3.19: The Empirical probability density function of frequency data during test period S1/S2/S3.

3.4 ROCOF evaluation of disturbances

Since the sampling frequency of 50 Hz containing some transient recordings and the accuracy of the 10 Hz implicit sampling frequency tends to be high(see Section 3.2.3) this has been chosen to evaluate the largest negative ROCOF in the NPS (generation trip etc.). These were sorted out from the data (covering 2006, 2012 and 2013) sorting the events of each year in the following manner: Locate all dips under a frequency of 49.80 Hz. These need to be at least 500 s apart in order to discard oscillatory behavior caused by the first frequency swing. To ensure that the observation starts before a disturbance an observation window of 600 s is created before and after the events minimum value, the initial frequency of the observation window, $f(t_0)$, must be above 49.9 Hz. This in order to ensure that the imbalance has started from a stable system. The maximum ROCOF during that observation window is then calculated and stored together with a time stamp and the temporary minimum frequency (TMF) of that event. The time stamps corresponding to the evaluated frequency window is also evaluated in order to ensure a continuous stream of data. It is important to note that the deviations are perhaps not more occurring in 2012 and 2013 than 2006 due to the increased number of points, even though it still seems like it. The lack of data coverage from 2006 makes this comparison difficult. The severity, temporary minimum frequency (TMF), of each disturbance is indicated by the colorbar to the right in the figures.

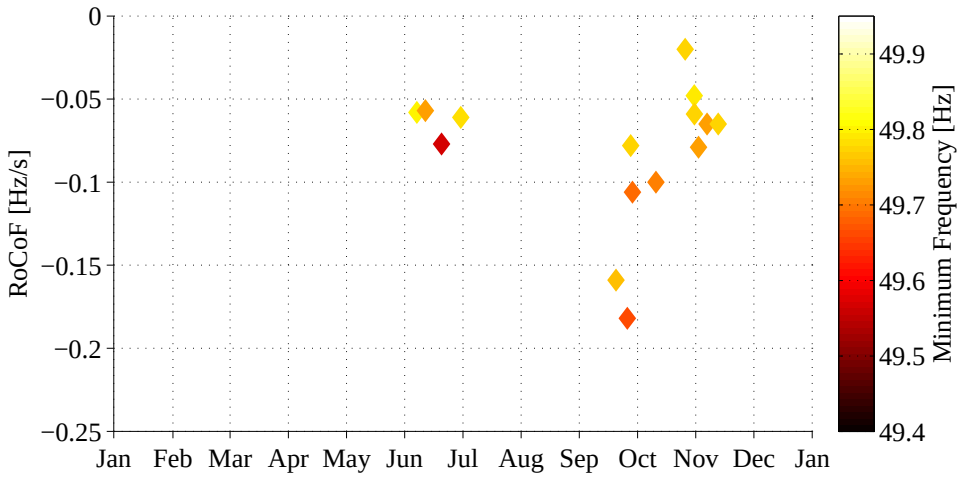

Figure 3.20: ROCOF evaluation for the year of 2006, coverage of data = 76.0 %

It should be noted that all these measurements are from a PMU in Lund. Thus when the closest and largest production unit trips, there can be much steeper frequency derivatives locally than at the further away bus-bars. Since one of Sweden's nuclear power stations (Ringhals) is situated in the vicinity (at least electrically) as well as the HVDC line from DK1 (Konti-Scan). This HVDC line is partly used as frequency responding reserve when not fully committed to delivering power to/from DK2 [27](150 MW at 49.8 Hz). Thus some of the bigger disturbances causing large ROCOF values (in Lund) are usually during trips of Ringhals (mostly around 1000 MW) causing big deviations initially. Then due to the quick reactions of the Konti-Scan this steep

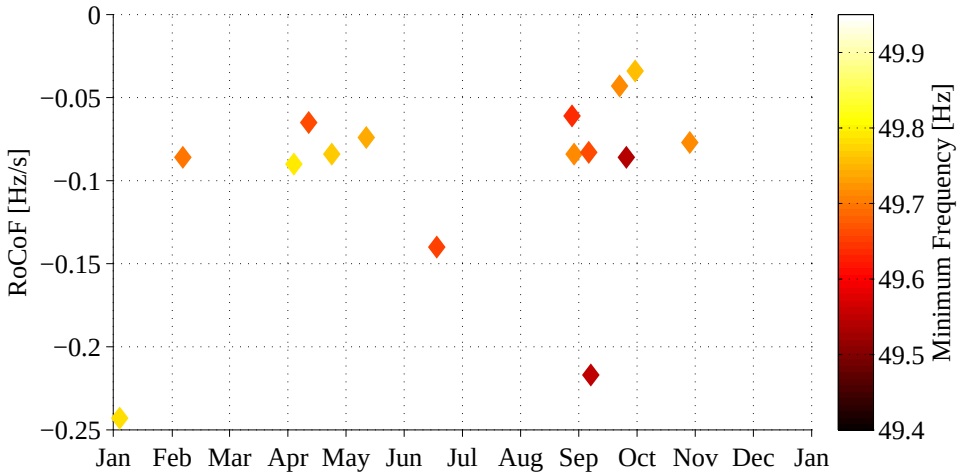

Figure 3.21: ROCOF evaluation for the year of 2012, coverage of data = 93.2 %

derivative is broken and system is balanced out fairly fast by other reserves. This does not mean that a big negative derivative will always cause a very low TMF (more on this in 3.4.2). However, considering the ROCOF limits of ASP and the events of 2012 and 2013 it can be observed that several erroneous trips may occur due to islanding protections, further worsening the situation during a high wind power production instance could occur due to the disconnection of more generation in an already constrained environment.

3.4.1 ROCOF evaluation - depending on location

Local frequency phenomena have been presented in mainly smaller grids due to the use of synchronized PMUs and their synchronized time stamps [46],[65][46]. During these evaluations it can be seen that the frequency during the initial seconds differ from different locations, see also 2.3. This has also been observed in the PMU data investigated for this study. As an example a planned trip of the nuclear station Forsmark 2 of 1100 MW the 14/5-2013 has been selected. The result of the disturbance is captured in Tampere, (Finland at 400 V), Lund (Sweden at 400 V) and Forsmark (Sweden at 400 kV, by SVK AB).

It can be observed from the two figures (Figure 3.23 and Figure 3.24) that the nadir of the disturbance does not change between the different measurements. The ROCOF values for the initial seconds could pose a problematic situation for regulators trying to implement Virtual/Emulated-inertia [66] since the ROCOF's are different and even become positive during the disturbance. A filtering stage and/or a delay seems to be necessary to avoid unintentional absorption of power during events that should in fact be characterized by an extra output of power from frequency regulating sources.

Seen from the point of view on primary regulation of the frequency these implications give no such problem for the disturbance observed since it acts on the frequency limits rather than the derivative of the frequency.

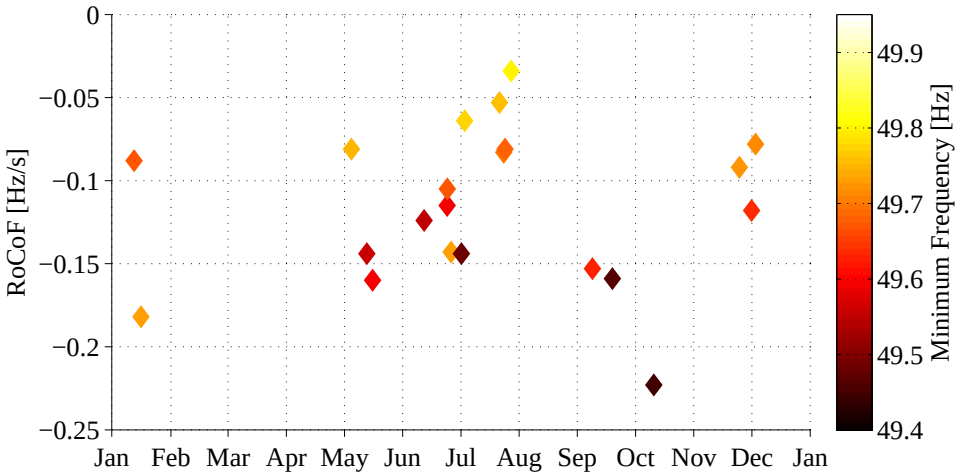

Figure 3.22: ROCOF evaluation for the year of 2013, coverage of data = 91.3 %

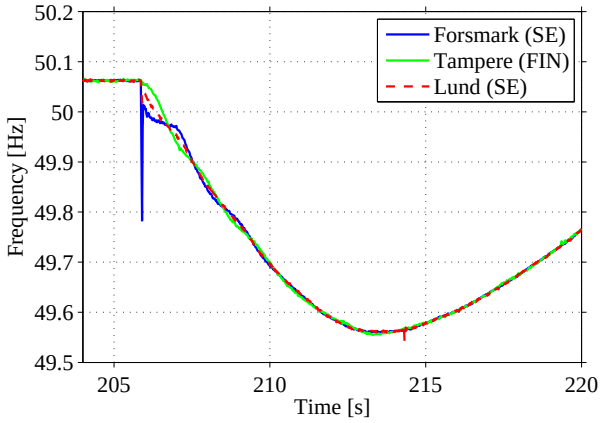

Figure 3.23: The first seconds of the Forsmark trip for different PMU locations

Considering the implication on generation protection, most DG (Distributed Generation) utilizes ROCOF-relays in order to detect islanded operation. Phase-shift relays are also used for islanding protection, however they have shown poor performance compared to ROCOF-relays (see Section 3.1). The settings of these relays are usually related to manufacturer data and hard to acquire. Fortum Sweden has a recommended (only for wind turbine connections to 10/20/30 kV) ROCOF settings of more than 0.3 Hz/s and a delay of 0.5 seconds in order to completely disconnect generators during island operation [67].

3.4.2 ROCOF evaluation - selected disturbances

One example of low frequency nadir (low TMF) and high ROCOF from 2013-10-11 is when Oskarshamn 3 trips, fairly far away from Lund, but with about 1300 MW. This causes a steep negative derivative until the FDR activates (noted by the red ring in Figure 3.25.)

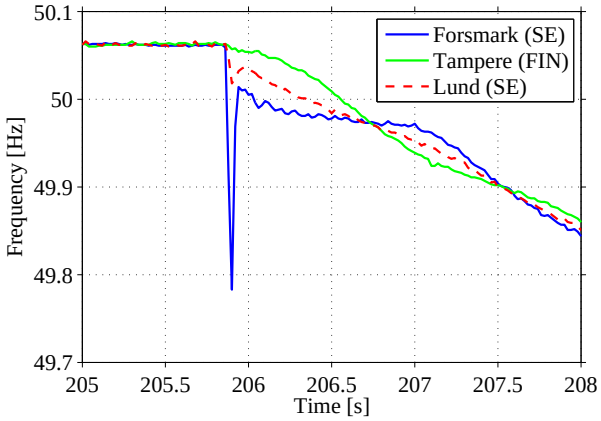

Figure 3.24: An enhanced view of the first seconds of the Forsmark trip for different PMU locations

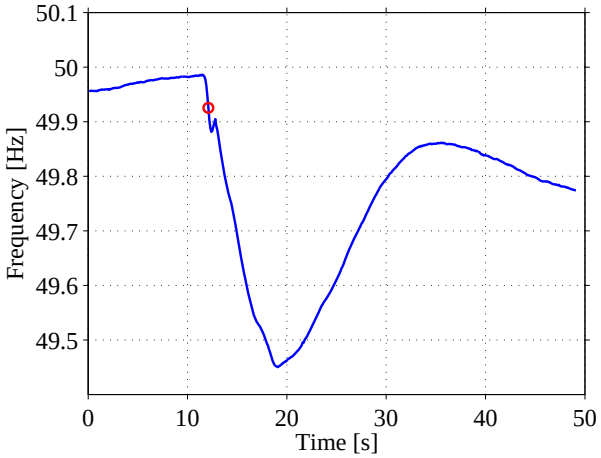

Figure 3.25: TMF = 49.4502 Hz, ROCOF = -0.2230 Hz/s, 2013-10-11

One example of High ROCOF but not as low TMF is when Ringhals 4 trips with about 935 MW fairly close to Lund and a quick relatively local action from Konti-Scan with at least 100 MW added power and a high initial frequency causes a fairly high TMF. Ringhals 4 - R4: 935 MW

3.5 Conclusions

A few concluding remarks from the chapter are presented below.

Considering the minute by minute allocation of frequency deviations presented in Section 3.3.3 it would be preferred to utilize the FRR-A during the hours of large disturbances. However it is important not to start the service exactly at the hour shift, recommendations based on Figure 3.13-3.14 result in 3:30-8:30 , 19:30-22:30, 15:15-18:15 and 19:30-22:30 GMT. This due to the fact that the frequency deviations start to occur prior to the market clearing of each

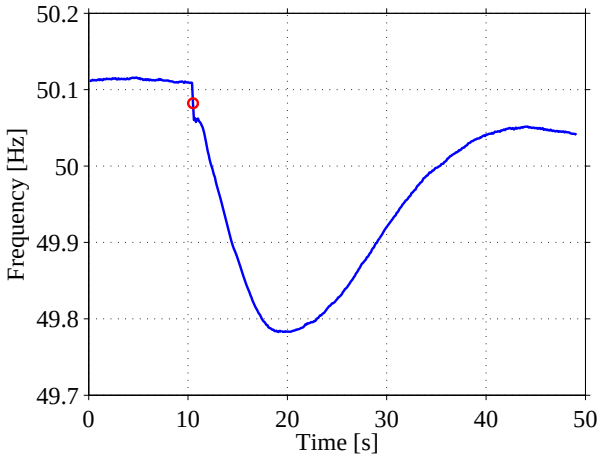

Figure 3.26: TMF = 49.7826 Hz, ROCOF = -0.2430 Hz/s, 2012-01-04

hour, as can be seen in Figure 3.15.

Another interesting behavior of the system has emerged during the studies, that the deviations in June and July, dominated by a relatively low load compared to January has a severe amount of frequency deviations. These deviations still seem to occur close to hour shifts but cannot be correlated to the variability of the load. A more reasonable reason could be that of the scheduled generation responsible for frequency control during the summer months. It is however clear that increased frequency regulation is necessary during the summer. During the year 2013 the FRR-A was inactive during the summer. The impact of this could be the reason for the increased deviations seen in the period. The benefit of BESS or VSWT with Virtual/Emulated Inertia or FCR support strategies is that they can produce a faster FCR response. However, an improved way of determining the state of the system must be found in order to realize the problem. simply waiting for the frequency to drop under 49.9 Hz is a to slow pattern for these sources and signals such as a pre-fault value, ROCOF-signal(filtered) and a frequency signal should be used in order to act as fast as possible. Preferably even as fast as not to trip ROCOF relays, which would further worsen the situation, see Chapter 5 for impact on ROCOF from temporary support strategies from VSWTs.

The over frequency behavior of the system is something that could be reduced with the help of frequency sensitive pitch regulators, since a pitch rate of 10 degrees/s is still faster than many of the generators governors. Acceleration of VSWT rotors is even faster and could be utilized to give a quicker response during constrained operation of over frequency, for more information see Chapter 6.

Financial incentives for a 15 min clearing of the market could be given to power systems that could handle it, considering the NPS and the concentration of hydro this is reasonable, as the main reason for hourly set-points is the limitations on old thermal units. This would in turn reduce the steps in generation in causing less stress on the frequency controlling reserves utilized. If the integration of wind turbines were to provide regulating power it would be better in order to balance these sources in order to increase the speed of temporary support. A market cleared 1 day ahead could be split into 12 h-ahead market to get better load and wind forecasts in the

system thus improving the situation even further.

The localized ROCOF measurements could result in a more optimized frequency reserve regulation. It could allow for reserve to be activated in the affected area in order to cover the loss of generation without causing congestion of transmission lines leading into that area. Generators close to points of disconnection can see a steeper ROCOF and would thus act faster, which is deemed a preferable strategy for VSWT and BESS due to their fast acting power electronic converters interface. Any recharging or re-acceleration could in the later stages be covered by slower generation sources. In order to evaluate an appropriate coordinated response to a disturbance it could be beneficial to first send frequency data to a central control unit compare the different initial frequency variations in order to set new set points for the reserve providing generators.

Chapter 4

Generation units modeling

4.1 Generation units modeling

4.1.1 Variable speed wind turbine

A basic model of VSWT (GE DFIG 3.6 MW) is implemented as presented in [68] and [69] and used in order to evaluate a power system [5],[68] during a power imbalance. Similar wind turbine models can be found for full power converter wind turbines (FPC-WT). One key figure for the frequency support is the inertia constant of the VSWT model used, it has been found to vary from 4-6 s depending on topology and rating of the VSWT. A One-mass model has been shown sufficient to model the behavior of the turbines during frequency variations especially since voltage is assumed to be constant during the periods of operation [70] it is also commonly utilized in well cited papers [7],[9],[71],[72]. Two-mass model parameters are available in [68] but the author recommends the use of the one mass-model. However, if voltage variations are considered it is recommended to utilize the two-mass model [73].

The conversion from wind into aero-dynamical power, in Watt, can be represented by:

$$P_{aero} = \frac{1}{2}\rho A C_p(\lambda, \beta) v_{wind}^3 \tag{4.1}$$

Where, ρ is the air density in kg/m^3 , A the swept area by the blades in m^2, $C_p(\lambda, \beta)$ is the power coefficient of the turbine and v_{wind} is the wind subjected to rotor blades in m/s.

The power coefficient, C_p, is determined by an analytical function seen in 4.2 [68].

$$C_p(\lambda, \beta) = \sum_{i=0}^{4} \sum_{j=0}^{4} \alpha_{i,j} \beta^i \lambda^j \tag{4.2}$$

Where λ is the tip speed ratio (TSR) of the turbine, β is the pitch angle of the blades and $\alpha_{i,j}$ are the constants given in Appendix A.1. λ is obtained using 4.3.

$$\lambda = R_{wt}\frac{\omega_{wt}}{v_{wind}} \tag{4.3}$$

Where R_{wt} is the radius of the turbine and ω_{wt} is the rotor speed of the turbine. The power coefficients dependency on λ and β are presented in Figure 4.1.

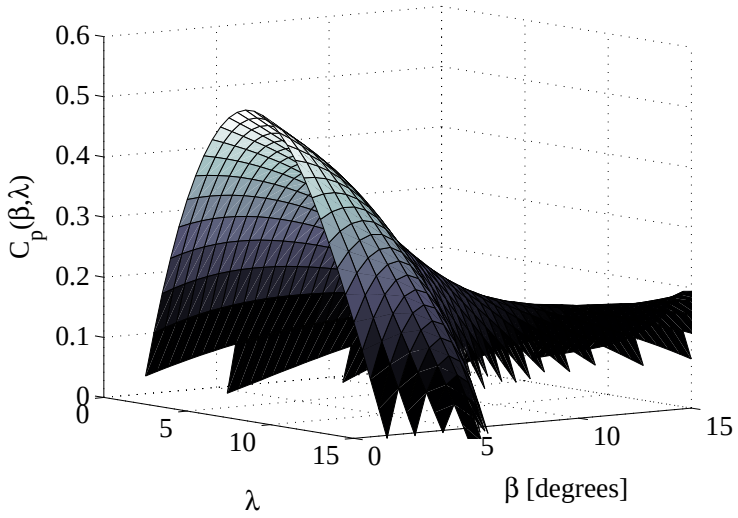

Figure 4.1: Power coefficient for different values of β and λ.

In Figure 4.1 the different operational points for a VSWT can be observed. It is important to note the change in C_p due to a change in pitch. This would imply the possibility to fast reduce the power output of the turbine by pitching the blades. However this possibility to change the output power is limited by the response of the pitch actuator. The option of alternating the rotor speed of the turbine beyond that of the optimum can also be used in order to adjust the power absorbed by the turbine from the wind, however this is not done in standard configurations. The speed reference (ω_{wt-ref}) of the turbine is generated with respect to the measured produced power in accordance with 4.4 when the output power is below 0.75 pu while above the speed reference is set to 1.2 pu.

$$\omega_{wt-ref} = -0.67P_{e-meas}^2 + 1.42P_{e-meas} + 0.51 \tag{4.4}$$

Where P_{e-meas} is the measured output power, acquired through a first order transfer function with a time constant T_{e-meas} of 5 s. When the rated speed is reached the pitch actuator is activated, the pitch actuator and model is based on [68]. It is modeled in accordance with Figure 4.2 and controls the rotation of the turbine during the high wind speed range when (v_{wind} >11.2 m/s).

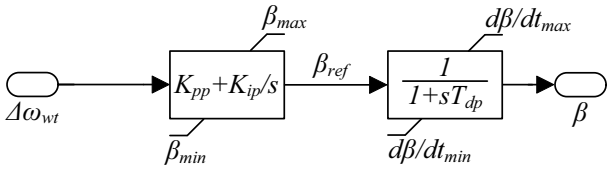

Figure 4.2: Pitch controller and actuator for standard pitch system utilized in VSWT model, parameters are presented in Table 4.1.

Where the pitch actuator is a first order transfer function with a time constant T_{dp}, rate limiter $d\beta/dt$ and max and minimum pitch angle[1]. The PI-controller is implemented as a parallel type with anti-windup. All settings can be found in Table 4.1.

TABLE 4.1: Parameters for the Pitch control.

Parameter	Value
K_{pp}	50
K_{ip}	4.5
T_{dp}	0.3 s
$d\beta/dt$	$\pm$ 10 °/s
β_{min}	0°
β_{max}	27°

The overall VSWT model presented in Figure 4.3.

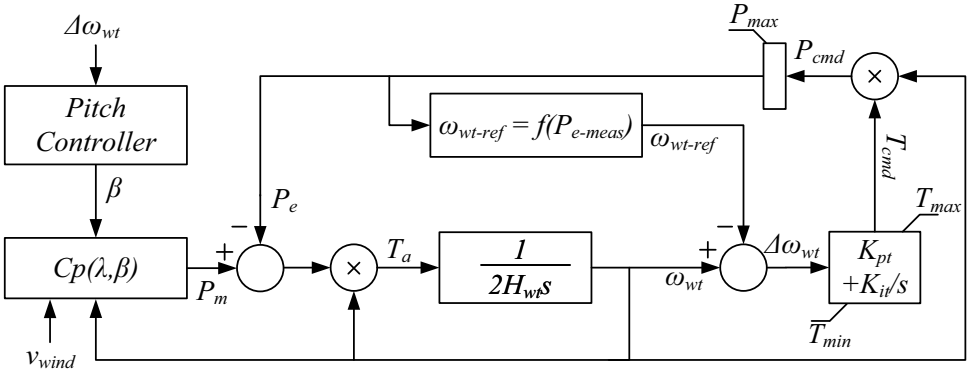

Figure 4.3: Wind turbine model.

The parameters of the VSWT modeled can be observed in Table 4.2.

[1]Improved modeling of pitch actuator systems utilizing a second order system can be found in [74] p. 16

TABLE 4.2: Parameters for the VSWT.

Parameter	Value
K_{pt}	3
K_{it}	0.3
T_{e-meas}	5 s
H_{wt}	5.19 s
T_{min}	0
T_{max}	0.833
P_{max}	1 pu

4.1.2 Hydro unit

A hydro generator was modeled in accordance with [49][2]. In order to provide a stable performance of the governors of hydraulic units a transient droop compensation is used. This due to the inherent reduction in power output during a change in governor position. The block diagram is presented in Figure 4.4 and contains transient droop in the speed governor and turbine characteristics.

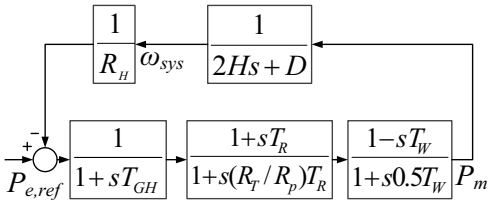

Figure 4.4: Hydro unit model.

TABLE 4.3: Parameters for the Hydro turbine [49].

Parameter	Value
R_H	0.05
T_{GH}	0.2 s
T_W	1.0 s
R_P	0.05
R_T	0.38
T_R	5.0 s
D	1.0
H	3.0 s

[2] For more information on the hydro turbine consider [49], p. 394-418 for functional information and p. 599-600 for modeling.

4.1.3 Reheat steam unit

A reheat steam generator was modeled in accordance with [49][3]. The steam turbines comes in formations with and without reheat, the reheated steam turbines have two separate systems to operate the steam energy within the turbine. The reheat turbine is commonly installed and will thus be modeled in order to represent a fast acting governor able to respond rapidly to power system instabilities. The model includes representation of the speed governor, turbine with the reheat function and the droop control for load-frequency analysis. A figure of the block diagram is presented in Figure 4.5 with the values of the parameters according to Table 4.4.

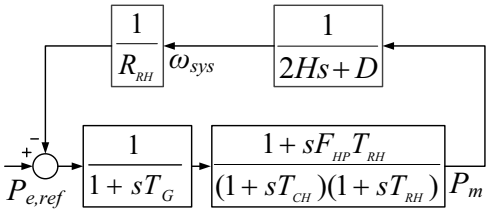

Figure 4.5: Reheat steam turbine model.

TABLE 4.4: Parameters for reheat steam turbine [49].

Parameter	Value
R_{RH}	0.05
T_G	0.2
F_{HP}	0.3
T_{RH}	7.0 s
T_{CH}	0.3 s
F_{LP}	0.7
D	1.0
H	3.0 s

4.1.4 Thermal unit

Since thermal units have a large penetration in the NPS it is of interest to model. The model used is an adaption of [75][4] disregarding the voltage regulation and is shown in Figure 4.6. The model considers steam valve transfer functions, turbine and low/high pressure parts of the shaft and its contribution to power output. The parameters can be seen in Table 4.5.

[3]For more information on the reheat steam turbines or non-reheat consider [49], p. 424-448 for functional information and p. 598-600 for modeling.

[4]The constant K_{KL} is selected to the operation point close to rated power output for the model (150 MW/60 MVAr).

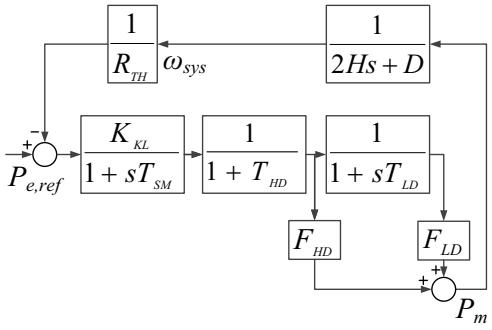

Figure 4.6: Thermal unit model.

TABLE 4.5: Parameters for Thermal turbine [75].

Parameter	Value
R_{TH}	0.05
K_{KL}	1.6
T_{SM}	0.06 s
T_{HD}	0.24 s
F_{HD}	0.2
T_{LD}	10.0 s
F_{LD}	0.36
D	1.0
H	3.0 s

4.2 Increasing wind penetration ratio

This is done by reducing the droop of each generator (R_H,R_{RH} and R_{TH}) by the percentage of WPR. The same for the inertia constant H of the generators, thus the variables vary in accordance with Table 4.6 and [69].

TABLE 4.6: Affect on parameters by alternating WPR

WPR	R_X	H
0 %	0.05	3 s
10 %	0.05/0.9	2.7 s
20 %	0.05/0.8	2.4 s
30 %	0.05/0.7	2.1 s
40 %	0.05/0.6	1.8 s
50 %	0.05/0.5	1.5 s

Where R_X is R_H,R_{RH} or R_{TH}.

4.3 Generation units during disturbances

In order to observe the primary and inertia response of the different units and their action to mitigate a load increase of 0.1 pu is simulated and shown in Figure 4.7(a), 4.7(b) and 4.7(c).

Figure 4.7(a) indicate the action of the turbine and its control parameters and their effect on the power system frequency during the power imbalance initiated at 0 s. Both the modeled thermal and reheat unit show similar behavior while the hydro unit performs worse, in the sense of TMF, ROCOF and time until a steady state frequency is reached. The reason for this behavior is represented in Figure 4.7(b) where the initial decrease in power from the hydro is visible at 0 s. This due the decrease of water pressure on the turbine blades during the change in valve position of the hydro unit as the governor is reacting to the disturbance. Figure 4.7(c) shows the immediate response from the directly coupled generator in order to balance the power imbalance as discussed in Section 2.3. Here however only one generator is responsible for providing the inertia to initially cover the power imbalance. Figure 4.7(b) also indicates the use of the droop controller's parameters (R_H,R_{RH},R_{TH}) and the interaction from the load dampening of the load as discussed in 2.12 in Section 2.3.

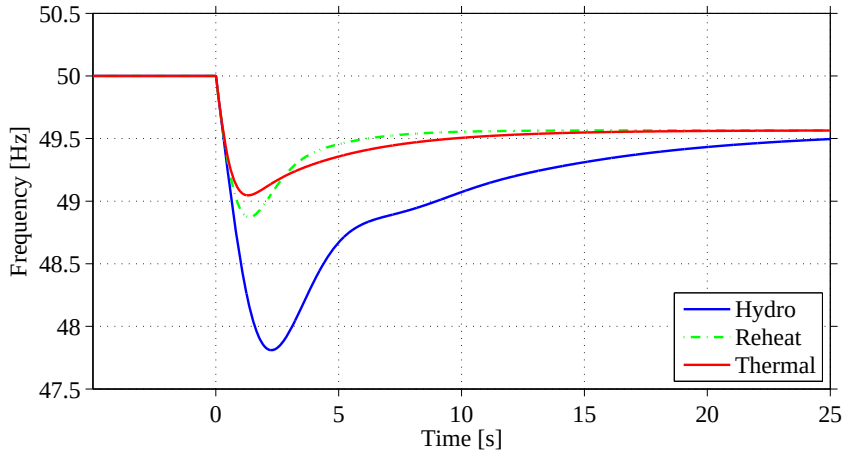

(a) Frequency response of the generators in a power system only based on that specific generator type.

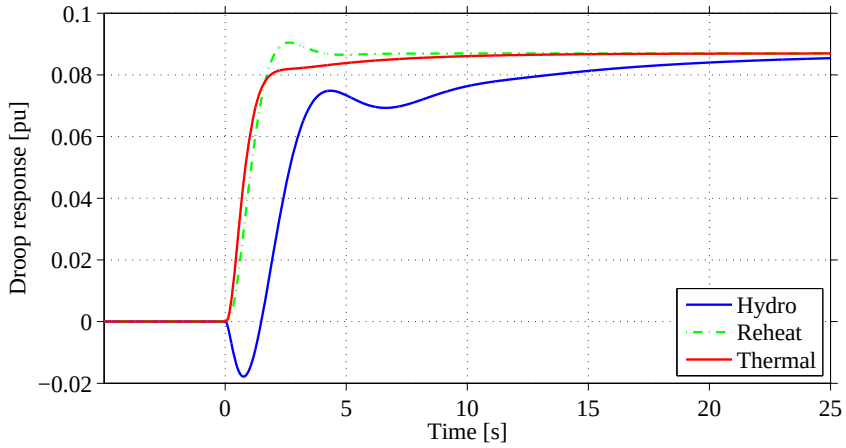

(b) Power output from the three generator models due to their primary support through droop.

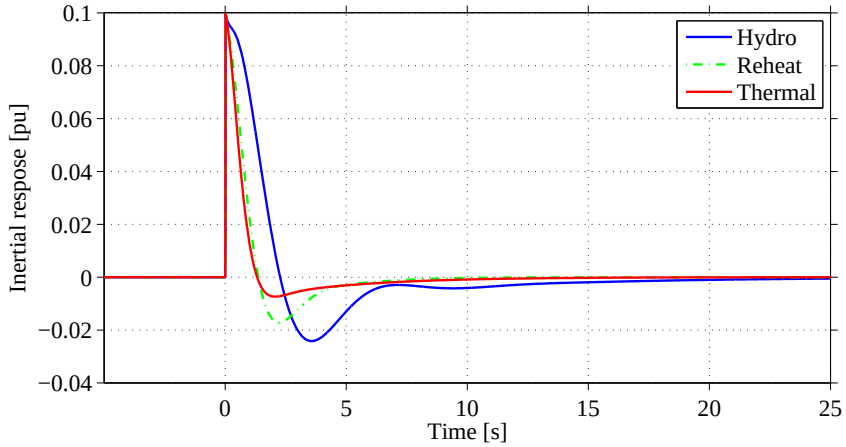

(c) Power removed from the inertia in the different generators during the disturbance.

Figure 4.7: The different generation unit's response to 0.1 pu load imbalance.

Chapter 5

Inertia support from wind plants

5.1 Introduction

An increase in the wind power penetration ratio (WPR) causes a decrease in the total system inertia. These factors may result in an increased frequency variation and instability issues in the future power system.

An overview of recent grid codes is presented in [20] related to wind power integration. Countries included are Denmark, Germany, Spain, United Kingdome, Ireland, United States and China. It is stated that the UK grid code was the strictest among the investigated related to frequency deviations, requiring a frequency span of 47.5 $<$f $<$52 Hz. In contrast, E.ON's (Germany) grid code on offshore installations is the least strict, allowing a frequency span of 46.5 $<$f $<$53.5 Hz.

Therefore there is a need for investigating different frequency control strategies supplied by VSWTs, especially during island operation. Previous publications have proposed an increase in the use of different frequency support actions by controlling the output power of a VSWT. The use of the pitch actuator or control strategies alternating around the maximum power point to reduce the power produced is presented in [76]. Temporary frequency support during short term power imbalance has also been investigated using the kinetic energy in the rotating mass through the use of additional control measures [77]. The Spanish grid code strongly suggest inertia emulation in future codes where a suitable additional 5 % power could be supplied with a response time of 50 ms. Thoughts of energy storage was also presented that it would be able to inject or absorb 10 % active power for at least 2 s. It is also stated that the dead band for inertia emulation should be $\pm$10 mHz. The inertia emulation should be disabled for voltages below 0.85 pu [20]. This most probably not to interfere with possible reactive control and limit the thermal overloading of transmission lines. However, studies within islanded operation are still needed to evaluate the frequency support strategies. Island operation of wind turbines is at this moment not required by grid codes. However, with a large share of generation capacity from wind farms (WFs), especially in islanded power systems, it is not feasible to disregard the frequency support that can be provided by the WFs. Different rates of WPR have been discussed but usually with the new capacity added to the previously existing production thus not reducing

the effect on the frequency nadir by an increase of wind power penetration (WPP) [8],[78],[79]. The WPR can vary greatly during a future islanded operation of a grid with frequency controlled VSWT. Therefore different support strategies for power imbalance needs to be evaluated. A study related to islanded systems with frequency dependent loads subjected to large wind power penetrations is also needed. The aspect of frequency derivative needs to be used in order to compare different strategies since low inertia usually means a low TMF and a steep ROCOF (See Section 3.4).

The chapter is structured in a short initial review of the frequency support strategies in Section 5.2. This is then followed by a modeling part in section 5.3 that describes the modeling of a small test power system. Section 5.4 then presents the results of two different test sessions, one with a 20 % WPR and one utilizing a 50 % WPR. An adaption to the presented strategies is presented and evaluated in both of the test sessions. Special attention is given to the frequency derivatives for the different cases. Furthermore, the response of a frequency dependent load is evaluated for the two test sessions. Concluding the chapter is a discussion regarding the results.

5.2 Inertia support strategies for VSWT

To take advantage of the fast control from VSWT can be seen through the basic simulations of the generation units in Section 4.3 and in frequency measurements presented in Section 3.4 and should thus give added frequency stability during large power imbalances. One possible way is to utilize the rotating mass in the turbine, which is further described in this chapter.

5.2.1 Instant power support

For the sake of limiting the initial frequency drop, a method proposed by [69] is implemented to show its performance during the initial stages of the power imbalance. An extra signal is the added on top of the power reference prior to the load disturbance to extract the rotational energy in accordance with a pre-defined pattern similar to Figure 5.1,

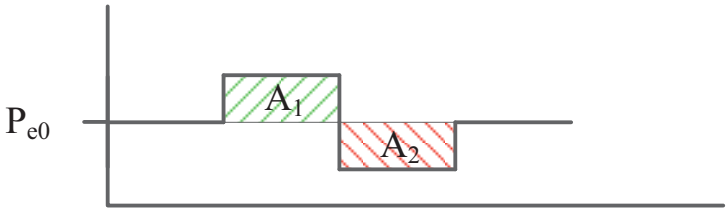

Figure 5.1: Instant inertia and its pre-defined pattern.

where P_{e0} is the pre-fault value of the maximum power point tracker. The P_{extra} is then added as a deceleration area (A_1) to extract energy from the rotation and a re-acceleration area (A_2) that are pre-defined to the amount of the rotational energy that should be utilized. It is important to note that the mechanical power during the locked operation window of A_1 and A_2 is considered constant, thus also the wind speed. Quick changes will however be smoothened out by the turbine inertia. For further evaluation of the potential implications with that assumption see Section 5.5. The time constant of the power controller of about 20 - 50 ms [68],[80] is neglected in the model.

5.2.2 Inertia emulation support

In order to provide a reduction in ROCOF and thus limit the TMF of a power system, inertia emulation can be added to the control system of the VSWTs. The inertial control signal is based on [77],[19]:

$$P_{extra} = 2KH\omega_{sys}\frac{d\omega_{sys}}{dt} \tag{5.1}$$

where P_{extra} is the additional power extracted from the rotational energy, ω_{sys} is the system frequency and H is the emulated moment of inertia. However, the constant K has been added to be able to adjust the level of inertia support.

5.3 Wind-Hydro system modeling

Figure 5.2 shows the test system used to analyze inertia frequency control of a wind-hydro system. Specifically, the following factors that affect system frequency response are evaluated:

1. The effect of wind power penetration level
2. Load frequency dependence
3. Two WT frequency support strategies
4. The interaction between the hydro and wind system.

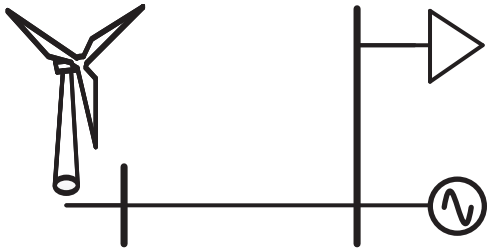

Figure 5.2: The analyzed power system.

The hydro generator model is used in accordance with Section 4.1.2 (since it has a slow and a less preferable initial behavior) and the basic VSWT-model is adopted as described in Section 4.1.1 and [69] connected as presented in Figure 5.3. To investigate the effect of a frequency dependent load, a load model is implemented based on [81]. The active load demand is represented as:

$$P_{load,pu} = \left(\frac{V}{V_0}\right)^{a_1} \frac{1}{1+sT_p}\left[\left(\frac{V}{V_0}\right)^{a_2-a_1}\left(1+\frac{L_f}{100}\Delta f\right)\right] \tag{5.2}$$

where V_0 is the initial load bus voltage, V the actual voltage, L_f the frequency characteristics coefficient for an active power load, α_1 and α_2 are the voltage characteristics of the load and T_p is the time constant for the active load, mainly depending on the interaction from induction machines. The voltage is assumed to be unchanged in the analysis. Thus 5.3 is re-written as:

$$P_{load,pu} = \frac{1}{1+sT_p}\left(1+\frac{L_f}{100}\Delta f\right) \tag{5.3}$$

The parameters are available in Appendix A.1.

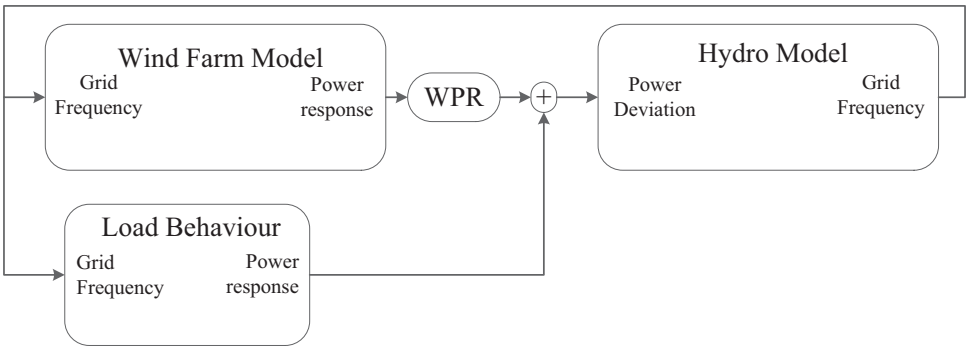

Figure 5.3: Schematic overview of the modeling of the test power system.

5.4 Simulation and data description

5.4.1 Case studies

Instant Power Support and Inertia Emulation Support strategies are then subjected to a base case of 20 % and 50 % WPR, a rotational speed of 0.9 pu at a constant wind speed of 7.5 m/s at this time the WT output power is 0.3 pu. Data on generators can be found in [69] and [49]. A load step increase of 0.1 pu is simulated at 0 s. Table 5.1 shows five cases presented with 20 % or 50 % WPR. One reference case with 100 % hydro power production, is also to be evaluated. A frequency change factor of L_f = 1 is used (see (5.3)) but evaluated in the upcoming subsections in Table 5.2 and 5.3.

TABLE 5.1: The five simulated cases and their descriptions, X = 20 % or 50%.

Case	Description
1	100 % Hydro
2	X % WPR WT without frequency support
3	X % WPR WT with Instant Power Support
4	X % WPR WT with Inertia Emulation Support, K=1
5	X % WPR WT with increased Inertia Emulation Support, K=3

5.4.2 Support strategies for 20 % WPR

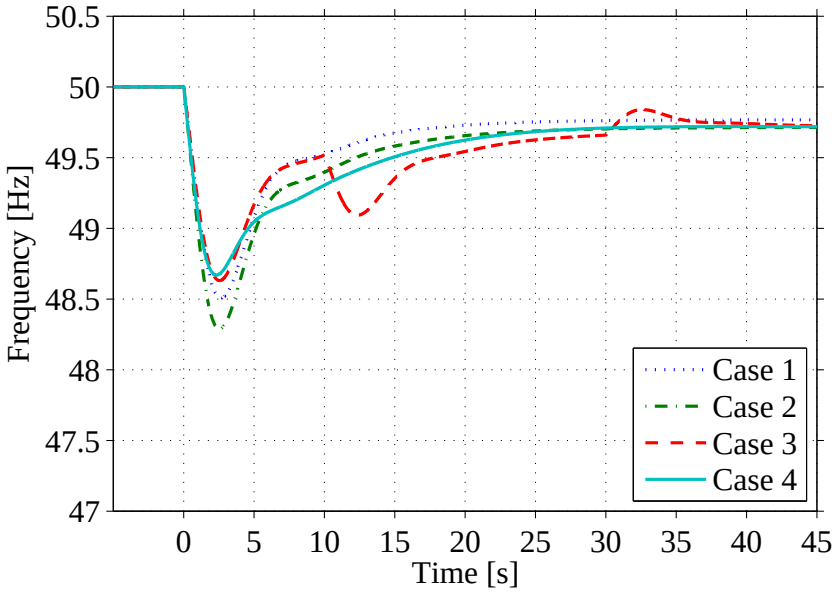

Figure 5.4: The frequency nadir for the simulated cases in accordance with Table 5.1 with a WPR of 20 %.

In Figure 5.4 and Figure 5.5 the response is presented for the different cases. The temporary minimum frequency (TMF) of each case is summarized in Table 5.2 utilizing L_f=1. It can be seen that Case #2 has the worst nadir presented, followed by the total hydro based scenario (Case #1). In Case #3 and #4 the interaction from the WT can be noted to reduce the drop in overall frequency. However, the re-acceleration of the rotor is more apparent in Case #3. Furthermore, Case #3 disconnects the speed controller during the time when the frequency support is active and at the time of its reconnection, at t = 30 s, a mismatch in speed and speed reference can be observed. This creates a small burst of power as the speed of the VSWT is reduced by the action of the speed controller.

To increase the response during the initial second a constant is introduced and evaluated, shown in (5.1). Case #4 is corresponding to equation with a K=1, Case #5 presented is similar to Case #4 but with K=3, thus utilizing more inertia. The resulting change in frequency nadir is presented in Figure 5.5. The resulting change due to the increased power output of the added constant to the equation results in a change in TMF but it needs to be evaluated towards the need of a quick return to the steady state frequency. TMF values for the cases in Figure 5.5 are presented in Table 5.2.

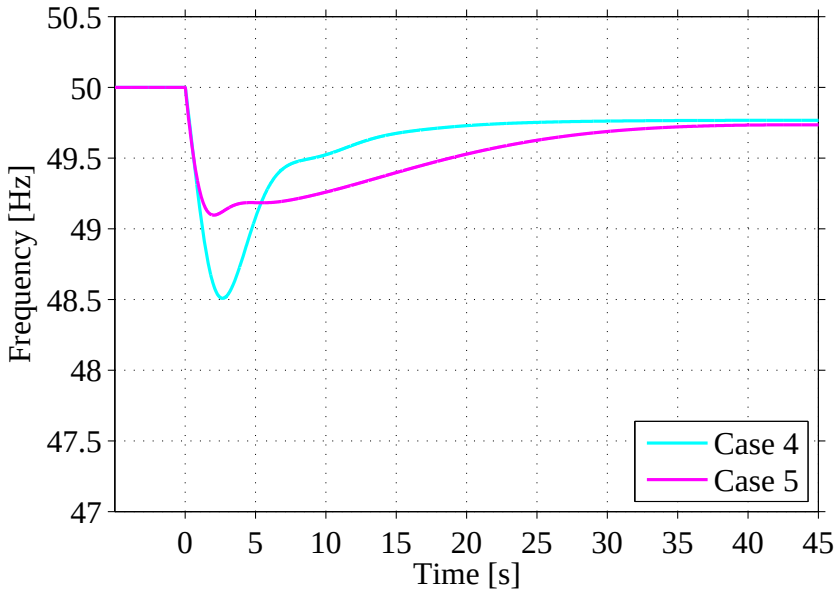

Figure 5.5: Frequency nadir of the presented adoption of inertia emulation compared to the original case.

TABLE 5.2: The interaction between the frequency dependent load parameter L_f and the temporary minimum frequency of the five cases for a WPR of 20 %.

Case	TMF [Hz], $L_f = 0$	TMF [Hz], $L_f = 1$	TMF [Hz], $L_f = 6$
1	48.31	48.51	49.07
2	48.02	48.29	49.00
3	48.41	48.63	49.20
4	48.50	48.67	49.15
5	49.02	49.10	49.36

The performance of the cases during the initial frequency dip for the first seconds is presented in Figure 5.6 below.

In Figure 5.6 it can be observed that Case #3 has a lower derivative than the other cases due to its rapid increase of power output after the frequency deviation is created. This shows a need for a fast response and thus to utilize the quick control of the power electronics in an improved manner. Case #5 is a clear improvement in this sense compared to Case #4. In the current situation (see Section 5.3) only 0.3 pu power is extracted from the WT. Thus, there is a lot of capacity of the WT system to deliver extra power from the rotational energy. One can therefore relate the inertia response depending on the power output and rating of the VSWT and its power electronics, a possible adaption to K depending on the current status of the system could be implemented. The different cases present different ways of producing the extra active power during the five evaluated cases and are presented in Figure 5.7. It is important to consider the interaction of the WPR in Figure 5.3 as a factor for this case. The extra power output is being multiplied by 0.2 from the wind farm. Thus, not all of the presented power will influence the frequency but only 20 % of it.

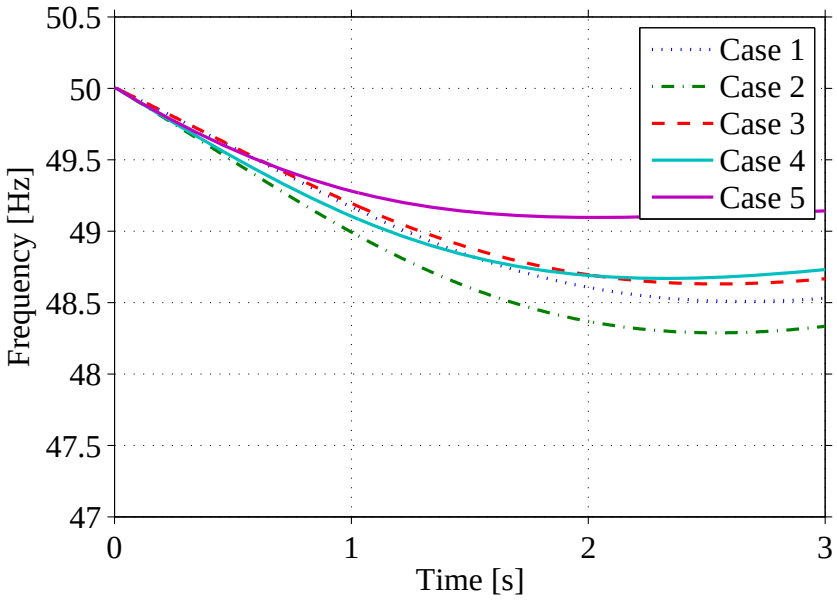

Figure 5.6: A enhanced view showing the different derivatives of the frequency nadir of the simulated cases in accordance with Table 5.1 for a WPR of 20 %.

At the same time as the wind turbine reacts to the frequency deviation the droop and the inertia response from the hydro unit also tries to balance the system, as represented in Figure 5.8 and Figure 5.9 with the droop power and the inertia response respectively.

In Figure 5.8 the difference between the inertia emulated cases can be seen as a higher but slower transition in Case #5 compared to Case #4. The abrupt change in power reference in Case #3 can also be observed mainly in Figure 5.9, which results in a new burst of inertial energy from the hydro when transitioning from A_1 to A_2. This due to the fact that this event is seen from the hydro unit that as a new dip in frequency and lack of power. However, this time without the support from the WT. This results in the second dip (see Figure 5.4).The impact this would have on a higher WPR is presented in subsection 5.4.3. The similar event is when the locked operation window transitions to ordinary maximum-power point tracking (MPPT) at 30 s where a loss of load (load being the P_{re-acc}) is experienced. As we extract rotational energy from the WT the rotor will slow down depending on the strategy used and the how the support strategy is implemented, as can be seen in Figure 5.10.

In Figure 5.10, the behavior of Case #3 and its de-acceleration and re-acceleration areas (A_1 and A_2 respectively) can be observed. Since Case #5 extracts the most energy compared to Case #4 a larger decrease in speed can be observed. The mismatch in speed reference can also be seen at 30 s for Case #3. None of the cases violate the minimum speed of the turbine of 0.7 pu.

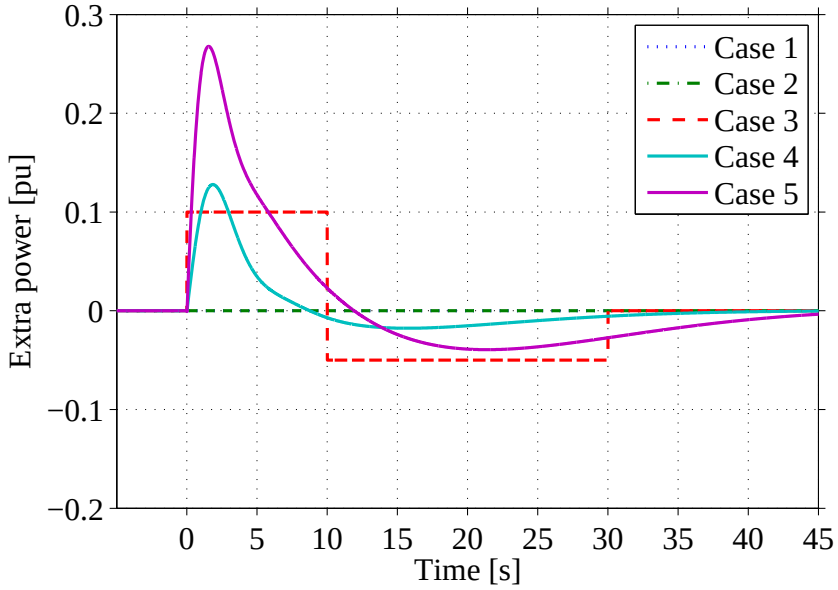

Figure 5.7: Power response from the VSWT for the various cases during a WPR of 20 %.

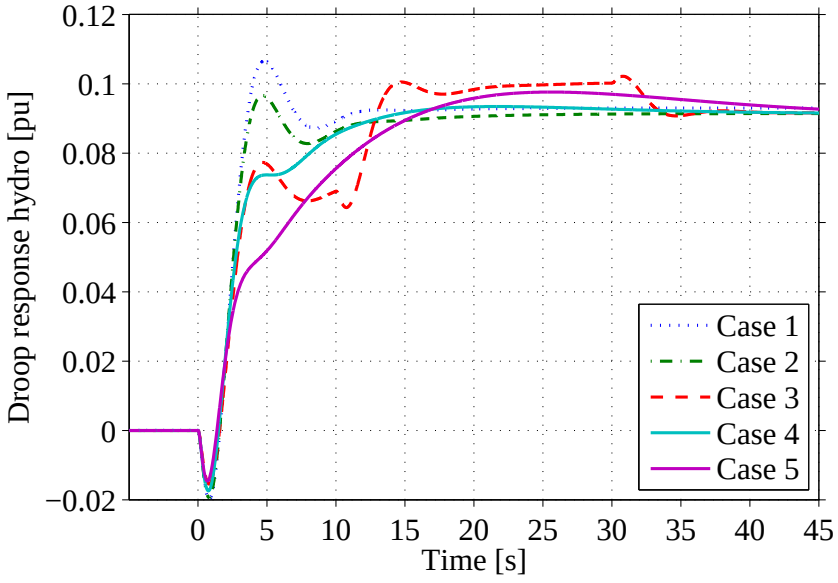

Figure 5.8: Power response due to the droop from the hydro unit with the various cases during a WPR of 20 %.

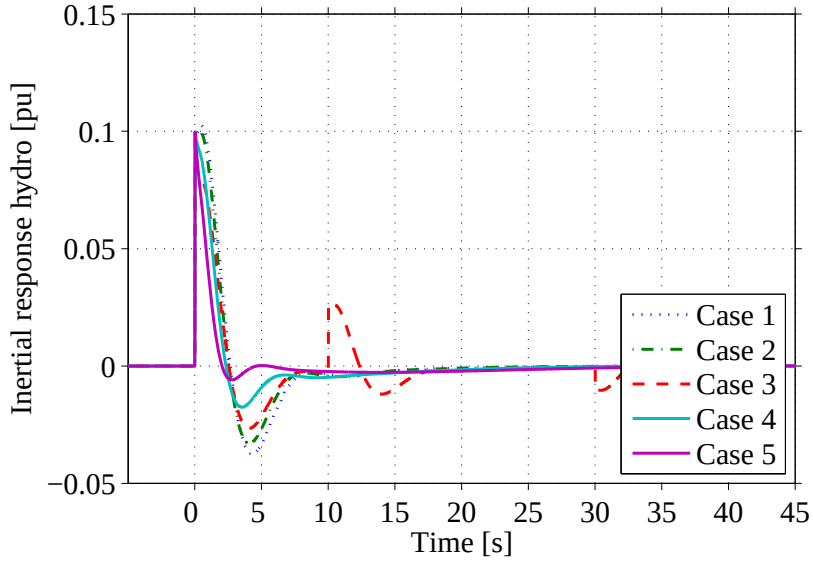

Figure 5.9: Inertial power response from the hydro unit with various cases during a WPR of 20 %.

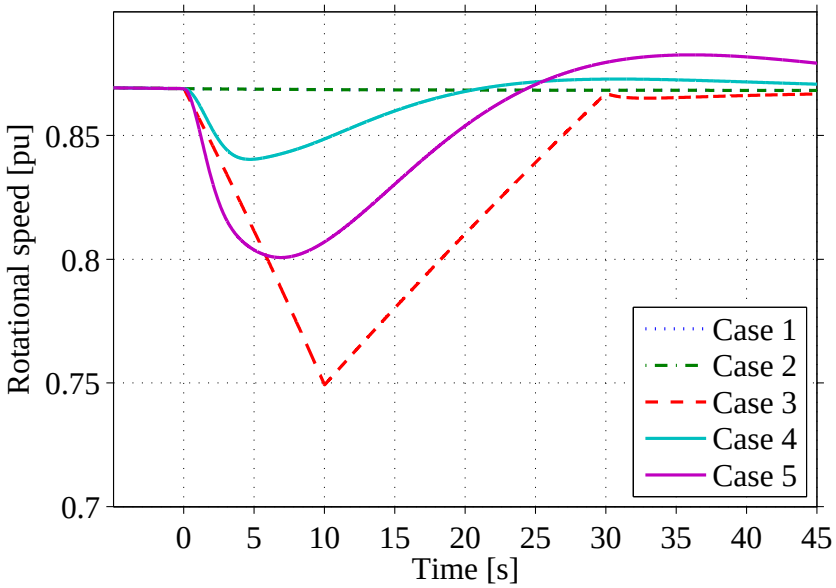

Figure 5.10: Response on the rotational speed of the VSWT during the different frequency support strategies during a WPR of 20 %.

Load frequency dependence

Figure 5.11 shows the result of the frequency dependent load and its interaction during the frequency dip.

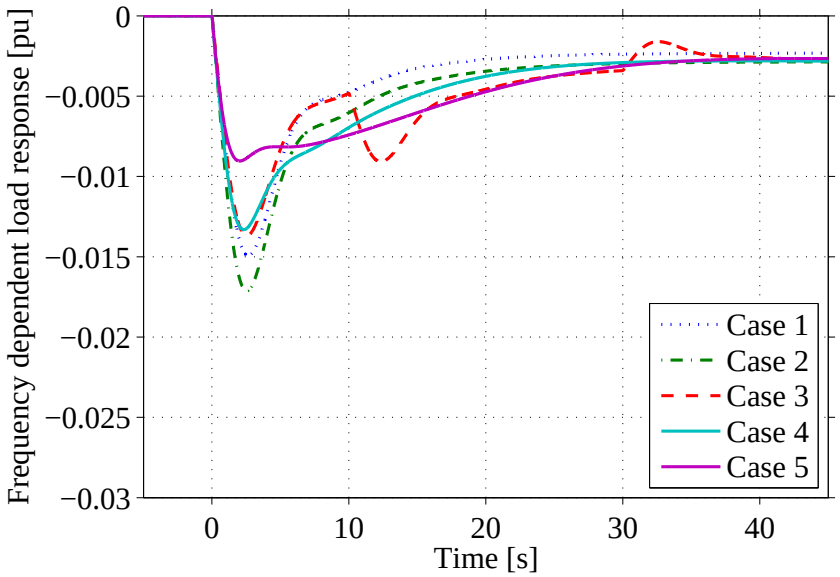

Figure 5.11: The response from the dynamic load model implemented and its interaction during the different cases with a WPR of 20 %.

It can be seen that the frequency dependence of the load is decreasing the power demand as the frequency reduces in the overall system. The frequency nadir is slightly improved compared to the case without the frequency dependent load. [81] states that the evaluated value of the frequency characteristics coefficient (L_f in 5.3) can vary between 0-6. The most common case being L_f = 1 this is therefore used as a base for all simulations. The case of L_f = 6 is also evaluated for the different WPR and the results shown in Table 5.2 as well as in Figure 5.12 in order to show its impact on the TMF. As a comparison an old study (from 1995) of the Nordic system presented a value of L_f = 0.7 during lightly loaded conditions [82].

It can be seen from Figure 5.12 that Case #2 has gained the most from the interaction from the load since the frequency change causes the reduction of power demand. The support from the WT in Case #3 does not depend on the actual frequency change and does therefore perform better than the inertia emulated control strategy represented by Case #4 when L_f = 6. Case #5 however reacts more to the frequency change and performs in the best way of the evaluated cases.

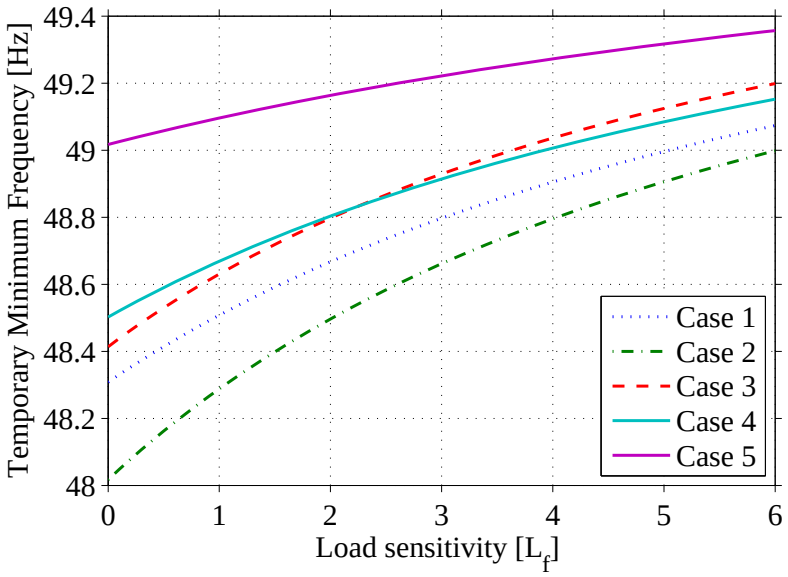

Figure 5.12: The interaction between the frequency dependent load parameter L_f and the temporary minimum frequency of the analyzed cases.

5.4.3 The effect of increasing WPR

Here the impact of an increased WPR of 50 % is evaluated. The axes are fixed to those of the previous sessions in order to allow for the possibility to compare the different frequency nadirs. Similarly to the first test session the system is subjected to a load step increase of 0.1 pu at 0 s and a similar case structure is compared and evaluated.

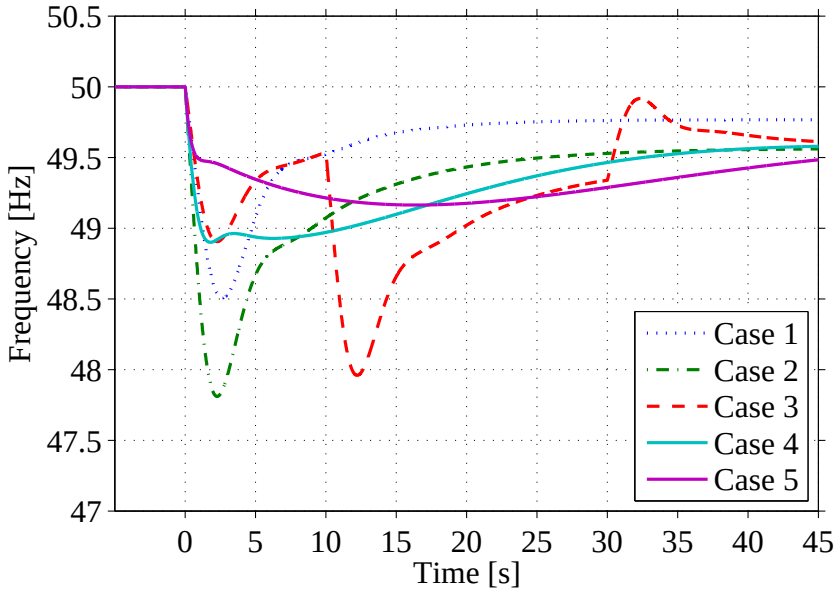

Figure 5.13: The frequency nadir for the simulated cases in accordance with Table 5.1 with a WPR of 50 %.

As expected from the previous tests the secondary dip of Case #3 is much larger here mainly due to the larger amount of mass that has to be re-accelerated as well as a smaller amount of inertia of the hydro system reacting to this second change. The response for Case #1 and #2 shows a level of complexity when comparing the results. Both cases representing a hydro unit but in order to reduce the size of the hydro unit also the permanent droop is increased. This gives a difference in the steady state frequency deviation between Case #1 and the other four test cases, in accordance with equation 5.4.

$$\Delta f = \frac{\Delta P}{D + \frac{1}{R}} \tag{5.4}$$

Where, Δf is the frequency deviation in steady state, D is the load damping constant, ΔP is the load change and R the effective speed droop.

TABLE 5.3: The interaction between the frequency dependent load parameter L_f and the temporary minimum frequency of the five cases for a WPR of 50 %.

Case	TMF [Hz], L_f = 0	TMF [Hz], L_f = 1	TMF [Hz], L_f = 6
1	48.31	48.51	49.07
2	47.33	47.81	48.87
3	47.61	47.96	48.83
4	48.78	48.90	49.27
5	49.10	49.16	49.41

The temporary minimum frequency presented in Figure 5.14 are similar of the events are similar to the case of a 20 % WPR presented in Figure 5.12. Here however the secondary dip of Case #3 (seen in Figure 5.13) causes the minimum frequency instead of the first dip.

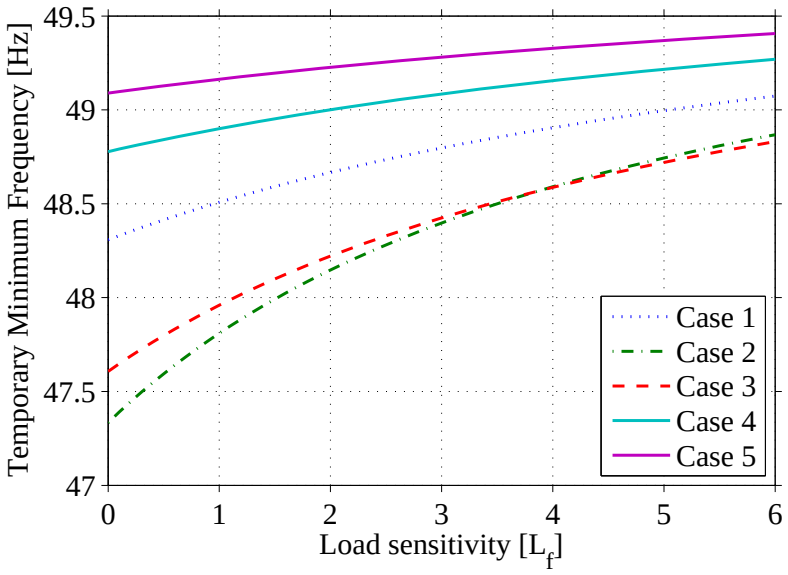

Figure 5.14: The interaction between the frequency dependent load parameter L_f and the temporary minimum frequency of the analyzed cases with a WPR of 50 %.

Even though the initial response is improved for Case #4 and #5 a larger contribution during the first second from Case #3 is utilized. An adaption of the characteristics of the extra power support might improve the performance by the inertia emulated cases. Compared to the previous test session the response from the WT creates a larger impact due to a WPR of 50 % compared to 20 % previously. The response provided by the WT during the power imbalance are presented in Figure 5.15.

Compared to the previous test session (see Figure 5.7) a lower interaction can be observed from the individual turbines due to the increased power input in total from the temporary support in case #4 and #5. However, the steady state frequency droop creates some problems for the

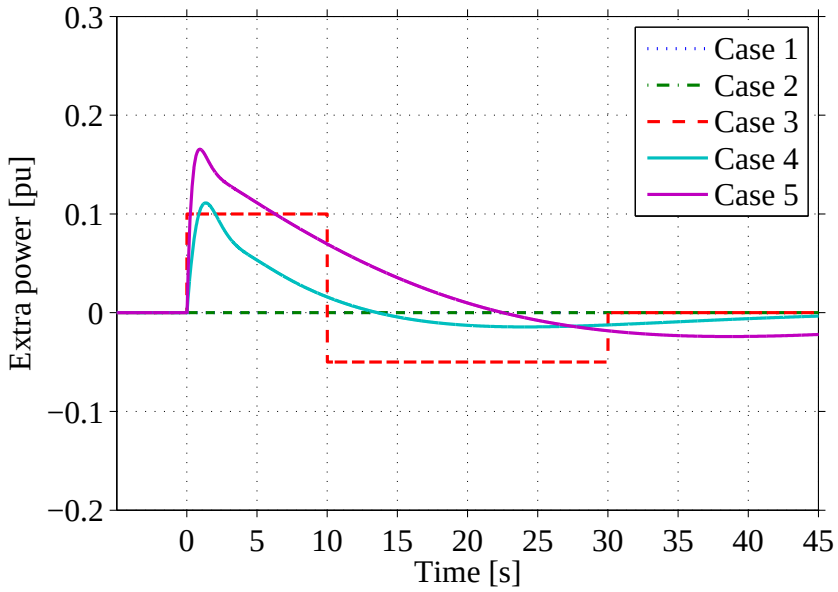

Figure 5.15: Power response from the various cases during a WPR of 50 %.

control system in the two cases creating a slow response. This would however be reduced by secondary frequency control.

5.4.4 Interaction between wind turbine and hydro unit

The support from the WT has a great effect on the hydro unit in the power system, the main support is provided at the time when the hydro output power change is negative. The interaction between the WT and Hydro unit during Case #4 is shown below in Figure 5.16 and compared to Case #1.

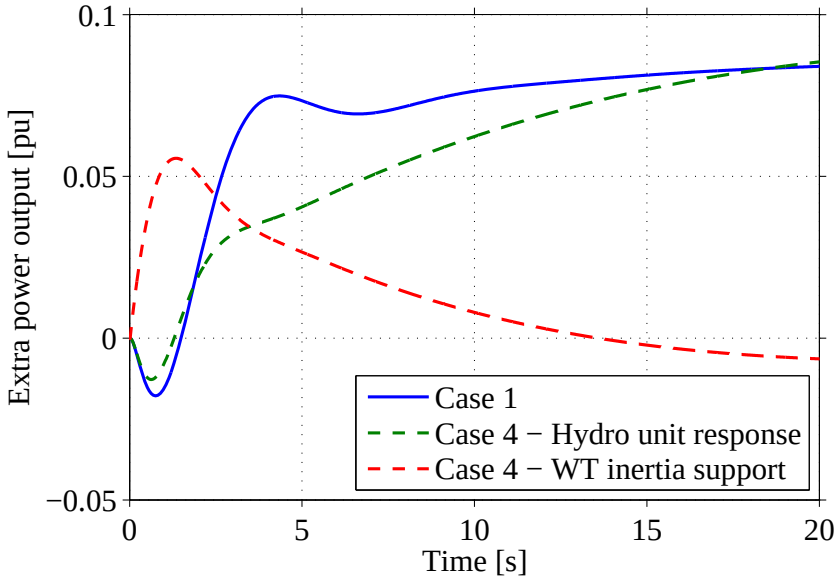

Figure 5.16: The interaction between the hydro and wind turbine in Case #4 during the disturbance and a WPR of 50 % compared to Case #1.

It can be shown that the support from the WT affects that of the hydro at this time. One benefit of the Case #3 structure is that the action of the WT is known for a longer period and could thus, in an already islanded operation, be sent as a signal to prepare the hydro unit mainly for the re-acceleration period of the turbine. Furthermore, Case #3 had several un-wanted characteristics (sharp transition from A_1 to A_2) in its profile these are improved by reducing the shift between de-acceleration and re-acceleration areas. This has been adapted and the result is presented below in Figure 5.17 as Case #6.

Case #6 is an improvement compared to Case #3 and the slopes attached to the frequency support profile shows a clear improvement to the frequency nadir that can be seen in Figure 5.20. The frequency dependence of loads transitioning to or operating in weak power systems should be taken into consideration. However, for stronger networks the affect would be smaller due to the larger inertia of the system, thus the response of a WPR of 20 % is presented in Figure 5.19 and Figure 5.20

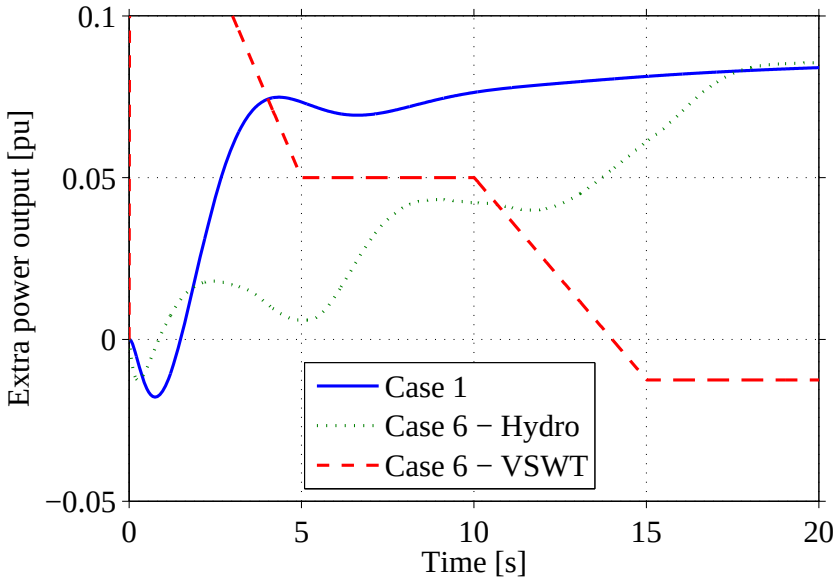

Figure 5.17: Adapted instant power support with extra error signal to the hydro unit for a WPR of 50 % compared to the hydro response of Case #1.

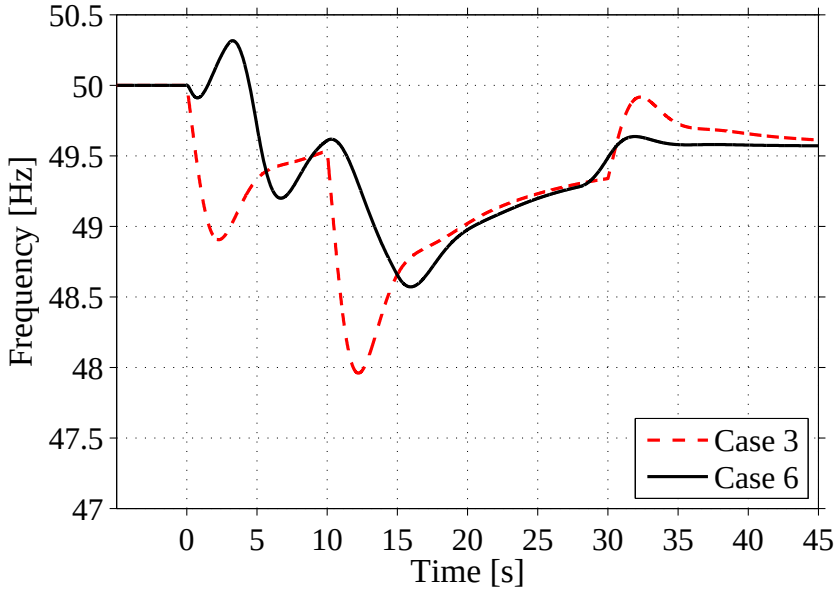

Figure 5.18: Frequency nadir of the two instant power strategies, Case #3 and the improved version Case #6 for a WPR of 20 %.

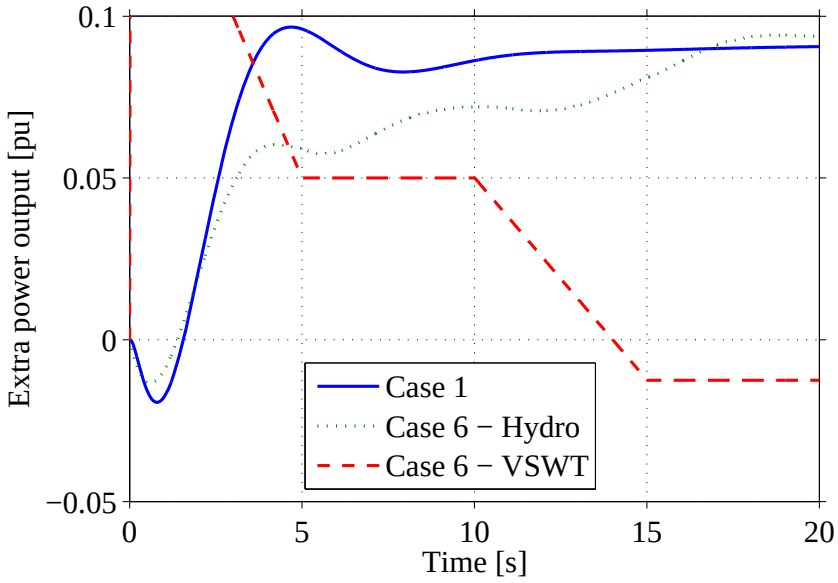

Figure 5.19: Adapted instant power support with extra error signal to the hydro unit for a WPR of 20 % compared to the hydro response of Case #1.

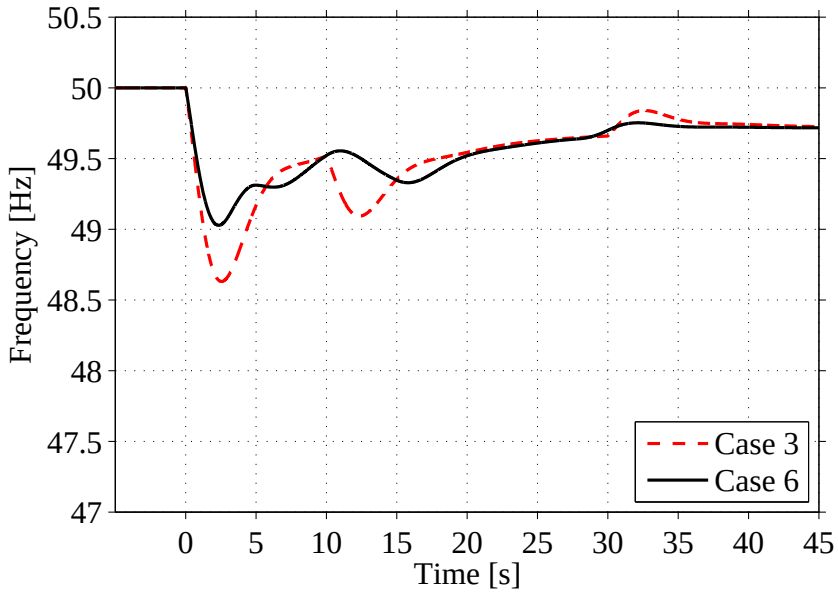

Figure 5.20: Frequency nadir of the two instant power strategies, Case #3 and the improved version Case #6 for a WPR of 20 %.

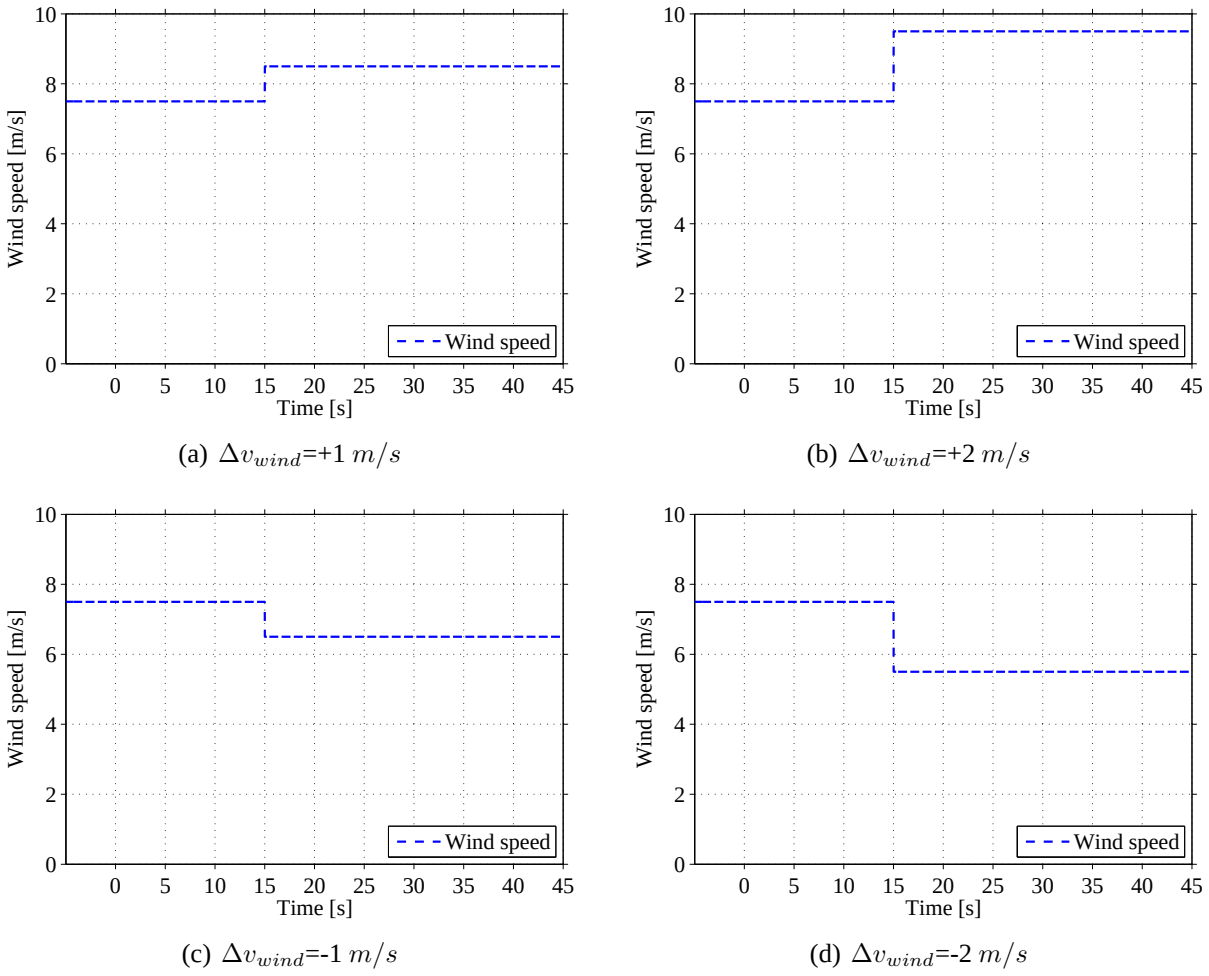

(a) Δv_{wind}=+1 m/s (b) Δv_{wind}=+2 m/s

(c) Δv_{wind}=-1 m/s (d) Δv_{wind}=-2 m/s

Figure 5.21: The different wind steps affecting the wind turbine during Case #3

5.5 Performance during variable wind

For the sake of Case #4 and Case #5, the impact of an increase in wind is not so severe since the control signal is placed on top of the MPPT operation, thus no reconnection or apparent re-acceleration areas are necessary. A smooth operation throughout the time of disturbance is thus obtained even if the mechanical power is decreased. Considering the Case #3 presented it locks the operation of the MPPT of the VSWT during the disturbance. One of the main assumptions is that the wind speed is constant for the duration of the strategy (here for 30 s). This section is meant to evaluate the effect of a wind speed step during the locked operational window of Case #3 and investigate the adoptions possible in order to improve the control strategy in order to handle this. Wind steps as per Figure 5.21 were subjected to the controller using the support structure Case #3, and its response in power output can be seen in Figure 5.22.

For the case of wind increase it can be observed in Figure 5.22 that since the controller expects the re-acceleration time to be constant the controller does not expect the added mechanical power which causes the rotor to accelerate faster, thus the rotation becomes higher than the

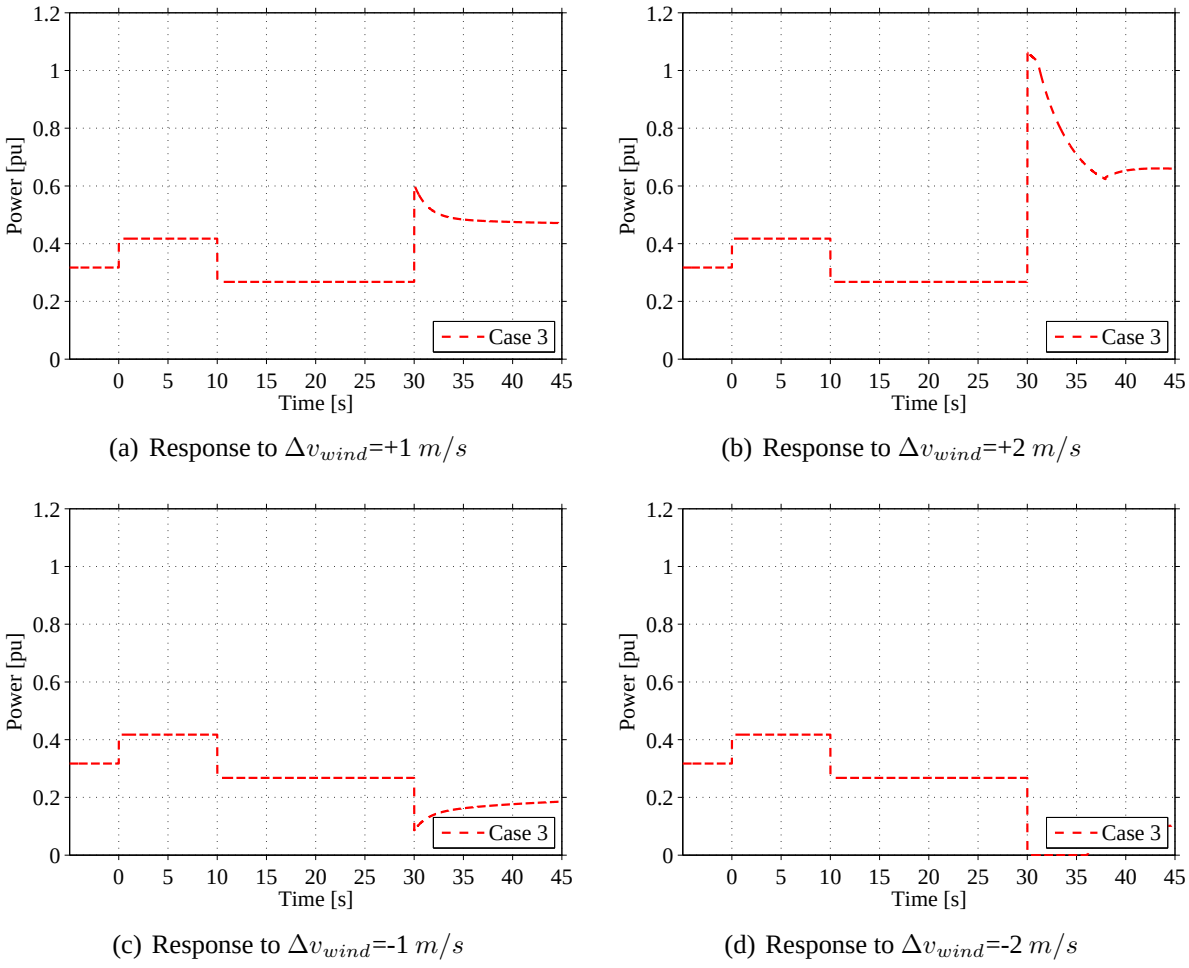

(a) Response to Δv_{wind}=+1 m/s

(b) Response to Δv_{wind}=+2 m/s

(c) Response to Δv_{wind}=-1 m/s

(d) Response to Δv_{wind}=-2 m/s

Figure 5.22: Power output with standard controller

pre-fault value. The speed error to the controller is thus big causing a big power burst when the turbine is de-accelerated down to MPPT-operation. This is done by requesting an increased amount of power from the turbine thus slowing it down similar to an inertia response action, here however it is unwanted since the main use is in the initial seconds of a disturbance. For the case of wind decrease during the locked operation window (when the Case #3 strategy is active) this causes the mechanical power to decrease. This in turn causes the rotation of the VSWT not to increase, even though re-acceleration power is consumed, especially if the wind step is big enough as compared to that of the re-accelerating power. However at this operational point there is no similar necessity for the wind turbine to regain its rotation. This since the wind decrease would any way cause it to reduce its power output to match the lower wind and stay in MPPT operation. Here however the MPPT is deviating too much from its given point and tries to re-accelerate the turbine by consuming power from the grid causing even zero power output for the response to Δv_{wind}=-2 in Figure 5.22(d).

5.5.1 Improvements to handle variable wind

If a wind increase occurs during the locked operation window of A_1 and A_2 in Figure 5.1 the turbine needs to know its pre-fault value of rotation to return to MPPT operation when it has re-accelerated to this value. Further re-acceleration area is not necessary. During a wind decrease, the control system needs to observe the derivative of the rotor speed of the wind turbine if it is negative. If that is the case during the re-acceleration area A_2 (in Figure 5.1), the controller is aware that the wind has decreased sufficiently not to provide its function (of re-acceleration) anymore so a MPPT operation is preferred. A filter on the rotor speed derivative could allow for some temporary wind decrease of the turbine while still operating in the controlled window. This would reduce the number of accidental breaks from the locked operational window. Lastly a very small wind decrease where the mechanical power does not drop as far as to cause a reduction in rotational speed the controller needs to continue to try to re-accelerate its rotor but still jump out of the control structure if not able to do so before $t = t_0 + t_{de-acc} + t_{re-acc}$.

The control structure is presented in Figure 5.23 and the results of it is presented in Figure 5.24. A first order transfer function (time constant $T_{rot-der}$= 1 s, process gain , $K_{rot-der}$ = 1) filters the rotor derivative prior to its evaluation.

The main purpose of the controller is to initially capture initial data P_{e0} (the initial power output) and ω_0 (the initial rotor speed). Then to output the predefined pattern of inertia support. While this occurs the control system evaluates if $d\omega_{wt}/dt$ (the derivative of the rotor speed) is less than zero, if ω_{wt} has reached ω_0 and if the overall time allowed for the locked window of operation is reached. If any of these three stages are valid the controller will break from its locked window of operation and return to MPPT-operation. It is important to note that the transfer from the locked operation window to MPPT-operation is blocked during the delivery of the extra energy for the first de-accelerating time (t_{de-acc}) during area A_1. The reason for this is that if a substantial wind increase ($\Delta P_{mech} > 0.1$ pu) were to occur during the de-acceleration phase, the turbine would still accelerate. This in turn would cause the possibility for the rotational speed to exceed its pre-fault value, such an event should not reconnect the MPPT-operation if temporary. If the wind increase is continuous the power increase will occur after the t_{de-acc}.

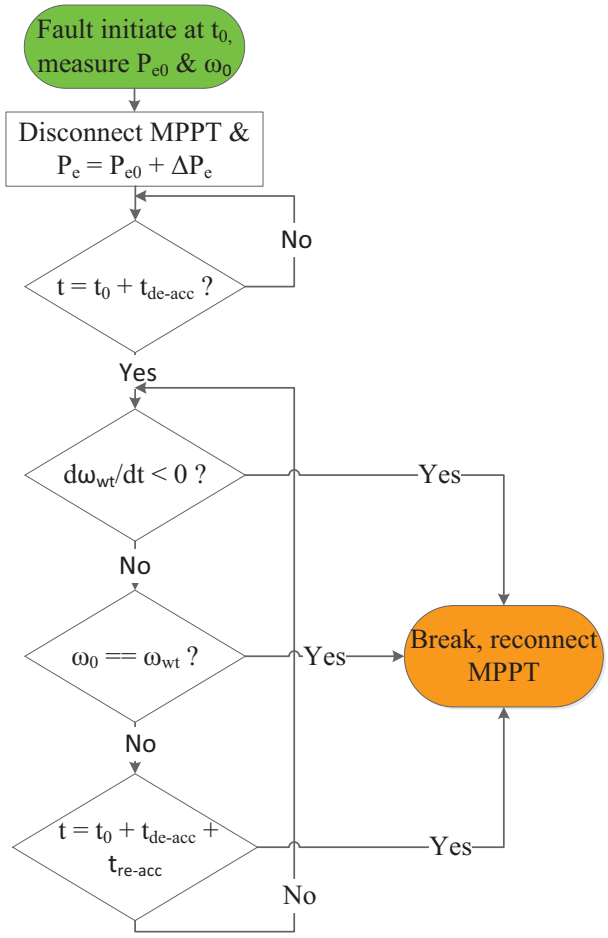

Figure 5.23: Schematics for the improved controller of Case #3 handling both wind increase and wind decrease during the locked operational window of the controller.

For the cases of wind increase (Figure 5.24(a) and Figure 5.24(b)) we can see a clear reduction of the necessary time for re-acceleration during the event. Prior to the change to the strategy clearing back to MPPT-operation at 30 s. A more stable return to the new wind increase can also be observed without any big power deviations during the reconnection of the MPPT.

The wind step decrease occurs at 15 s in Figure 5.24(c) and Figure 5.24(d) and the decrease in rotor speed is detected by the controller and MPPT-operation is continued, mowing the VSWT towards the new operational point with a lower power output. In addition, here a smooth return can be seen without sharp drops in the power output as can be seen in Figure 5.22(c) and Figure 5.22(d).

5.5.2 Verification of adaptation to real wind data

If the controller is subjected to a variable wind speed such as one with average wind of 8.1 m/s seen in Appendix A.3 its behavior of the adapted Case #3 can be observed in Figure 5.25.

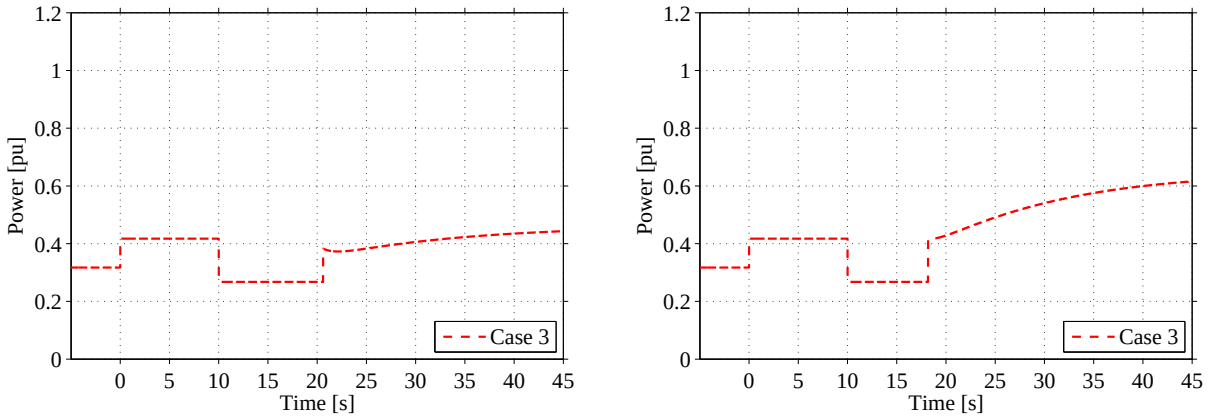

(a) Response to Δv_{wind}=+1 m/s

(b) Response to Δv_{wind}=+2 m/s

(c) Response to Δv_{wind}=-1 m/s

(d) Response to Δv_{wind}=-2 m/s

Figure 5.24: Power output with improved controller

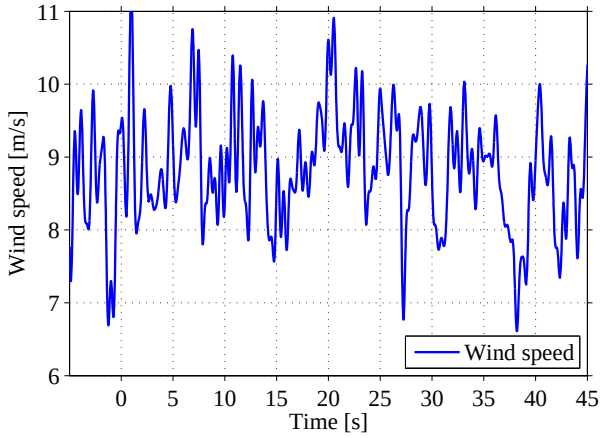

(a) Wind speed

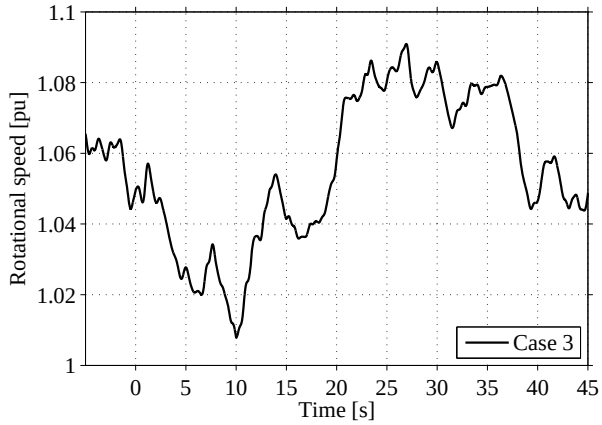

(b) Rotor speed

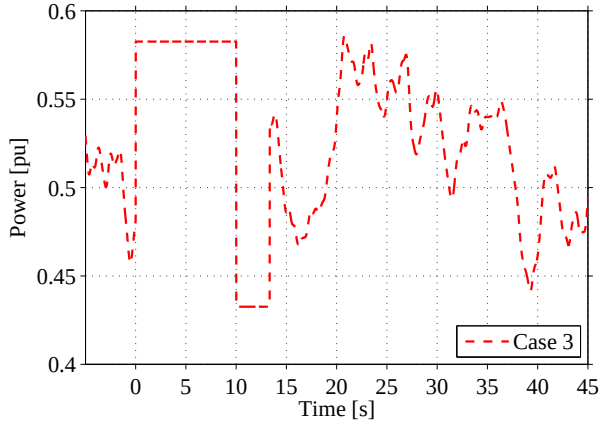

(c) Power output

Figure 5.25: Adapted controller and its performance during wind session 2 in Appendix A.3.

As can be observed in Figure 5.25 the re-acceleration area, A_2, is shortened by the increase of mechanical power during the re-acceleration phase, due to an average wind increase during the period 7-13 s after the activation of the controller. A small dip in the rotational speed (at around 12 s) is observed in Figure 5.25(b). Due to the filter in the controller it does not react to such a small deviation but continues in the locked operation first breaking back to MPPT when the rotational speed has reached its pre-fault value. After the reconnection there is a small period where the output power increases following MPPT-operation before the overall wind decreases again. Notable is also that during the initial seconds of the activation of the support strategy we see an increase of the rotor speed above the pre-fault value, however the controller is set to deliver the full 10 s of 0.1 pu extra power and since the rotor speed at 10 s is not up to pre-fault the re-acceleration is started.

5.6 Conclusions

The improvement of the frequency nadir by 1 Hz from Case #2 to Case #5 has been presented in the case of 20 % WPR considering a non-frequency dependent load. To extract extra energy quickly is a benefit of a VSWT and the inertia emulation support should also be designed in accordance with these possibilities. The frequency dependence of loads transitioning to or operating in weak power systems should be taken into consideration. However, for stronger networks the affect would be smaller due to the larger inertia of the system. Future VSWT will utilize the inertia emulation strategies; however it is of great interest to investigate how this energy should be extracted. The extra active power supported needs to be activated as soon as possible but still depend on the frequency and the outlook of the system. Even if Case #3 has its downsides it also provides the knowledge of what will happen for the 30 s while it's active. A coordinated control between the hydro and wind turbine in this case could solve the issues of a second dip especially for Case #3 where the behavior of the wind turbine is predefined and could thus be known for the hydro governor. The interaction in islanded systems between the different production units in a smart grid could improve the behavior during a load mismatch or when the transition to islanded operation occurs. However, this needs to be investigated further. The behavior of the load demand due to supply voltage should be evaluated since a temporary voltage reduction over the load could improve the frequency behavior further by reducing the load power.

5.6.1 Variable wind conclusions

The improvements to the instant power support strategy to contribute with inertia support during variable wind is evaluated and determined. The controller is improved and its adaption presented and evaluated through fixed step in wind speed. To evaluate the filter of the rotational derivative is vital for it to handle variable winds and should be evaluated in future research. The benefit of being able of acting on the market is however still very important, a fixed amount of power support could be sold and traded on a market that allowed for such an action.

Chapter 6

Frequency control strategies from wind plants

6.1 Introduction

The potential area for contributing with control measures from VSWT is not only valid during large power imbalances such as the disconnection of generators or loads. During high levels of WPR and low inertia in a power system the variations in power output from the VSWT can be a cause of frequency fluctuation. Attention to frequency fluctuations has been given in several publications, a brief summary is presented below.

[83] presents recommendations on frequency control in power systems with high WPR (around 50 %) through the use of delta control which means that the avalible wind power is estimated and a fixed limit under this value is set as the power output. Even though this causes relatively large amouts of power to be spilled, the presented case utilizing a 20 % delta control proves to provide large improvements to the minimum frequency of the power system during the simulated time of 700 s. The backup units[1]utilized in the model are consisting of a mix of gas, steam and diesel units. [84] uses a variable droop concept of the interaction between the power system frequency and the wind turbine, the droop is changed from 2 % to 6 %. A rather high inertia constant (10 s) was simulated in the power system, frequency control came from from a diesel generator (with fairly fast response time), thus large frequency variations where not seen in the overall simulation time of 450 s. The paper contains several meaningful discussions regarding the setting of the droop parameter and thorough discussions on the results of the proposed controllers.

Lastly [85] presents an islanded power system operating in a 2:1 wind power to load ratio, where no other generation is affecting the system behavior after the disconnection of a circuit breaker. Several wind speeds are evaluated for a simulation time of 300 s. The paper base several control signals on the available wind to the turbine, which can be difficult to estimate. Both reactive power and active power control is provided during the simulation window.

[1]The term backup units is referred to as the power production units in the power system in charge of frequency

Interesting contributions to these articles are the difference depending on the type of generation unit that is responsible for the main frequency control. Furthermore, the interaction due to delays in the control system as well as the dead band settings needed for a frequency responding VSWT should be evaluated. This chapter is focusing on low inertia power systems with high wind penetration, real wind data of different wind speeds, various generation units responsible for frequency control (through AGC) and possible support strategies from VSWT and their effect on the power system frequency. The focus will be on the frequency variations caused by the wind variability and thus the power fluctuations.

6.2 System modeling

The generation units and their models are presented in Chapter 4. In this section a case setup and added functions to the power control and pitch control will be presented. Dead band and delay settings are investigated and a sensitivity analysis due to these parameters are investigated before evaluating the power response possible from a VSWT in islanded operation with a WPR of 50 % similar to the system studied in Section 5.3 but with alternating backup generation. However the section starts with the acquirement of wind data to the aerodynamical model (see Section 6.2.1) and tuning of AGC (see Section 6.2.2).

6.2.1 Wind data

Wind data was acquired from wind measurements in southern Sweden (farmland) where wind turbines were already in place. The anemometer was installed at the top of a measurement mast at a height of 30 m where wind speed measurements were acquired at a sampling rate of 4 Hz. The wind speeds are then transferred to a hub height of 90 m (though it is site dependent) of the GE 3.6 MW turbine modeled by using the Hellmann approach [86] seen in 6.1 using α=0.20.

$$v_{wind,h} = v_{wind,ref}\left(\frac{h}{h_{ref}}\right)^{\alpha} \tag{6.1}$$

Where $v_{wind,h}$ is the wind speed at height h, $v_{wind,ref}$ is the wind speed at the measured height h_{ref} and α is the Hellmann exponent.

The wind speed measurements are divided into four different wind speed sessions after being converted to hub height and are presented in Table 6.1

control, excluding any VSWT with that added functionality.

TABLE 6.1: The different wind speed sessions to be evaluated in the case setup for the frequency controlled VSWT. The wind profiles can be seen in Appendix A.3.

Wind speed session [#]	Average wind speed [m/s]
1	7.36
2	10.24
3	12.84
4	14.63

The wind speed is averaged out across the swept area of the rotor of the WT utilizing a linear filter $H_{\psi,0}(s)$ obtained from [87], that was also used for similar applications in [88]. The filter is presented in 6.2 below:

$$H_{\psi,0}(s) = \frac{0.99 + 4.79ds}{1 + 7.35ds + 7.68(ds)^2} \tag{6.2}$$

where s is the Laplace operator, d = R/V_0 where R is the radius of the rotor and V_0 is the average wind speed for the simulated time. The filtered wind data is linearly interpolated to fit the discrete time steps of the simulation of 100 Hz. The entire procedure from measured wind speed to the input of the simulation can be seen in Figure 6.1 and the result from the output of the filter is depicted in Figure 6.2.

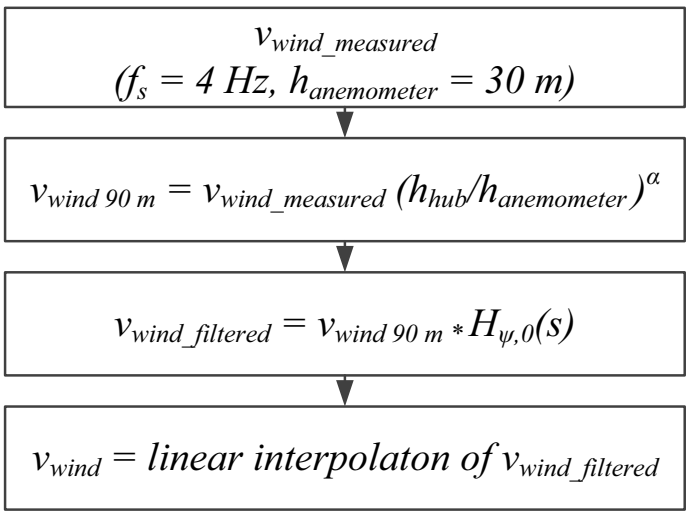

Figure 6.1: The procedure of acquiring wind speed data for the model. Starting from measured wind speed data, shifting it to hub height and filtering it prior to input to the VSWT-model.

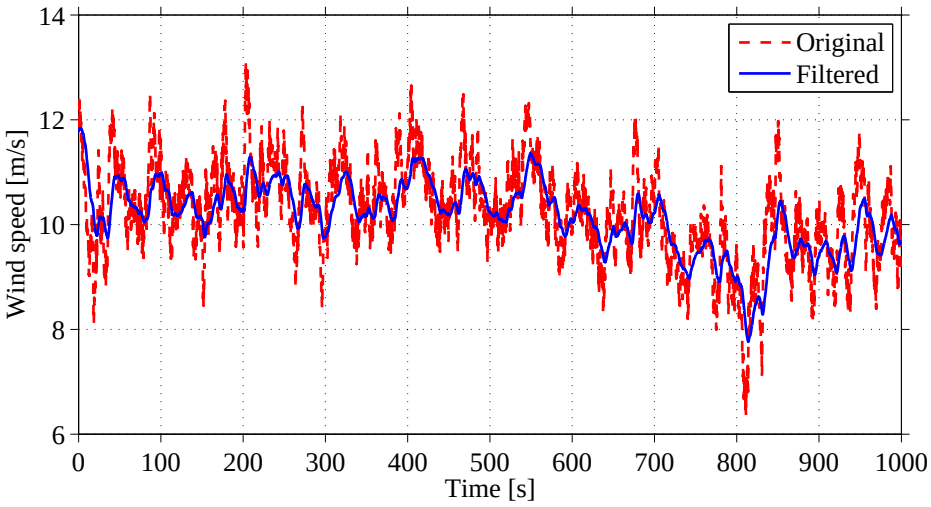

Figure 6.2: The filtered and unfiltered data of wind speed session 2 with an average value of 10.24 m/s at a hub height of 90 m.

It can be observed in Figure 6.2 that the utilized filter has a large impact on the variations of the wind speed implicating that the use of an unfiltered wind speed would result in a larger power variation from a modeled VSWT than a filtered wind speed.

6.2.2 AGC-tuning

In order to return to nominal frequency during the simulation the AGC are individually tuned for each generation system presented in Section 4. This results in different AGC settings for the various generator units, which should perform as stable as possible in order to balance a power system with high wind penetration. A power system based on a certain type of generator unit could then prove to handle a high WPR better than others, due to the fact that a more rapid response (see Section 4.3) would be preferred in order to balance power fluctuations. The integrators (K_{agc}) of the generation units where tuned using the method of pole placement, previously utilized in power system applications by for example [89],[90] and is explained in detail in [91]. The AGC is modeled as presented in Figure 6.3. The result of the pole placement can be seen in Table 6.2.

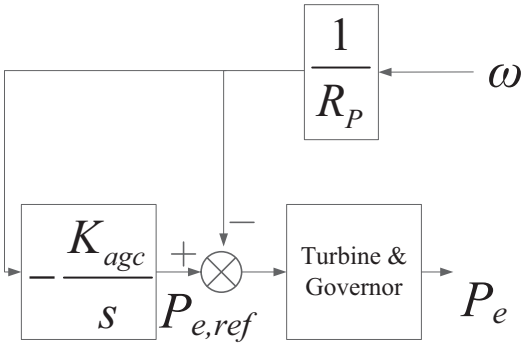

Figure 6.3: A schematic overview of the AGC adjusting the power reference through the use of the integrator constant K_{agc}.

In Figure 6.3 the R_p is the droop of the investigated generator (R_H,R_{RH},R_{TH} in Section 4) and K_{agc} is the integrator constant of the AGC. The result of the pole placement can be seen in Table 6.2.

TABLE 6.2: Parameters for the AGC controller presented in Figure 6.3.

Generation unit	K_{agc}
Hydro	3.4
Reheat	4.2
Thermal	7.0

From Table 6.2 it can be seen that the Thermal unit has a largest K_{agc} of the generators modeled, this would further imply a larger, more force full reaction to frequency deviations for this specific unit in comparison to the others.

AGC tuning for Hydro generation

In this section a short presentation of the results of the pole placement for the hydro unit is presented. The most interesting poles (closest to the real zero axis) are illustrated in Figure 6.4. The pole placement and the transfer functions of the other generators are presented in Appendix A.2. The response for a change in frequency due to a change in power for the hydro unit is presented in 6.3.

$$\frac{\Delta P_L}{\Delta f} = \frac{1}{(D+2Hs)\left(1+\frac{R_p\left(\frac{1}{R_H}+\frac{K_{agc}}{s}\right)(1+T_R)(1-0.5T_w s)}{(D+2Hs)(1+T_{GH}s)(R_p+R_T T_R s)}\right)} \tag{6.3}$$

The poles of the unit is iterated by increasing K_{agc} from zero, indicated by green circle in Figure 6.4, until the most beneficial point has been reached. For the modeled hydro unit the poles are initially close to the Re(poles)=0 but as the integrator constant increases they move

further away indicating a more stable region. However the top and bottom poles are moving towards a more unstable region, thus indicating a limit to the size the variable. K_{agc} was chosen to 3.4 for the hydro unit as depicted with a red circle in Figure 6.4.

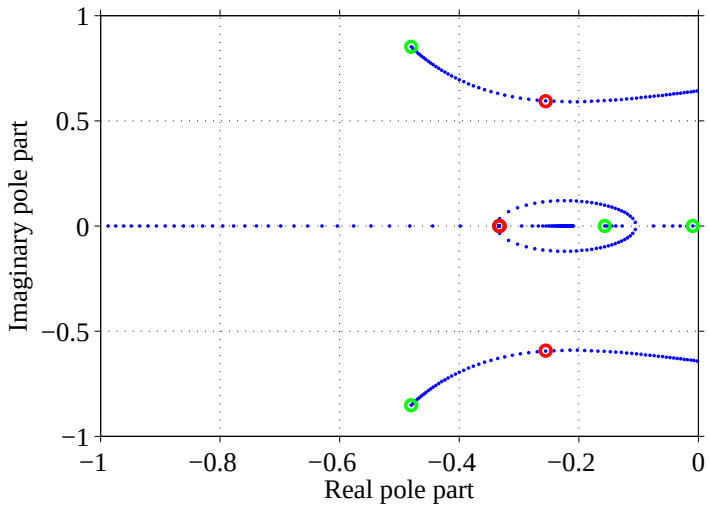

Figure 6.4: Pole placement strategy for the AGC of the hydro unit and the chosen integrator gain noted by red K_i=3.4, green circle showing the performance without integrator.

For the sake of frequency control it is important to evaluate the wind session creating the largest impact on the power output of the VSWT. Considering the low wind speed sessions, where the VSWT is working at an maximum power point (MPP) it would not provide a big step in power output during a wind increase considering that the output power is proportional to the cubic of wind speed. During high wind speeds over 11.2 m/s the turbine starts to pitch in order to limit its mechanical power. A wind increase in that region is met with an increased pitch angle thus not creating an increased power output. The wind speed to be evaluated should thus be the one with an average wind speed of 10.24 m/s (wind speed session 2) presented in Figure 6.2, the other wind speed sessions are presented in Appendix A.3. The evaluation of the impact of the various wind speed sessions were conducted utilizing a 50 % WPR and a hydro unit reposigle for the AGC. The VSWT simulated did not provide any frequency regulation to see the impact of average wind speed level on the variations in frequency. The empirical probability distribution can be seen in Figure 6.5.

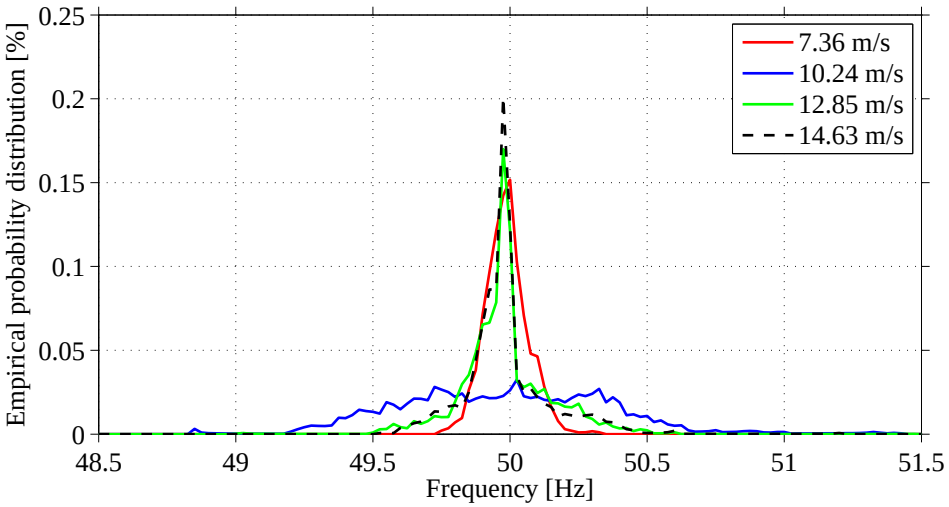

Figure 6.5: Empirical probability distribution of power system frequency with various wind speed sessions from Table 6.1.

It can be observed, from Figure 6.5, that as expected the wind data with an average of 10.24 m/s is by far the worst seen from a hydro unit out of the four wind speed sessions. It is thus chosen as the base case for the various methods of improving frequency quality by utilizing frequency control by VSWT. It can also be seen that the higher wind speeds cause more occurring under frequency deviations. This is due to the fact that a positive derivative in wind speed is mainly balanced out by the pitch actuator and is therefor not providing any change in power output. However, when the wind speed decreases and goes below 11.2 m/s a more apparent drop in output power from the VSWT cause a more evident drop in frequency before the reaction of the, in this case slower, hydro governor in order to balance the power system.

6.2.3 Various generation units frequency regulation during 50 % WPR

In order to evaluate the response time and ramp-rates of the various generation units they were all subjected to 50 % WPR and an average wind of 10.24 m/s as discussed in Section 6.2.1

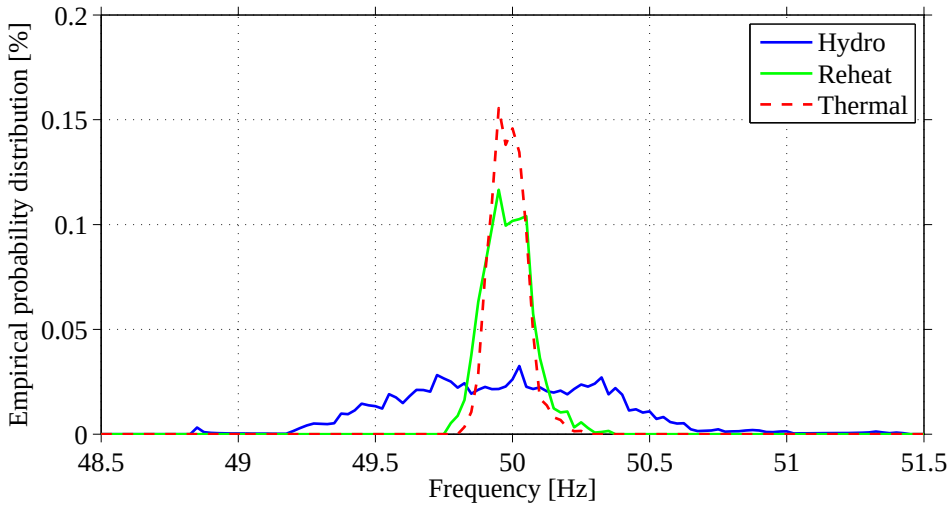

Figure 6.6: Empirical histogram of the frequency during normal operation of VSWT at an average wind speed of 10.24 m/s.

It can be observed from Figure 6.6 that the hydro unit performs in a worse manner than the reheat and thermal-unit during the WPR of 50 %. The actual power output during the evaluation period is presented below in Figure 6.7.

From Figure 6.7(a) the power produced is noted to be very similar for the various generation units, the differences still exist and cause the larger differences considering the variations in the frequency behavior presented in Figure 6.7(c).

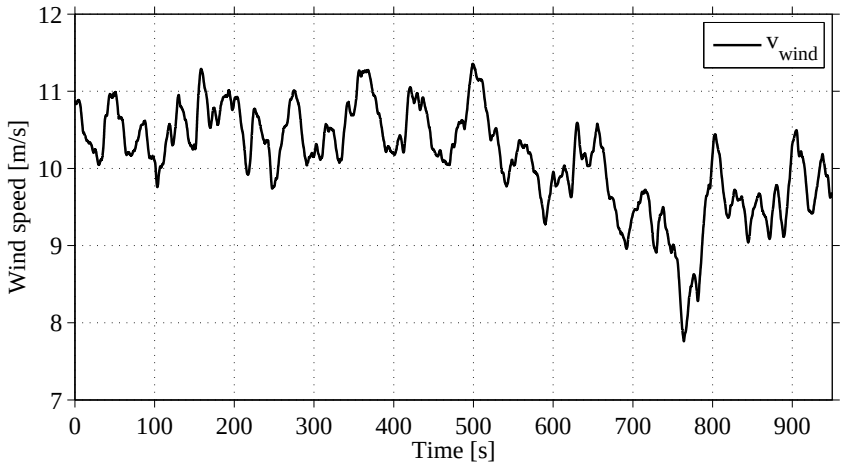

(a) Wind speed subjected to VSWT in default configuration.

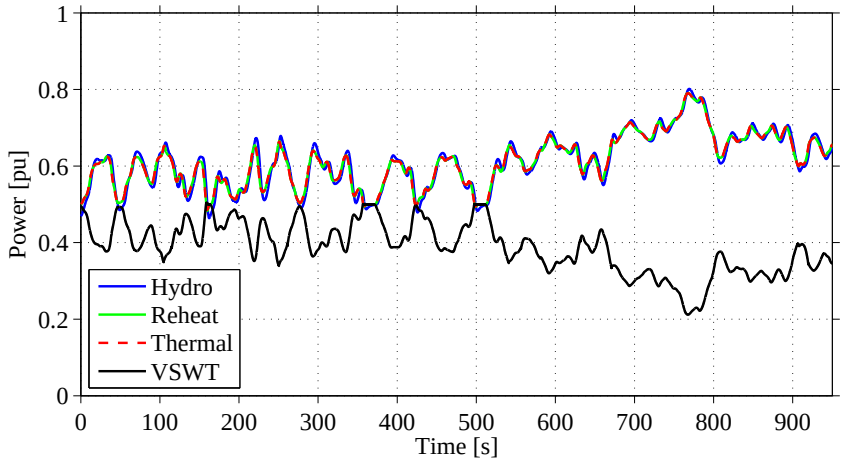

(b) Power output from respective generator.

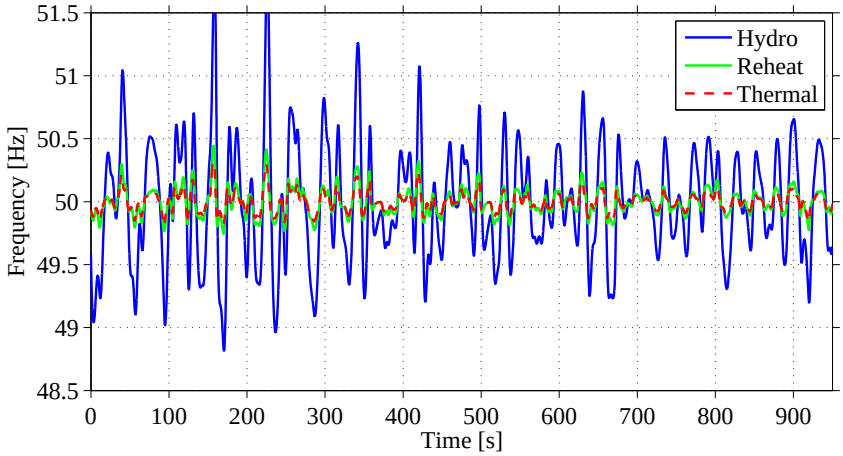

(c) Frequency during the various types of backup generation.

Figure 6.7: The response from the generation units to a VSWT subjected to wind speed session 2.

6.3 Frequency control strategies for wind plants in island operation

Several of the discussed controllers in Section 6.1 utilize the energy for accelerating or de-accelerating the rotor, this pushes the VSWT to operate at operating points away from what is optimum causing the spillage of wind. The energy produced during the operational window is therefore evaluated as a consequence. Limitations such as dead band setting to any control algorithm on frequency control are of interest and are therefore presented prior to the sections on frequency control that include sensitivity analysis of both dead band and delay.

Dead band

The dead band decides how often a generation unit should interact towards the system frequency. After a short literature review on settings of dead band of the controllers are set to 50 mHz, (0.001 pu). Typical values are presented to $\pm$ 10 mHz (0.0002 pu) according to [92] for a 50 Hz system. In [93] and [94] the Electric Reliability Council of Texas (ERCOT) present their impact of decreasing their dead band strategy from $\pm$ 0.036 Hz (0.0006 pu) to $\pm$ 0.01666 (0.00028 pu) Hz on 60 Hz system frequency. ERCOT also alters their design from a step response droop characteristic, implying that a step is incorporated into the droop characteristics, towards a non-step response design but with the previously mentioned lower dead band. The North American Electric Reliability Corporation (NERC) also considers $\pm$ 0.0006 pu as a typical limit [95]. A more recent publications regarding BESS and its contribution to frequency support considers a $\pm$ 0.001 pu dead band [96]. National Grid (UK grid code) restricts the frequency dead band to $\pm$ 0.015 Hz in frequency sensitive mode (FSM) [97] and EirGrid has a similar restriction [98]. The old grid code considering the NPS allowed for a dead band of $\pm$ 0-50 mHz on large thermal generators [27].

6.3.1 Droop control

Droop control strategies are a common way to allow multiple generators to interact towards the stabilization of the grid frequency. Here the quick action of the power electronics is utilized through a steeper droop than that of the other generator units.

For example, a 5 % droop (as utilized here by all governors) or regulation means that a 5 % frequency deviation causes 100 % change in valve position or power output. This is a common setting for generation units capable of acting on frequency deviations. For the cases were the VSWT is used to repond to frequency a quick response in contrast to the other units in the power system is preferred. During a disturbance of $\pm$ 5 % with a $\pm$ 0.2 pu extra power output (ΔP_{wt}), seen in Figure 6.9, thus R_{wt} is set in accordance to 6.4.

$$R_{wt} = \frac{\Delta f}{\Delta P_{wt}} = \frac{0.05}{0.2} = 0.25 \tag{6.4}$$

The implementation of the droop controller into the structure is presented in Figure 6.8 and its implications on power output illustrated in Figure 6.9. The P_{droop} signal is the added to the P_e-signal of the VSWT in Section 4.1.1 in Figure 4.3.

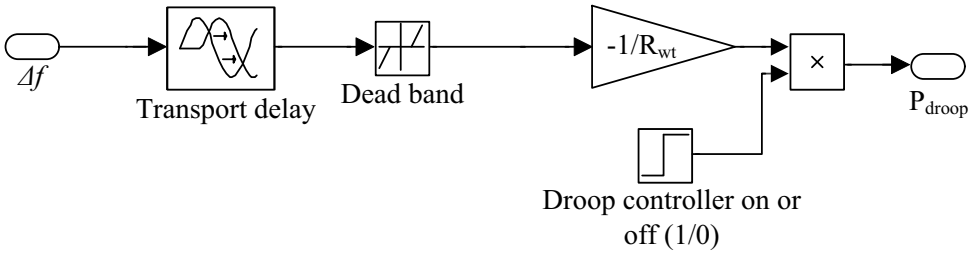

Figure 6.8: Droop controller implementation in overall structure.

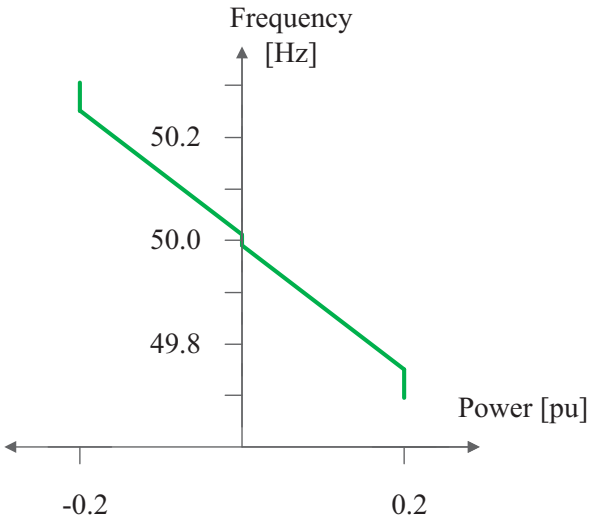

Figure 6.9: Tuning of droop controller and slope.

Droop controller - Delay parameter sensitivity

The delay parameter is implemented in order to make a drastic simplification of the acquiring of a frequency signal. Either if this is by a moving average window as presented is Section 3.2.1 in Figure 3.1 or by using a circular buffer[2]in order to create an average frequency signal. The impact of signal delay could also be incorporated into this delay, especially considering a centralized frequency measurement that through supervisory control is sent to the VSWT in order to get an identical response from several turbines distributed throughout a possible power system.

The droop controller was subjected to a simulated frequency signal increasing from 50 Hz to 51 Hz with a ROCOF of 2 Hz/s. The response signal is presented in Figure 6.10 together with the change in the frequency signal in pu.

[2]For more information regarding circular buffers see p. 506-507 in [99].

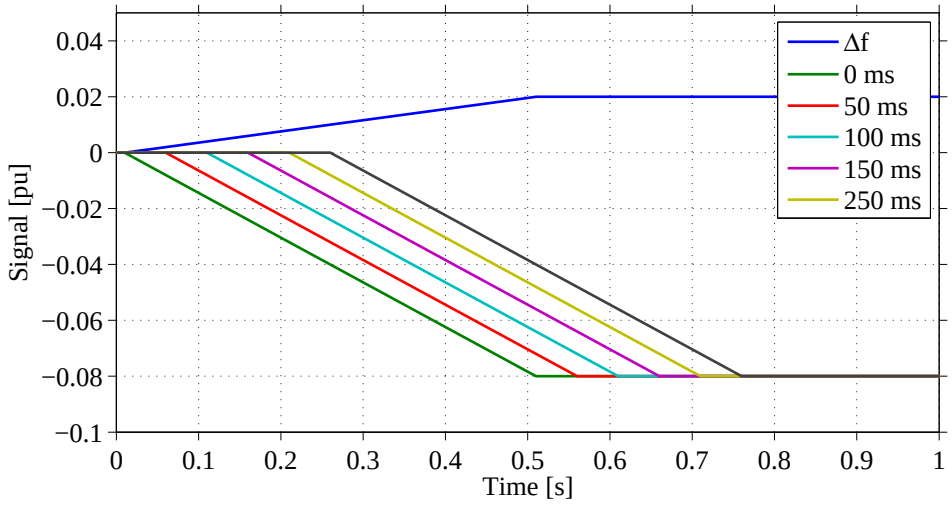

Figure 6.10: Delay parameter sensitivity and the simulated frequency signal and the impact on P_{droop}-signal.

Droop controller - Dead band parameter sensitivity

Several dead band settings were presented in Section 6.3. In order to evaluate the severity of an erroneous or to high setting of the dead band a sensitivity evaluation was performed on the controller and the results are presented below in Figure 6.11.

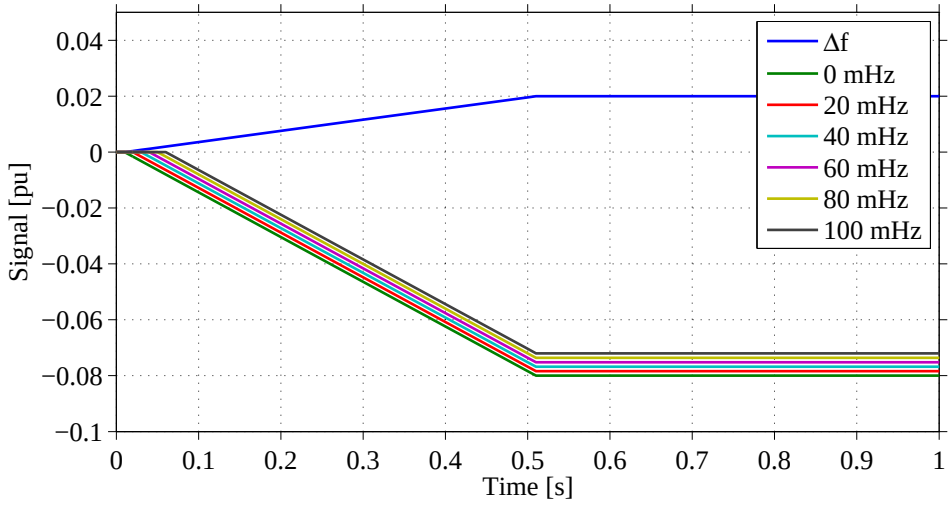

Figure 6.11: Dead band parameter sensitivity and the simulated frequency signal and the impact on P_{droop}-signal.

Parameters for the controllers are chosen as can be observed in Table 6.3.

TABLE 6.3: Parameters for the frequency respondent controllers.

Parameter	Value
Dead band	50 mHz
Delay	100 ms

In Figure 6.11 it can be observed that the way the dead band is constructed it acts in a similar way as the delay. However added to the behavior is also an offset error to the power request of the controller. This since the output of the dead band controller is an offset of that of the dead band limits.

6.3.2 Frequency controlled pitch actuator (FCPA)

Since over frequency is a reoccurring event, observed in the frequency studies of the NPS as seen in Chapter 3 a frequency controlled pitch actuator (FCPA)(see Figure 6.12) is considered as a process to decrease the over frequency events in the power system during constrained times of operation. The pitch actuator is however slow compared to that of the power electronics in the VSWT controlling the power output. A situation of over frequency, causing pitch to increase thus lowering the C_p of the VSWT, followed by a decrease in wind speed could cause a much more severe power decrease from the VSWT with a FCPA than a VSWT without the FCPA function.

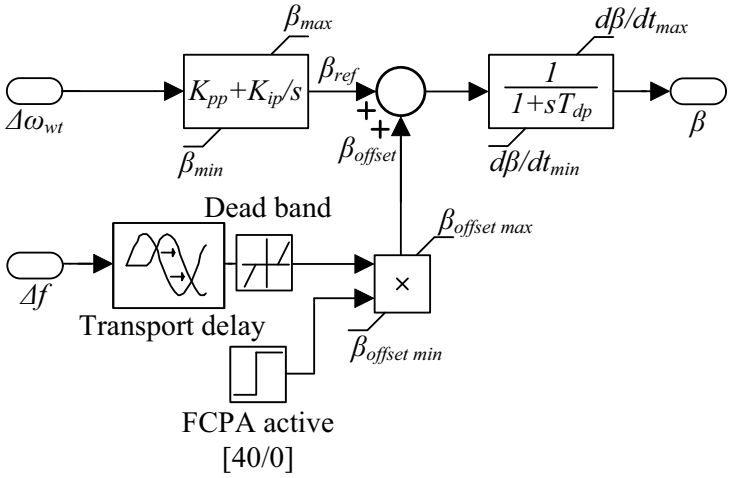

Figure 6.12: Frequency responding pitch actuator.

The incoming change in frequency (in pu) is multiplied with a constant gain of 40, this after providing various 1000 s wind data series with a average wind ranging from 5 m/s - 16 m/s into the simulation. This value resulted in the most promising result seen to the increase in frequency quality over the entire wind spectra. The signal β_{offset} is then fed through and added to β_{ref}, limitations $\beta_{offsetmax}$ = 10 and $\beta_{offsetmin}$ = 0. Presented below are the various operational points during the wind speed session #2 chosen in Section 6.2.1 together with the droop frequency controller presented in Figure 6.8.

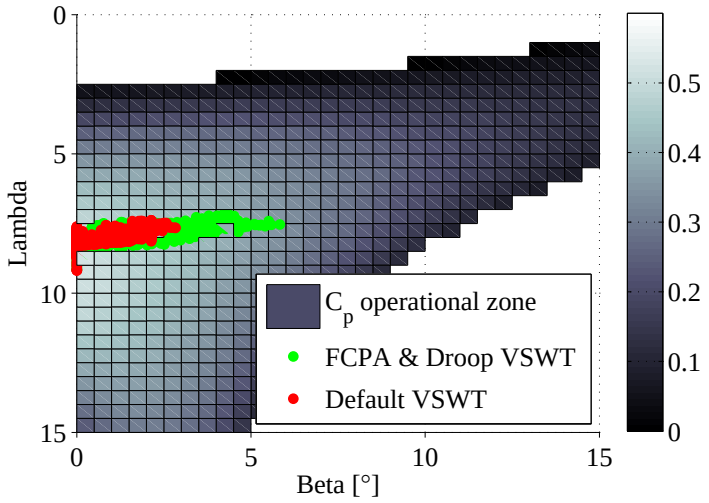

Figure 6.13: The introduction of FCPA and its effect on operational points of VSWT during active droop controller. For a 3d-curve see Figure 4.1.

It can be observed from Figure 6.13 that the operation points are extended throughout the β-axis. This together with the droop controller causes a wider spread of operation points over the C_p-plane. The implications this has on the energy that actually can be sold will be further analyzed in Section 6.4.

6.4 Droop controller and FCPA - In islanded power system

It can be seen from Figure 6.13 that the impact of the FCPA causes the VSWT to operate at higher pitch angles more often then without it as expected. It is important that since both speed and pitch is utilized to control the frequency at the same time this reduces the deviation from the MPP of the turbine compared to when the controls are used separately. The results of the FCPA combined with the droop controller is presented in Figure 6.14 and cause an increased frequency quality compared to the case without frequency support from the VSWT. This can further be seen in a histogram of the frequency during 950 s in Figure 6.15.

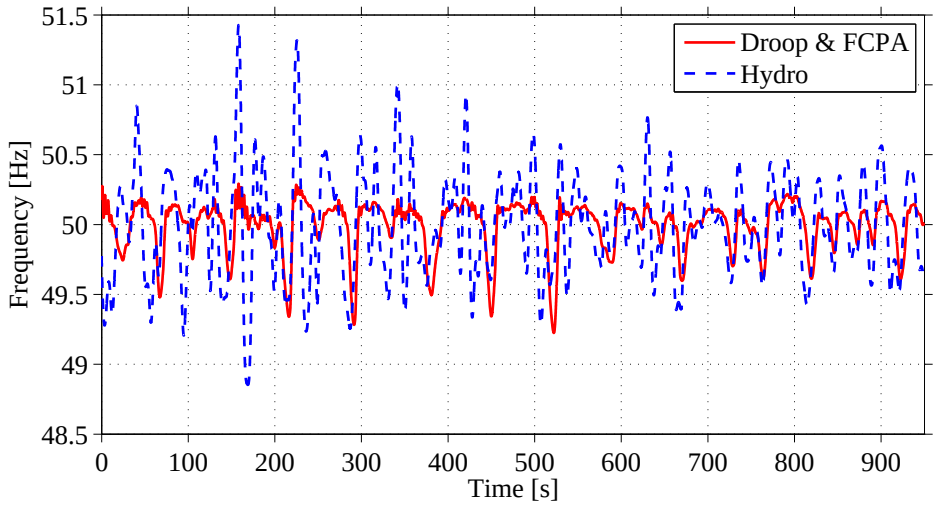

Figure 6.14: Frequency of the two cases of Droop controller and FCPA compared to ordinary hydro unit and 50 % WPR that is non responsive to frequency variations.

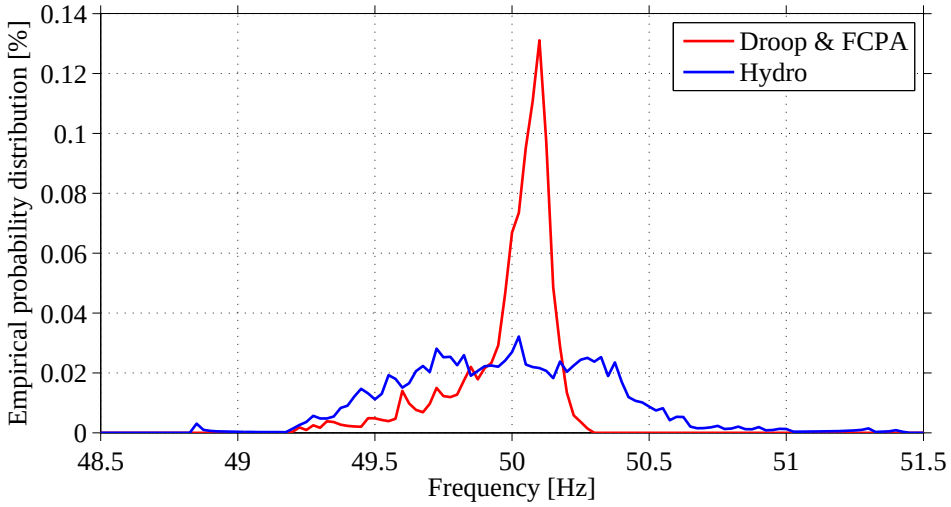

Figure 6.15: Histogram of Droop controller and FCPA compared to ordinary hydro unit and 50 % WPR.

A vast improvement in the frequency quality in the modeled power system can be seen in Figure 6.14 and Figure 6.15.

A standard VSWT would produce a total relative energy value (REV), of 712 pu s during the simulation window. Considering the energy lost for the wind farm owner while not operating at an optimum level throughout the simulated time 667 pu s is produced when both droop and FCPA is active. Considering a fixed price for the simulation time on the spot market this would cause a reduction of profits of about 6 % when participating in frequency regulation in the studied case. This does however not consider the increased wear and tear that is placed on the

components in the VSWT. The improved frequency quality could reduce the wear and tear of the hydro unit.

TABLE 6.4: The duration within various frequency ranges with and without the implemented droop & FCPA strategy during a WPR of 50 % in a hydro based power system system.

Frequency interval [Hz]	Droop & FCPA duration [%]	Hydro (WT at MPPT) duration [%]
$f \geq 50.8$	0	2
$50.5 \leq f < 50.8$	0	5
$50.1 \leq f < 50.5$	33	32
$49.9 \leq f < 50.1$	47	19
$49.5 \leq f < 49.9$	17	32
$49.2 \leq f < 49.5$	3	9
$49.2 < f$	0	1

In Table 6.4 the different durations within the different frequency intervals can be observed in percent of the total simulation time. A clear improvement to the span of 49.9 Hz $\leq f <$50.1 Hz of 28 percentage points in this primary operation area for the power system. The most severe under and over frequency occurances has also reduced when introducing the combined frequency controller onto the VSWT. The maximum frequency during the evaluation period was noted to 50.29 Hz and 51.43 Hz for the frequency controlled VSWT and un-controlled case respectively. The minimum frequency during the evaluation period was noted to 49.22 Hz when utilizing the combined controller and 48.85 Hz when the VSWT were controlled as default.

The increased variance of different parameters associated to the use of the system as well as the wear and tear of components are presented in Table 6.5.

TABLE 6.5: The variance of different parameters affected by the frequency adaption of the VSWT during a WPR of 50 %.

Variance of parameter	Droop & FCPA	Hydro (WT at MPPT)
f	0.18	0.38
P_{hydro}	0.0570	0.0628
AGC	0.1118	0.1454
beta	1.2326	0.3191
wt_{rot}	0.0492	0.0423

A drastic change can be seen (Table 6.5) in the variance of the frequency of the system when comparing the two cases. A reduction of the usage of the hydro unit, both the AGC-signal and the actual droop response (P_{hydro}) can also be observed due to the interactions from the VSWT utilizing the FCPA and the suggested droop controller. The FCPA causes the droop to act to a greater extent than it would in the case without FCPA. The variance in the rotation of the wind turbine in also increased due to the droop controller. This could give rise to an increased wear and tear to bearings, gearboxes and generators. These impacts on wear and tear would probably be limited since the action of the pitch also decreases the mechanical stresses of

these components in the drive train. Pitch actuators will however be forced to have an updated maintenance plan in order to cope with its increased use.

If one considers the other generators discussed previous a big improvement can be seen here, however the rapid response of these governors and generator units are vastly outperforming the hydro based case.

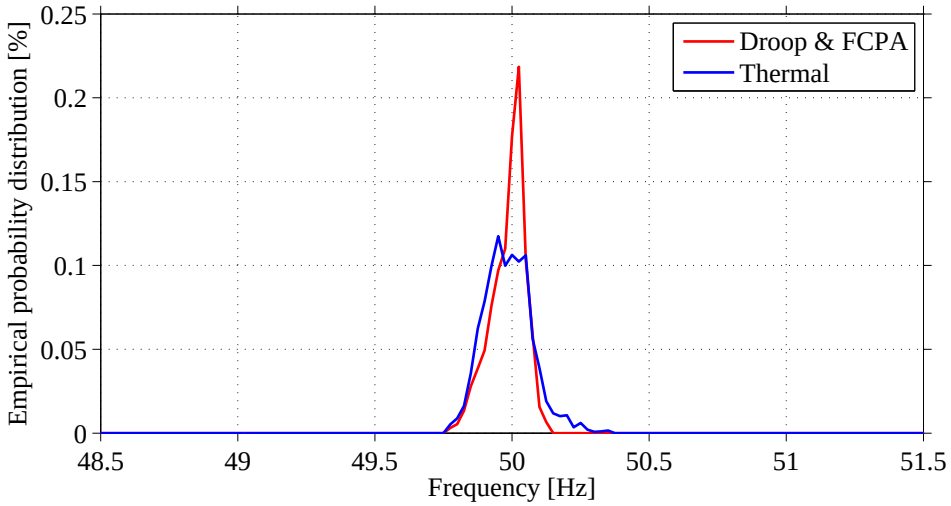

Figure 6.16: Histogram of Droop controller and FCPA compared to ordinary reheat unit and 50 % WPR.

REV values for the case with a reheat unit in charge of backup generation are noted to E_{gen} = 698 pu s with the combined frequency control from the VSWT (in default VSWT operation the E_{gen} = 712 pu s). This indicates the reduced need from contributing to frequency control from VSWT when operating with a reheat unit as a backup generation.

TABLE 6.6: The duration within various frequency ranges with and without the implemented droop & FCPA strategy during a WPR of 50 % in a reheat based power system system.

Frequency interval [Hz]	Droop & FCPA duration [%]	Reheat (WT at MPPT) duration [%]
$f \geq 50.8$	0	0
$50.5 \leq f <50.8$	0	0
$50.1 \leq f <50.5$	2	10
$49.9 \leq f <50.1$	89	77
$49.5 \leq f <49.9$	9	13
$49.2 \leq f <49.5$	0	0
$49.2 < f$	0	0

It can be observed from Table 6.6 that a the frequency control VSWT improves the behavior even of the fast generation unit such as the reheat-unit. The maximum frequency during the evaluation period was noted to 50.15 Hz with the frequency controlled VSWT and 50.36 Hz

with the VSWT controlled as default. Considering the minimum frequency during the evaluation period was noted to 49.78 Hz for both cases. This implies that the droop could interaction from the VSWT could be increased depending on the backup generation unit in order to aid more during under-frequency events.

Considering the thermal unti and its behaviour a histogram of the frequency during the simulation time is presented below in Figure 6.17.

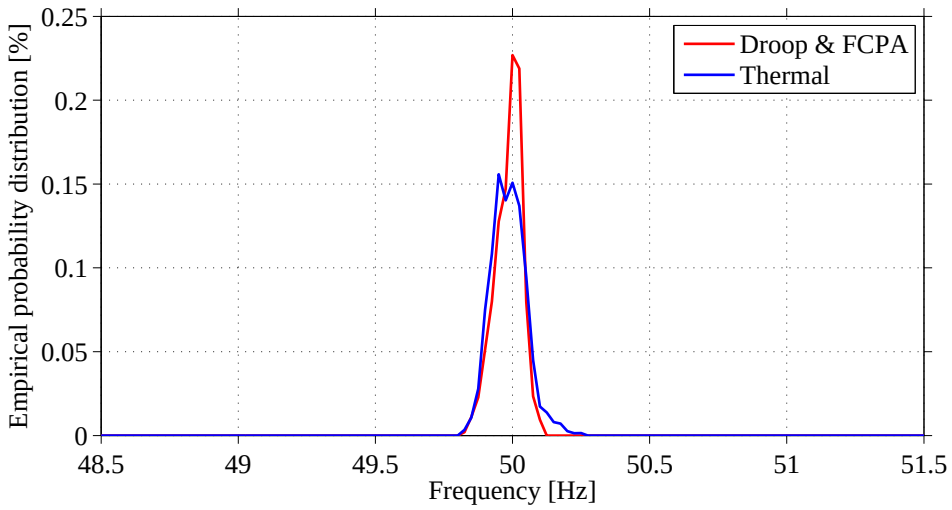

Figure 6.17: Histogram of Droop controller and FCPA compared to ordinary thermal unit and 50 % WPR.

REV values when the thermal unit was in charge of backup generation are noted to E_{gen} = 702 pu s with the combined frequency control from the VSWT (in default VSWT operation the E_{gen} = 712 pu s). This indicates the reduced need from contributing to frequency control from VSWT when operating with a thermal unit as a backup generation.

TABLE 6.7: The duration within various frequency ranges with and without the implemented droop & FCPA strategy during a WPR of 50 % in a thermal based power system system.

Frequency interval [Hz]	Droop & FCPA duration [%]	Thermal (WT at MPPT) duration [%]
$f \geq 50.8$	0	0
$50.5 \leq f <50.8$	0	0
$50.1 \leq f <50.5$	1	5
$49.9 \leq f <50.1$	95	91
$49.5 \leq f <49.9$	4	4
$49.2 \leq f <49.5$	0	0
$49.2 < f$	0	0

The modeled thermal unit performs slightly better than the reheat unit for both cases, with and without frequency support from the VSWT considering the duration in the range of $49.9 \leq f$

$<$50.1 Hz. The maximum frequency during the evaluation period was noted to 50.12 Hz with the combined frequency controllers for the VSWT and 50.26 Hz for VSWT in default operation. The minimum frequency during the evaluation period was noted to 49.84 Hz for both cases, a similar result as shown in the case of the reheat unit where no improvement was done to the minimum frequency of the simulated time.

6.5 Conclusions

Two support strategies are evaluated together against various wind speeds and generation mixes. The strategies consider parameters such as delays and dead band settings.

The two strategies combined improve the overall frequency quality in the power system for all wind speeds and all generation mixes presented. Variations in the backup generation are reduced and transferred to the VSWT. The fast regulating generation units (thermal and re-heat) perform better than the slower hydro unit and has less problems handling the frequency variations caused by the wind turbines, even without using the combined frequency controller.

Even though pitching and utilizing the droop alters the operational points of the VSWT the energy sold by the wind turbines in frequency control is marginally affected.

Un-filtered wind data, could cause big differences in the wind variation and thus the power produced further causes implications to the frequency quality.

Due to the activation of the pitch controller the need for fast up regulation can be considered one of the biggest issues faced by TSOs in hydro based power systems with high wind penetration.

Delay parameters that are presented worsen the frequency quality while dead bands mainly affect the histogram reducing the distribution just around the rated frequency especially for the hydro based power system one should consider the demands set in Table 2.3.

Chapter 7

Conclusions and future work

7.1 Conclusions

This thesis has dealt wind integration of variable speed wind turbines and the effect that this has on the system frequency in low inertia power systems. Special interest has been put to the frequency quality in the Nordic power system, the ability to provide synthetic inertia in hydro dominated systems and to provide a type of temporary primary support to an islanded power system. Literature studies on generator grid codes on frequency has been evaluated, implications on poor frequency quality and dead band settings has also been considered in the thesis.

The studies have shown on large variations in ROCOF depending on locations which are backed up by theoretical derivations. The local frequency measurements show the implication on acting on local frequency signals when dealing with large generation trips such as the case of the trip of the nuclear station Forsmark. The action of local support strategies could prove increasingly difficult especially for the case of inertia emulation strategies since on occasion the frequency derivative could become positive during a big disturbance to later on continue with a large frequency nadir.

Sampling frequencies when estimating ROCOF needs to be at least 10 Hz in order not to give a pessimistic view of the disturbance. Providing ROCOF calculations based on 1 Hz measurements is not deemed reasonable since it gives to large errors. If the TSO utilizes several PMU they could average a response from different locations to give a supervisory control frequency to be sent to the VSWTs. The implication of this would be a longer delay after a disturbance and most probably a steeper ROCOF during the initial second during high WPR and low inertia, due to the communication delay.

Updated grid codes on ROCOF protection is deemed necessary, at least considering the Swedish ASP. Future power systems with lower inertia will result in a steeper ROCOF during large n-1 contingencies and should not trip island protections of VSWT.

Two strategies of utilize the rotating mass of the VSWT in order to balance 20 and 50 % VSWT instantaneous wind penetration ratios (WPR) in a islanded power system based on a hydro unit. The temporary frequency drop for a wind penetration of 50 % was improved from 47.33 Hz, for

the uncontrolled case, to 49.10 Hz. This is a functionallity that should be considered due to its large possible contributions to frequency stability increase of weak power systems. To assume a constant wind speed might be reasonable when at first designing an inertia strategy from a VSWT for short power imbalances. Its application(inertia support) will however be utilized in another more dynamic situation where wind variations and power injection from other sources needs to me modeled simultaneously. Dynamic simulations put larger stress on an accurate model of the wind turbine control system including pitch controller/actuator. The presented adaptations to the inertia support shows that this is possible with few alterations to the control logic.

The high levels of wind penetration modeled could cause problems to the frequency due to periodic power oscillations during especially medium wind speeds in small power systems (by size). Up regulation is at these occurrences more important than down regulation since down regulation could be solved with pitch actuators. The suggested combined controller (Droop & FCPA) alters the power in a small way but is sufficient to alter the frequency behavior of the presented hydro dominated system. It indicates also that large quantities of energy does not need to be spilled in order to improve the power system behavior in the main operational frequency range of a power system. Improvements from the combined controller are shown even for faster backup generators (reheat and thermal) who seem to handle the wind variations without added control from the VSWT. For the generalized hydro model this in however not the case and the VSWT needs to provide frequency support in order not to experience severe load shedding in the system.

7.2 Future work

The implication of using a simplified power system is that all changes in power, speed, frequency and event timings are rather easy to observe. The IEEE 9/14 - bus system have been used in transient studies, similar studies on these systems could be made in order to get the representation of the fault at different locations. Studies on the integration of a supervisory control vs that of a local control for inertia support should be evaluated. Included in this analysis fast support units such as the ones provided by the HVDC links or future battery storage systems.

The lack of inertia in any system is hard to observe without an all knowing system. However, knowing what generators that are connected and generating each hour, assuming that the TSO has this knowledge, inertia-support from operational VSWT can be ordered to keep the n-1 criteria to be held without load shedding in case of too low power system inertia.

If wind turbines provide inertia, there is a reason for them to provide inertia to the power system, they want to sell their produced power. Still it is important to realize that other synchronous generators already provide their inertia without getting compensation for it. This could also be the case for a VSWT and suggestions on grid code recommendations for an inertia support should be considered.

Market implications of shifting to a 15 min cleared spot market could be of importance as well as market designs for a inertia market (if not choosing grid code requirements) in order

to compensate VSWT owners for their participation in aiding the power system during sevear power imbalances.

The action of the FCPA during high wind speeds should be further evaluated to ensure that the added reference signal to the pitch actuator does not cause increased mechanical stresses and over speeding of the rotor. This is mainly due to the derivative of the power coefficient related to a change in pitch at high pitch angles, which is lower than at low pitch angles. A dynamic FCPA that adjusts the gain of the controller due to the operational points of the VSWT could improve the situation.

In the future smart grid VSWT would be interconnected towards slower AGC-units in order to coordinate their response without causing overshoot in the frequency due to the interaction of the two during a generation trip. The fast power electronics should be utilized to handle the first initial dip with a defined inertial power, that with communication could be sent to AGC units in order to handle this temporary but fast support.

Transient stability enhancement could be considered for the initialization of a frequency deviation to ensure that the first rotor swing not causes connected generators to loose synchronism.

References

[1] EWEA, *"The European offshore wind industry - key trends and statistics 2014"*, Jan 2015.

[2] ——, *"Wind energy scenarios for 2020"*, Jul 2014.

[3] B.-M. Hodge, D. Lew, M. Milligan, H. Holttinen, S. Sillanpää, E. Gómez-Lázaro, R. Scharff, L. Söder, X. G. Larsén, G. Giebel *et al.*, "Wind power forecasting error distributions: An international comparison," 2012.

[4] G. Ramtharan, J. Ekanayake, and N. Jenkins, "Frequency support from doubly fed induction generator wind turbines," *Renewable Power Generation, IET*, vol. 1, no. 1, pp. 3–9, 2007.

[5] E. Vittal, M. O'Malley, and A. Keane, "Rotor angle stability with high penetrations of wind generation," *Power Systems, IEEE Transactions on*, vol. 27, no. 1, pp. 353–362, Feb 2012.

[6] Y. Zhang, J. Bank, E. Muljadi, Y.-H. Wan, and D. Corbus, "Angle instability detection in power systems with high-wind penetration using synchrophasor measurements," *Emerging and Selected Topics in Power Electronics, IEEE Journal of*, vol. 1, no. 4, pp. 306–314, Dec 2013.

[7] P.-K. Keung, P. Li, H. Banakar, and B. T. Ooi, "Kinetic energy of wind-turbine generators for system frequency support," *Power Systems, IEEE Transactions on*, vol. 24, no. 1, pp. 279–287, Feb 2009.

[8] I. Erlich, K. Rensch, and F. Shewarega, "Impact of large wind power generation on frequency stability," in *Power Engineering Society General Meeting, 2006. IEEE*, 2006, pp. 8 pp.–.

[9] R. de Almeida and J. Peas Lopes, "Participation of doubly fed induction wind generators in system frequency regulation," *Power Systems, IEEE Transactions on*, vol. 22, no. 3, pp. 944–950, Aug 2007.

[10] G. C. Tarnowski, P. C. Kjær, J. Østergaard, and P. E. Sørensen, "Frequency control in power systems with high wind power penetration."

[11] J. Ekanayake and N. Jenkins, "Comparison of the response of doubly fed and fixed-speed induction generator wind turbines to changes in network frequency," *Energy conversion, IEEE transactions on*, vol. 19, no. 4, pp. 800–802, 2004.

[12] J. Björnstedt, "Integration of non-synchronous generation," Ph.D. dissertation, Lund University, 2012.

[13] G. C. Tarnowski, "Coordinated frequency control of wind turbines in power systems with high wind power penetration," Ph.D. dissertation, Technical University of Denmark (DTU), 11 2011.

[14] Z. Xu, J. Ostergaard, M. Togeby, and F. Isleifsson, "Evaluating frequency quality of nordic system using pmu data," in *Power and Energy Society General Meeting - Conversion and Delivery of Electrical Energy in the 21st Century, 2008 IEEE*, July 2008, pp. 1–5.

[15] Z. Li, O. Samuelsson, and R. Garcia-Valle, "Frequency deviations and generation scheduling in the nordic system," in *PowerTech, 2011 IEEE Trondheim*, June 2011, pp. 1–6.

[16] H.-W. Kim, S.-S. Kim, and H.-S. Ko, "Modeling and control of pmsg-based variable-speed wind turbine," *Electric Power Systems Research*, vol. 80, no. 1, pp. 46 – 52, 2010. [Online]. Available: http://www.sciencedirect.com/science/article/pii/S0378779609001771

[17] C. Abbey and G. Joos, "Supercapacitor energy storage for wind energy applications," *IEEE Transactions on Industry Applications*, vol. 43, no. 3, p. 769, 2007.

[18] D. Y. J. Zhu, H. Urdal, "Synthetic inertia control strategy for double-fed induction generator wind turbine generators using energy from dc capacitor," in *Wind Integration Workshop Proceedings, 2013-1165*, 2013.

[19] Y.-Z. Sun, Z.-S. Zhang, G. jie Li, and J. Lin, "Review on frequency control of power systems with wind power penetration," in *Power System Technology (POWERCON), 2010 International Conference on*, Oct 2010, pp. 1–8.

[20] M. Altin, O. Göksu, R. Teodorescu, P. Rodriguez, B.-B. Jensen, and L. Helle, "Overview of recent grid codes for wind power integration," in *Optimization of Electrical and Electronic Equipment (OPTIM), 2010 12th International Conference on*, 2010, pp. 1152–1160.

[21] M. Liserre, R. Cardenas, M. Molinas, and J. Rodriguez, "Overview of multi-mw wind turbines and wind parks," *Industrial Electronics, IEEE Transactions on*, vol. 58, no. 4, pp. 1081–1095, April 2011.

[22] SVK, Åsa Åhlén Hagman, *Utvärderingsrapport för delövning Simuleringsövning 3 (in Swedish)*, Jun. 2013.

[23] 'Nordic Energy Regulators, *"Nordic Market report 2013 - Report 6/2013"*, July 2013.

[24] Danish Energy Agency. (2014, Dec) Register of wind turbines - data on operating and decommisioned wind turbines (as at end of october 2014).

[25] Energinet.dk, *Energinet.dk's Analyseforudsætninger 2013-2035 - Dok. 78482/13, Sag 12/427*, 2013.

[26] Svenska Kraftnät, *Avtal om Balansansvar för el mellan Affärsverket svenska kraftnät ("Svenska Kraftnät") och*, Jan. 2014. [Online]. Available: http://www.svk.se/Global/06_Energimarknaden/Pdf/El/BA_avtal_1_januari_2014_remiss.pdf

[27] Nordel, "Nordic grid code (nordic collection of rules)," Report, 2007.

[28] ENTSO-E, *Network Code on Load-Frequency Control and Reserves*, Jun. 2014. [Online]. Available: http://www.svk.se/Global/06_Energimarknaden/Pdf/El/BA_avtal_1_januari_2014_remiss.pdf

[29] The NERC Resources Subcommittee, *Balancing and Frequency Control*, Jan. 2011. [Online]. Available: http://www.nerc.com/docs/oc/rs/NERC%20Balancing%20and%20Frequency%20Control%20040520111.pdf

[30] M. H. Bollen and F. Hassan, *Integration of distributed generation in the power system*. John Wiley & Sons, 2011, vol. 80.

[31] M. Kuivaniemi, "Estimation of generator inertia in the Nordic power system," Master's thesis, Tampere University of Technology, Finland, 2014.

[32] *Harmonised Ancillary Services Consultation*, April 2014. [Online]. Available: http://www.eirgrid.com/media/HAS%20Consultation%20Paper%202014-2015.pdf

[33] Entso-e. (2012, Oct.) Introduction in automatic frr - 17 october 2012. [Online]. Available: http://www.svk.se/PageFiles/52463/Bilaga-1-LFC-Christer-Back.pdf

[34] P. Kundur, J. Paserba, V. Ajjarapu, G. Andersson, A. Bose, C. Canizares, N. Hatziargyriou, D. Hill, A. Stankovic, C. Taylor, T. Van Cutsem, and V. Vittal, "Definition and classification of power system stability ieee/cigre joint task force on stability terms and definitions," *Power Systems, IEEE Transactions on*, vol. 19, no. 3, pp. 1387–1401, Aug 2004.

[35] E. Potamianakis and C. Vournas, "Modeling and simulation of small hybrid power systems," in *Power Tech Conference Proceedings, 2003 IEEE Bologna*, vol. 2, June 2003, pp. 7 pp. Vol.2–.

[36] EirGrid and SONI, *"All Island TSO Facilitation of Renewables Studies"*. [Online]. Available: http://www.eirgrid.com/media/HAS%20Consultation%20Paper%202014-2015.pdf

[37] J. Machowski, J. Bialek, and J. Bumby, *Power System Dynamics: Stability and Control*. Wiley, 2011.

[38] EWEA, *"Wind in power - 2012 European statistics"*, Feb 2013.

[39] Energinet.dk, "Technical regulations 3.2.5 for wind power plants with power output greater than 11 kw," Report, 2010.

[40] Rede Eléctrica Nacional, "Diário da república, 1.ª serie - n.,° 147 - 30 de julho de 2010 and entidade reguladora dos serviços erergéticos - manual de procedimentos do gestor do sistema," Report, 2009.

[41] ——, "Disposición 10690 del boe núm. 191, issn: 0212-033x and technical requiremets for wind power and photovoltaic installations and any generating facilities whose technology does not consist on a synchronous generator directly connected to the grid, offprint form the o.p. 12.2 outline," Report, 2012.

[42] EirGrid, "Eirgrid grid code version 4.0, controllable wind farm power station grid code provisions," Report, 2011.

[43] E.ON Netz GbbH, "Grid connections regulations for high and extra high voltage," Report, 2006.

[44] ——, "Requirements for offshore grid connections in the e.on netz network," Report, 2008.

[45] ENTSO-E, *ENTSO-E Network code for requirements for grid connection applicable to all generators*, Mar. 2013.

[46] K. Creighton, M. McClure, R. Skillen, J. O'Higgins, T. McCartan, and A. Rogers, "Increased wind generation in ireland and northern ireland and the impact on rate of change of frequency," in *Proceedings of the 12th Wind Integration Workshop*, 2013.

[47] W. Wiser, *Energy Resources: Occurrence, Production, Conversion, Use*. Springer New York, 2012.

[48] B. J. Kirby, J. Dyer, C. Martinez, D. R. A. Shoureshi, R. Guttromson, and J. Dagle, "Frequency control concerns in the north american electric power system (ornl/tm-2003/41)," Report, 2002.

[49] P. Kundur, *Power System Stability And Control*, ser. EPRI power system engineering series. McGraw-Hill Education (India) Pvt Limited, 1994.

[50] M. Persson and W. Baig, "Modeling and measurements of transformer behavior at different voltages and frequencies," 2011.

[51] J. Andersson, "Modeling and measurements of the response of asynchronous machines exposed to voltage dips," 2010.

[52] B. J. Kirby, *Demand Response For Power System Reliability: FAQ*. Oak Ridge National Laboratory., 2006.

[53] M. G. Andy Beddoes, Peter Thomas, "Loss of mains protection relay performances when subjected to network disturbances / events," in *CIRED - 18th International Conference on Electricity Distribution*, 2005.

[54] W. Freitas, W. Xu, C. Affonso, and Z. Huang, "Comparative analysis between rocof and vector surge relays for distributed generation applications," *Power Delivery, IEEE Transactions on*, vol. 20, no. 2, pp. 1315–1324, April 2005.

[55] J. Vikesjö and L. Messing, "Wind power and fault clearance," *Elforsk*, vol. 10, no. 99, pp. 99–101, Apr. 2011.

[56] Åke Larsson and R. Larsson, "Anslutning av större produktions anläggning till elnätet," *Elforsk*, vol. 06, no. 10, pp. 39–40, Dec. 2006.

[57] M. Bongiorno and A. Petersson, "Development of a method for evaluation of wind turbines ability to fulfil swedish grid codes," *Elforsk*, vol. 09, no. 25, pp. 54–55, Feb. 2009.

[58] Eirgrid and SONI, "Rocof modification proposal - tsos recommendations," Report, 2012.

[59] Nord Pool Spot, *No. 18/2012 - Implementation of Load Frequency Control in the Nordic synchronous system*, May 2012.

[60] ——, *No. 26/2013 - Update on contracted FRR-A capacity in the Nordic synchronous system*, May 2013.

[61] ——, *No. 49/2013 - Update on contracted FRR-A capacity in the Nordic synchronous system*, Sep. 2013.

[62] ——, *No. 64/2013 - Update on FRR-A capacity in the Nordic synchronous system*, Nov. 2013.

[63] ——, *No. 67/2013 - Update on Exchange Information No. 64/2013 (2014 FRR-A contracting)*, Dec. 2013.

[64] ——, *No. 19/2014 - Update on Exchange Information No. 08/2014 (2014 FRR-A contracting)*, Apr. 2014.

[65] K. Kook, Y. Liu, and M. J. Bang, "Global behaviour of power system frequency in korean power system for the application of frequency monitoring network," *Generation, Transmission Distribution, IET*, vol. 2, no. 5, pp. 764–774, September 2008.

[66] M. Persson, P. Chen, and O. Carlson, "Frequency support by wind farms in islanded power systems with high wind power penetration," in *PowerTech (POWERTECH), 2013 IEEE Grenoble*, June 2013, pp. 1–6.

[67] Fortum, "Tekniska krav vid anslutning av vindkraftverk till 10/ 20/ 30 kv nÄtet (rn2105-10122)," Teknisk specifikation, 2011.

[68] N. W. Miller, *"GE Energy - Modeling of GE Wind Turbine-Generators for Grid studies - V4.2"*, June 2008.

[69] N. Ullah, T. Thiringer, and D. Karlsson, "Temporary primary frequency control support by variable speed wind turbines; potential and applications," *Power Systems, IEEE Transactions on*, vol. 23, no. 2, pp. 601–612, May 2008.

[70] J. Fortmann, *Modeling of Wind Turbines with Doubly Fed Generator System*, ser. Springer Vieweg. Springer Fachmedien Wiesbaden, 2014.

[71] T. Knuppel, J. Nielsen, K. Jensen, A. Dixon, and J. Otergaard, "Power oscillation damping controller for wind power plant utilizing wind turbine inertia as energy storage," in *Power and Energy Society General Meeting, 2011 IEEE*, July 2011, pp. 1–8.

[72] N. Strachan and D. Jovcic, "Stability of a variable-speed permanent magnet wind generator with weak ac grids," *Power Delivery, IEEE Transactions on*, vol. 25, no. 4, pp. 2779–2788, Oct 2010.

[73] A. Perdana, *Dynamic models of wind turbines*. Chalmers University of Technology, 2008.

[74] E. van der Hooft, P. Schaak, and T. van Engelen, *Wind turbine control algorithms*, ser. DOWEC-F1W1-EH-03-094/0, 2003.

[75] J. van Amerongen, H. Barends, P. Buys, and G. Honderd, "Modeling and control of a 180 mw power system," *Automatic Control, IEEE Transactions on*, vol. 31, no. 9, pp. 874–877, Sep 1986.

[76] G. Tarnowski, P. Kjær, S. Dalsgaard, and A. Nyborg, "Regulation and frequency response service capability of modern wind power plants," in *Power and Energy Society General Meeting, 2010 IEEE*, 2010, pp. 1–8.

[77] J. Ekanayake and N. Jenkins, "Comparison of the response of doubly fed and fixed-speed induction generator wind turbines to changes in network frequency," *Energy Conversion, IEEE Transactions on*, vol. 19, no. 4, pp. 800–802, 2004.

[78] G. C. Tarnowski, P. C. Kjær, P. E. Sørensen, and J. Østergaard, "Study on variable speed wind turbines capability for frequency response."

[79] J. Duval and B. Meyer, "Frequency behavior of grid with high penetration rate of wind generation," in *PowerTech, 2009 IEEE Bucharest*, 2009, pp. 1–6.

[80] N. R. Ullah, *Wind Power-Added Value for Network Operation*. Chalmers University of Technology, 2008.

[81] K. Yamashita, M. Asada, and K. Yoshimura, "A development of dynamic load model parameter derivation method," in *Power Energy Society General Meeting, 2009. PES '09. IEEE*, July 2009, pp. 1–8.

[82] G. le Dous and A. Holmer, "Frequency dependence of the load in the nordic power system - No. 95/96:02," Master's thesis, Chalmers University of Technology, Sweden, 1995.

[83] I. Margaris, S. Papathanassiou, N. Hatziargyriou, A. Hansen, and P. Sorensen, "Frequency control in autonomous power systems with high wind power penetration," *Sustainable Energy, IEEE Transactions on*, vol. 3, no. 2, pp. 189–199, April 2012.

[84] K. Vidyanandan and N. Senroy, "Primary frequency regulation by deloaded wind turbines using variable droop," *Power Systems, IEEE Transactions on*, vol. 28, no. 2, pp. 837–846, May 2013.

[85] F. Kanellos and N. Hatziargyriou, "Control of variable speed wind turbines equipped with synchronous or doubly fed induction generators supplying islanded power systems," *Renewable Power Generation, IET*, vol. 3, no. 1, pp. 96–108, March 2009.

[86] M. Kaltschmitt, W. Streicher, and A. Wiese, *Renewable energy: technology, economics and environment*. Springer, 2007.

[87] P. Sørensen, A. D. Hansen, and P. A. C. Rosas, "Wind models for simulation of power fluctuations from wind farms," *Journal of wind engineering and industrial aerodynamics*, vol. 90, no. 12, pp. 1381–1402, 2002.

[88] A. Pujante-López, E. Gomez-Lazaro, and J. Fuentes-Moreno, "Performance comparison of a 2 mw dfig wind turbine model under wind speed variations."

[89] J. Chow and J. Sanchez-Gasca, "Pole-placement designs of power system stabilizers," *Power Systems, IEEE Transactions on*, vol. 4, no. 1, pp. 271–277, Feb 1989.

[90] Y.-n. Yu and Q.-h. Li, "Pole-placement power system stabilizers design of an unstable nine-machine system," *Power Systems, IEEE Transactions on*, vol. 5, no. 2, pp. 353–358, May 1990.

[91] K. J. Åström and B. Wittenmark, *Adaptive Control - Second Edition*. Mineola, New York: DOVER PUBLICATIONS, INC, 2008.

[92] W. S. James DiCampli, "Grid stability: Gas turbines for primary reserve," in *ASME Turbo Expo 2013: Turbine Technical Conference and Exposition*, June 2013, pp. 1–6.

[93] S. Niemeyer, *"BAL-001-TRE-1 - Governor Droop and Dead-Band Settings and Their Impact on Grid Frequency Control"*, Jan. 2010.

[94] K. M. Sydney Niemeyer, *"FERC Technical Conference Frequency Response*, Sept 2010.

[95] R. W. Cummings, *"Overview of Frequency Response Initiative*, March 2010.

[96] T. Ono and J. Arai, "Frequency control with dead band characteristic of battery energy storage system for power system including large amount of wind power generation," *Electrical Engineering in Japan*, vol. 185, no. 3, pp. 1–10, 2013.

[97] National Grid, "The grid code , section cc.6.1.3 - issue 5, revision 10," Report, 2014.

[98] EirGrid, "Eirgrid grid code version 5.0," Report, 2013.

[99] S. Smith, "The scientist and engineer's guide to digital signal processing," 1997.

References

Appendix A

Appendix

A.1 Inertia modelling parameters

Load model, V_0 = 1, V=1, 0 $<\beta <$6, T_p = 51 ms, α_1 =2 and α_2 = 1. Inertia emulation: H_{wt} = 5.19 , (to get equal energy output during de-acceleration area between case #3 and #4 for 20 % WPR), K=3 or 9. Instant power support: A1 ; t_{de-acc} = 10 s , A2 ; t_{re-acc} = 20 s, ΔP_e = 0.1 pu during t_{de-acc} and 0.05 pu during t_{re-acc}.

C_p coefficients

$a_{0,0}$=-4.1909e-1; $a_{0,1}$=2.1808e-1; $a_{0,2}$=-1.2406e-2; $a_{0,3}$=-1.3365e-4; $a_{0,4}$=1.1524e-5;

$a_{1,0}$=-6.7606e-2; $a_{1,1}$=6.0405e-2; $a_{1,2}$=-1.3934e-2; $a_{1,3}$=1.0683e-3; $a_{1,4}$=-2.3895e-5;

$a_{2,0}$=1.5727e-2; $a_{2,1}$=-1.0996e-2; $a_{2,2}$=2.1495e-3; $a_{2,3}$=-1.4855e-4; $a_{2,4}$=2.7937e-6;

$a_{3,0}$=-8.6018e-4; $a_{3,1}$=5.7051e-4; $a_{3,2}$=-1.0479e-4; $a_{3,3}$=5.9924e-6; $a_{3,4}$=-8.9194e-8;

$a_{4,0}$=1.4787e-5; $a_{4,1}$=-9.4839e-6; $a_{4,2}$=1.6167e-6; $a_{4,3}$=-7.1535e-8; $a_{4,4}$=4.9686e-10;

A.2 AGC Tuning

AGC tuning - Hydro generation

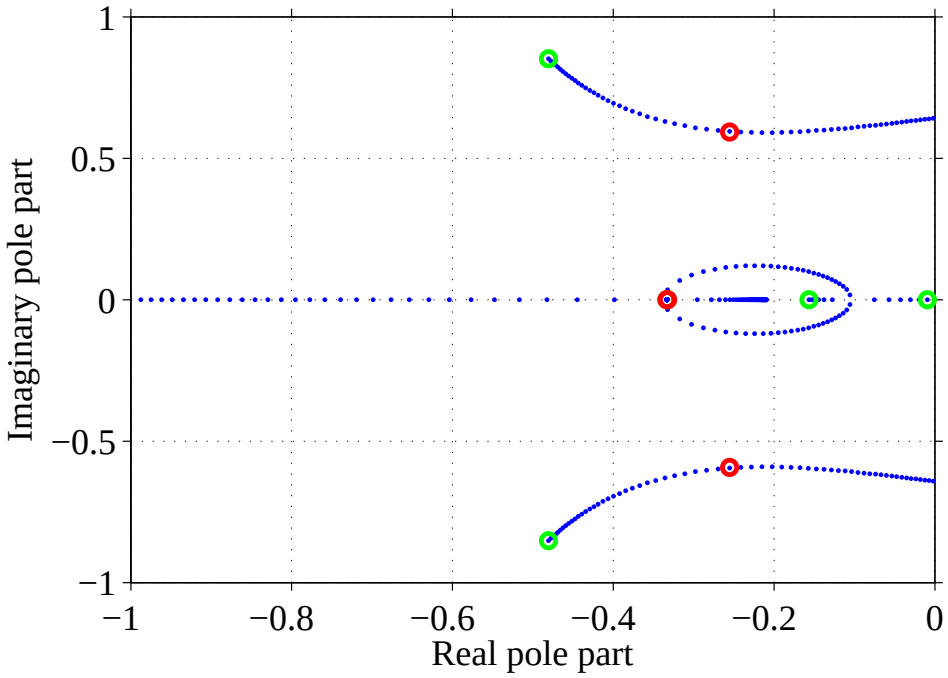

Figure A.1: Pole placement strategy for the AGC of the hydro unit and the chosen integrator gain noted by red K_{agc}=3.4, green circle showing the performance without integrator.

$$\frac{\Delta P_L}{\Delta f} = \frac{1}{(D+2Hs)\left(1+\frac{R_p\left(\frac{1}{R_p}+\frac{K_{agc}}{s}\right)(1+T_R)(1-0.5T_w s)}{(D+2Hs)(1+T_{GH}s)(R_p+R_T T_R s)}\right)} \tag{A.1}$$

AGC tuning - Reheat generation

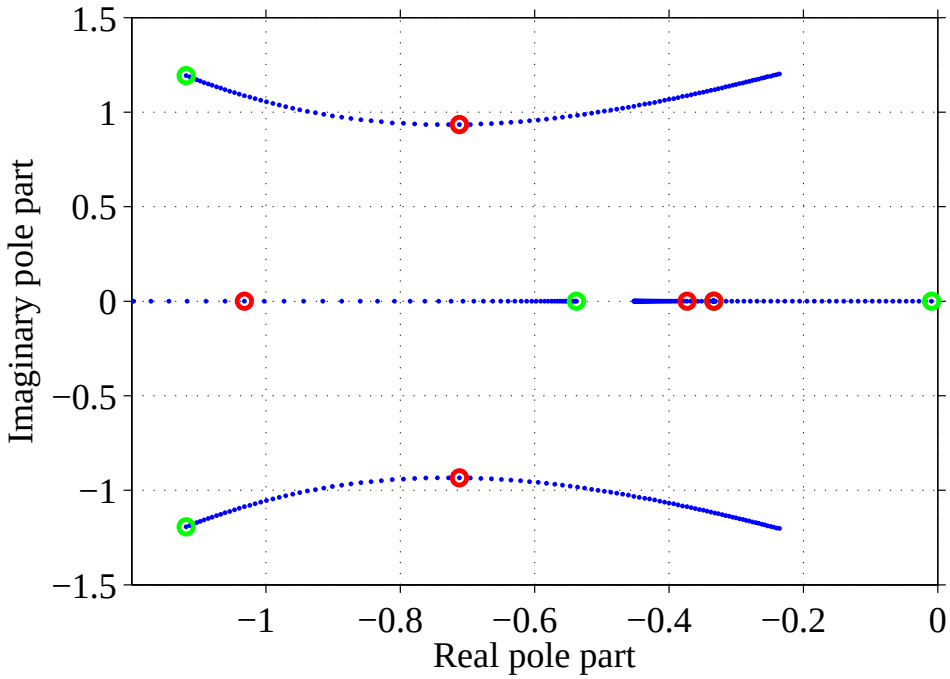

Figure A.2: Pole placement strategy for the AGC of the reheat steam unit and the chosen integrator gain noted by red K_{agc}=4.0, green circle showing the performance without integrator.

$$\frac{\Delta P_L}{\Delta f} = \frac{1}{(D+2Hs)\left(1+\frac{\left(\frac{1}{R_{RH}}+\frac{K_{agc}}{s}\right)(1+F_{HP}T_{RH}s)}{(D+2Hs)(1+T_{CH}s)(1+T_G)(1+T_{RH}s)}\right)} \tag{A.2}$$

AGC tuning - Thermal generation

$$\frac{\Delta P_L}{\Delta f} = \frac{1}{(D+2Hs)\left(1+\frac{K_{KL}(K_{agc}R_{TH}+s)(F_{HD}+F_{LD}+F_{HD}T_{HD}s)}{R_{TH}s(D+2Hs)(1+T_{HD}s)^2(1+T_{SM}s)}\right)} \tag{A.3}$$

A.3 Wind data series

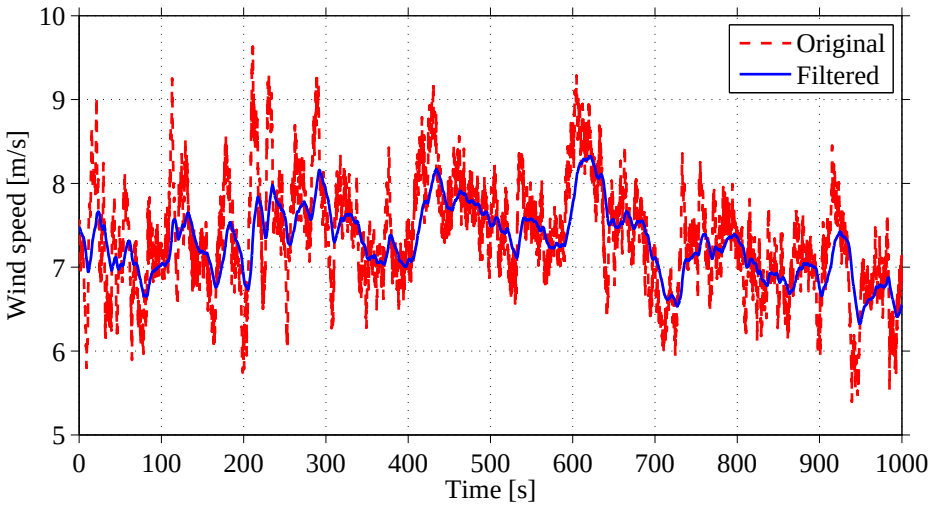

Figure A.3: Wind speed data session 1 with an average wind speed (unfiltered) of 7.36 m/s at hub height.

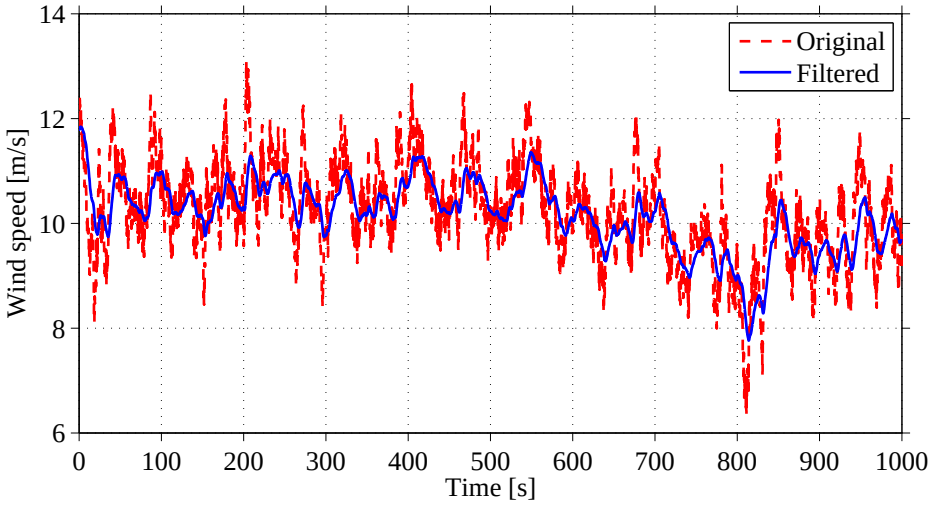

Figure A.4: Wind speed data session 2 with an average wind speed (unfiltered) of 10.24 m/s at hub height.

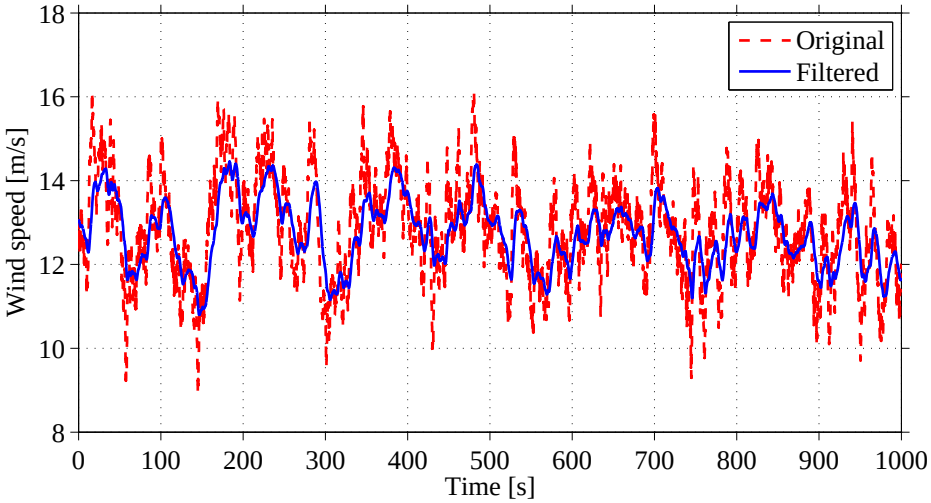

Figure A.5: Wind speed data session 3 with an average wind speed (unfiltered) of 12.84 m/s at hub height.

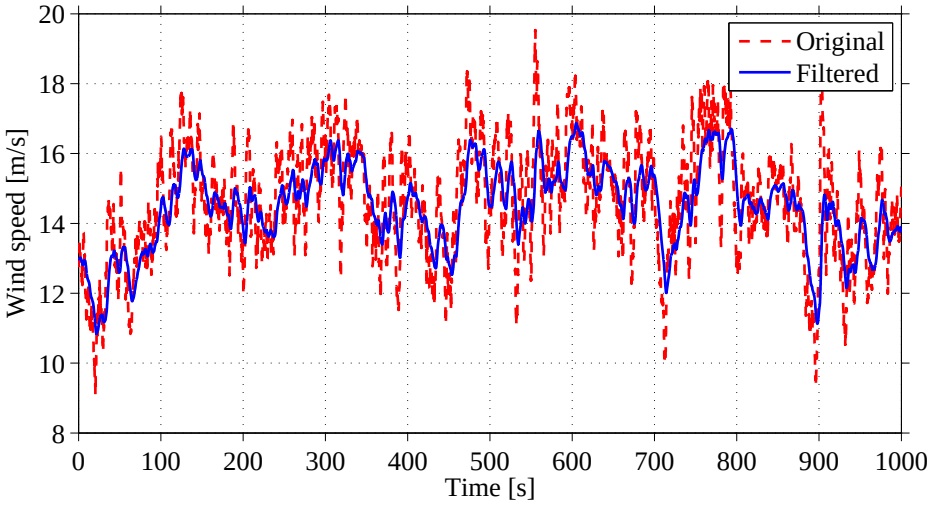

Figure A.6: Wind speed data session 4 with an average wind speed (unfiltered) of 14.64 m/s at hub height.